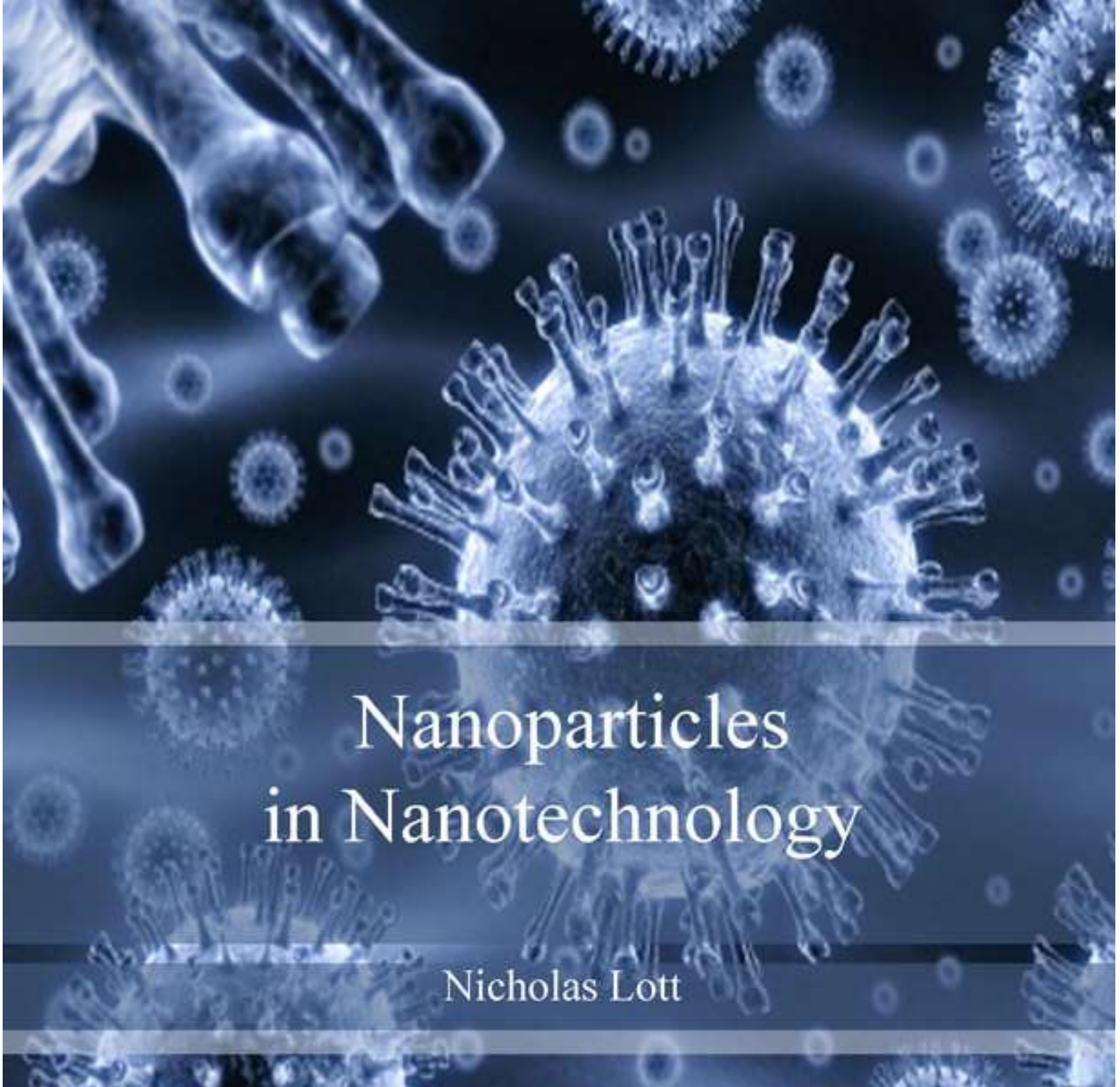

Nanoparticles in Nanotechnology

Nicholas Lott

First Edition, 2011

ISBN 978-93-81157-90-9

© All rights reserved.

Published by:
The English Press
4735/22 Prakashdeep Bldg,
Ansari Road, Darya Ganj,
Delhi - 110002
Email: info@wtbooks.com

Table of Contents

WT

Chapter- 1

Introduction to Nanoparticle

In nanotechnology, a particle is defined as a small object that behaves as a whole unit in terms of its transport and properties. It is further classified according to size: in terms of diameter, fine particles cover a range between 100 and 2500 nanometers, while ultrafine particles, on the other hand, are sized between 1 and 100 nanometers. Similar to ultrafine particles, **nanoparticles** are sized between 1 and 100 nanometers. Nanoparticles may or may not exhibit size-related properties that differ significantly from those observed in fine particles or bulk materials. Although the size of most molecules would fit into the above outline, individual molecules are usually not referred to as nanoparticles.

Nanoclusters have at least one dimension between 1 and 10 nanometers and a narrow size distribution. Nanopowders are agglomerates of ultrafine particles, nanoparticles, or nanoclusters. Nanometer-sized single crystals, or single-domain ultrafine particles, are often referred to as nanocrystals. Nanoparticle research is currently an area of intense scientific interest due to a wide variety of potential applications in biomedical, optical and electronic fields.

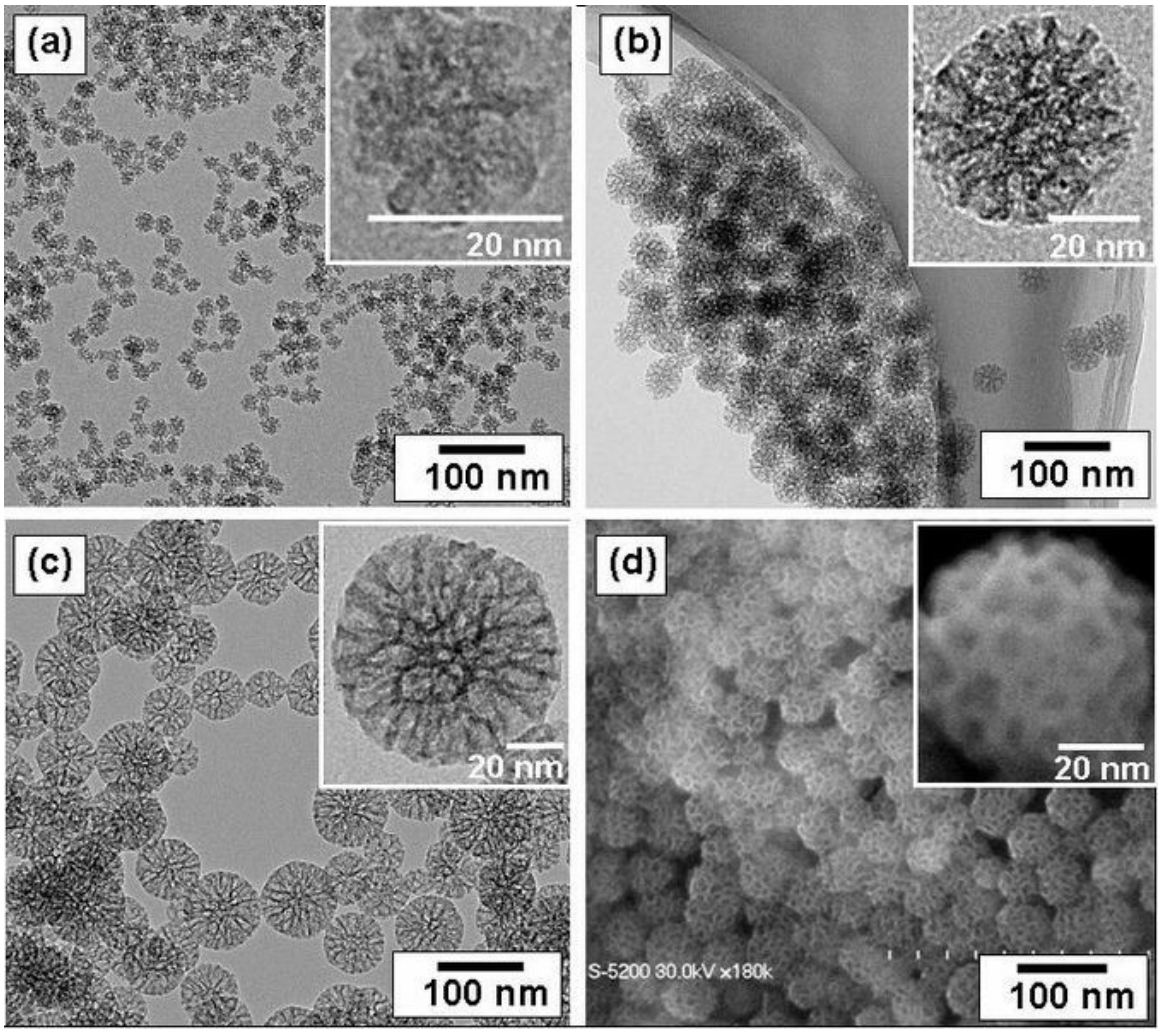

TEM (a, b, and c) images of prepared mesoporous silica nanoparticles with mean outer diameter: (a) 20nm, (b) 45nm, and (c) 80nm. SEM (d) image corresponding to (b). The insets are a high magnification of mesoporous silica particle.

The National Nanotechnology Initiative has led to generous public funding for nanoparticle research in the United States.

Background

Although nanoparticles are generally considered an invention of modern science, they actually have a very long history. Nanoparticles were used by artisans as far back as the 9th century in Mesopotamia for generating a glittering effect on the surface of pots.

Even these days, pottery from the Middle Ages and Renaissance often retain a distinct gold or copper colored metallic glitter. This so called luster is caused by a metallic film that was applied to the transparent surface of a glazing. The luster can still be visible if the film has resisted atmospheric oxidation and other weathering.

The luster originated within the film itself, which contained silver and copper nanoparticles dispersed homogeneously in the glassy matrix of the ceramic glaze. These nanoparticles were created by the artisans by adding copper and silver salts and oxides together with vinegar, ochre and clay, on the surface of previously-glazed pottery. The object was then placed into a kiln and heated to about 600 °C in a reducing atmosphere.

In the heat the glaze would soften, causing the copper and silver ions to migrate into the outer layers of the glaze. There the reducing atmosphere reduced the ions back to metals, which then came together forming the nanoparticles that give the colour and optical effects.

Luster technique showed that ancient craftsmen had a rather sophisticated empirical knowledge of materials. The technique originated in the islamic world. As Muslims were not allowed to use gold in artistic representations, they had to find a way to create a similar effect without using real gold. The solution they found was using luster.

Michael Faraday provided the first description, in scientific terms, of the optical properties of nanometer-scale metals in his classic 1857 paper. In a subsequent paper, the author (Turner) points out that: "It is well known that when thin leaves of gold or silver are mounted upon glass and heated to a temperature which is well below a red heat (~500 °C), a remarkable change of properties takes place, whereby the continuity of the metallic film is destroyed. The result is that white light is now freely transmitted, reflection is correspondingly diminished, while the electrical resistivity is enormously increased."

Uniformity

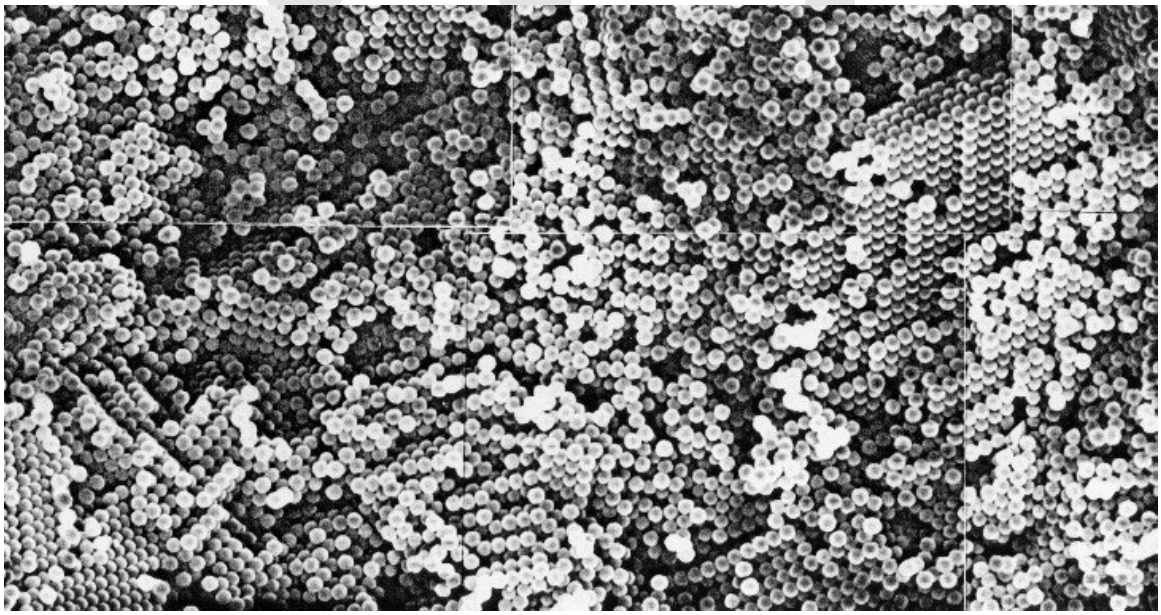

Colloidal crystal composed of amorphous hydrated colloidal silica (particle diameter 600 nm)

The chemical processing and synthesis of high performance technological components for the private, industrial and military sectors requires the use of high purity ceramics, polymers, glass-ceramics and material composites. In condensed bodies formed from fine powders, the irregular particle sizes and shapes in a typical powder often lead to non-uniform packing morphologies that result in packing density variations in the powder compact.

Uncontrolled agglomeration of powders due to attractive van der Waals forces can also give rise to in microstructural inhomogeneities. Differential stresses that develop as a result of non-uniform drying shrinkage are directly related to the rate at which the solvent can be removed, and thus highly dependent upon the distribution of porosity. Such stresses have been associated with a plastic-to-brittle transition in consolidated bodies, and can yield to crack propagation in the unfired body if not relieved.

In addition, any fluctuations in packing density in the compact as it is prepared for the kiln are often amplified during the sintering process, yielding inhomogeneous densification. Some pores and other structural defects associated with density variations have been shown to play a detrimental role in the sintering process by growing and thus limiting end-point densities. Differential stresses arising from inhomogeneous densification have also been shown to result in the propagation of internal cracks, thus becoming the strength-controlling flaws.

It would therefore appear desirable to process a material in such a way that it is physically uniform with regard to the distribution of components and porosity, rather than using particle size distributions which will maximize the green density. The containment of a uniformly dispersed assembly of strongly interacting particles in suspension requires total control over interparticle forces. Monodisperse nanoparticles and colloids provide this potential.

Monodisperse powders of colloidal silica, for example, may therefore be stabilized sufficiently to ensure a high degree of order in the colloidal crystal or polycrystalline colloidal solid which results from aggregation. The degree of order appears to be limited by the time and space allowed for longer-range correlations to be established. Such defective polycrystalline colloidal structures would appear to be the basic elements of submicrometer colloidal materials science, and, therefore, provide the first step in developing a more rigorous understanding of the mechanisms involved in microstructural evolution in high performance materials and components.

Properties

Silicon nanopowder

Nanoparticles are of great scientific interest as they are effectively a bridge between bulk materials and atomic or molecular structures. A bulk material should have constant physical properties regardless of its size, but at the nano-scale size-dependent properties are often observed. Thus, the properties of materials change as their size approaches the nanoscale and as the percentage of atoms at the surface of a material becomes significant. For bulk materials larger than one micrometer (or micron), the percentage of atoms at the surface is insignificant in relation to the number of atoms in the bulk of the material. *The interesting and sometimes unexpected properties of nanoparticles are therefore largely due to the large surface area of the material, which dominates the contributions made by the small bulk of the material*.

For example, nanoparticles of usually yellow gold and gray silicon are red in color. Gold nanoparticles melt at much lower temperatures (~300 °C for 2.5 nm size) than the gold slabs (1064 °C); . And absorption of solar radiation in photovoltaic cells is much higher in materials composed of nanoparticles than it is in thin films of continuous sheets of material. I.E. the smaller the particles, the greater the solar absorption.

Other size-dependent property changes include quantum confinement in semiconductor particles, surface plasmon resonance in some metal particles and superparamagnetism in magnetic materials. Ironically, the changes in physical properties are not always desirable. Ferromagnetic materials smaller than 10 nm can switch their magnetisation

direction using room temperature thermal energy, thus making them unsuitable for memory storage.

Suspensions of nanoparticles are possible since the interaction of the particle surface with the solvent is strong enough to overcome density differences, which otherwise usually result in a material either sinking or floating in a liquid. Nanoparticles also often possess unexpected optical properties as they are small enough to confine their electrons and produce quantum effects. For example gold nanoparticles appear deep red to black in solution.

The high surface area to volume ratio of nanoparticles provides a tremendous driving force for diffusion, especially at elevated temperatures. Sintering can take place at lower temperatures, over shorter time scales than for larger particles. This theoretically does not affect the density of the final product, though flow difficulties and the tendency of nanoparticles to agglomerate complicates matters. Moreover, nanoparticles have been found to impart some extra properties to various day to day products. For example the presence of titanium dioxide nanoparticles imparts what we call the self-cleaning effect, and the size being nanorange, the particles can not be observed. Zinc oxide particles have been found to have superior UV blocking properties compared to its bulk substitute. This is one of the reasons why it is often used in the preparation of sunscreen lotions. , and is completely photostable.

Clay nanoparticles when incorporated into polymer matrices increase reinforcement, leading to stronger plastics, verifiable by a higher glass transition temperature and other mechanical property tests. These nanoparticles are hard, and impart their properties to the polymer (plastic). Nanoparticles have also been attached to textile fibers in order to create smart and functional clothing.

Metal, dielectric, and semiconductor nanoparticles have been formed, as well as hybrid structures (e.g., core-shell nanoparticles). Nanoparticles made of semiconducting material may also be labeled quantum dots if they are small enough (typically sub 10 nm) that quantization of electronic energy levels occurs. Such nanoscale particles are used in biomedical applications as drug carriers or imaging agents.

Semi-solid and soft nanoparticles have been manufactured. A prototype nanoparticle of semi-solid nature is the liposome. Various types of liposome nanoparticles are currently used clinically as delivery systems for anticancer drugs and vaccines.

Nanoparticles with one half hydrophilic and the other half hydrophobic are termed Janus particles and are particularly effective for stabilizing emulsions. They can self-assemble at water/oil interfaces and act as solid surfactants.

Synthesis

There are several methods for creating nanoparticles, including both attrition and pyrolysis. In attrition, macro or micro scale particles are ground in a ball mill, a planetary

ball mill, or other size reducing mechanism. The resulting particles are air classified to recover nanoparticles. In pyrolysis, a vaporous precursor (liquid or gas) is forced through an orifice at high pressure and burned. The resulting solid (a version of soot) is air classified to recover oxide particles from by-product gases. Pyrolysis often results in aggregates and agglomerates rather than single primary particles.

A thermal plasma can also deliver the energy necessary to cause evaporation of small micrometer size particles. The thermal plasma temperatures are in the order of 10,000 K, so that solid powder easily evaporates. Nanoparticles are formed upon cooling while exiting the plasma region. The main types of the thermal plasma torches used to produce nanoparticles are dc plasma jet, dc arc plasma and radio frequency (RF) induction plasmas. In the arc plasma reactors, the energy necessary for evaporation and reaction is provided by an electric arc which is formed between the anode and the cathode. For example, silica sand can be vaporized with an arc plasma at atmospheric pressure. The resulting mixture of plasma gas and silica vapour can be rapidly cooled by quenching with oxygen, thus ensuring the quality of the fumed silica produced. In RF induction plasma torches, energy coupling to the plasma is accomplished through the electromagnetic field generated by the induction coil. The plasma gas does not come in contact with electrodes, thus eliminating possible sources of contamination and allowing the operation of such plasma torches with a wide range of gases including inert, reducing, oxidizing and other corrosive atmospheres.

The working frequency is typically between 200 kHz and 40 MHz. Laboratory units run at power levels in the order of 30–50 kW while the large scale industrial units have been tested at power levels up to 1 MW. As the residence time of the injected feed droplets in the plasma is very short it is important that the droplet sizes are small enough in order to obtain complete evaporation. The RF plasma method has been used to synthesize different nanoparticle materials, for example synthesis of various ceramic nanoparticles such as oxides, carbours/carbides and nitrides of Ti and Si.

Inert-gas condensation is frequently used to make nanoparticles from metals with low melting points. The metal is vaporized in a vacuum chamber and then supercooled with an inert gas stream. The supercooled metal vapor condenses into nanometer-sized particles, which can be entrained in the inert gas stream and deposited on a substrate or studied in situ.

Sol-gel

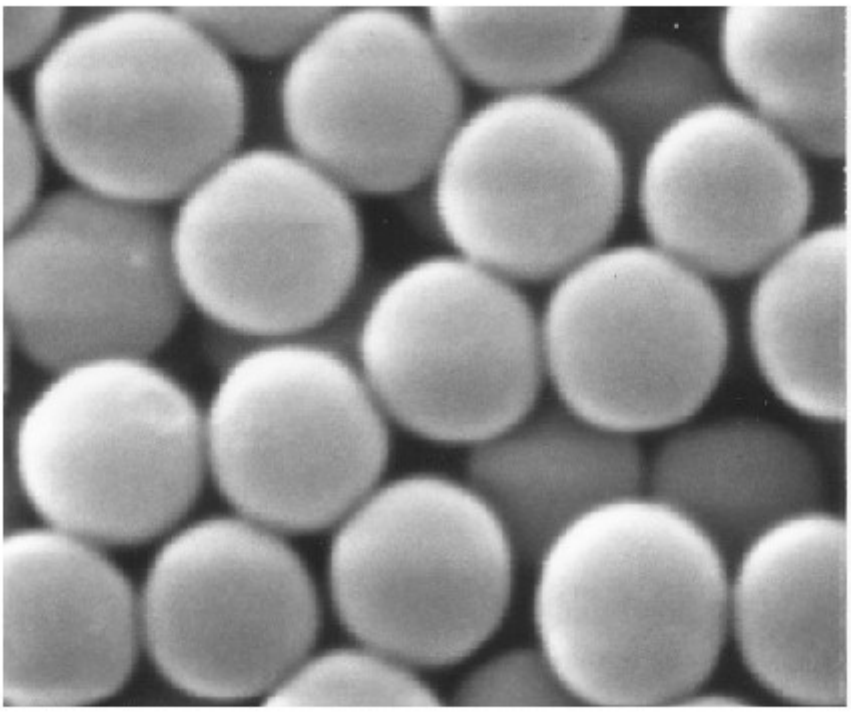

SEM micrograph of amorphous colloidal silica particles (average particle diameter 600 nm) formed in basic solution from TEOS.

The sol-gel process is a wet-chemical technique (also known as chemical solution deposition) widely used recently in the fields of materials science and ceramic engineering. Such methods are used primarily for the fabrication of materials (typically a metal oxide) starting from a chemical solution (*sol*, short for solution) which acts as the precursor for an integrated network (or *gel*) of either discrete particles or network polymers.

Typical precursors are metal alkoxides and metal chlorides, which undergo hydrolysis and polycondensation reactions to form either a network "elastic solid" or a colloidal suspension (or dispersion) – a system composed of discrete (often amorphous) submicrometer particles dispersed to various degrees in a host fluid. Formation of a metal oxide involves connecting the metal centers with oxo (M-O-M) or hydroxo (M-OH-M) bridges, therefore generating metal-oxo or metal-hydroxo polymers in solution. Thus, the sol evolves towards the formation of a gel-like diphasic system containing both a liquid phase and solid phase whose morphologies range from discrete particles to continuous polymer networks.

In the case of the colloid, the volume fraction of particles (or particle density) may be so low that a significant amount of fluid may need to be removed initially for the gel-like properties to be recognized. This can be accomplished in any number of ways. The most simple method is to allow time for sedimentation to occur, and then pour off the

remaining liquid. Centrifugation can also be used to accelerate the process of phase separation.

Removal of the remaining liquid (solvent) phase requires a drying process, which is typically accompanied by a significant amount of shrinkage and densification. The rate at which the solvent can be removed is ultimately determined by the distribution of porosity in the gel. The ultimate microstructure of the final component will clearly be strongly influenced by changes implemented during this phase of processing. Afterwards, a thermal treatment, or firing process, is often necessary in order to favor further polycondensation and enhance mechanical properties and structural stability via final sintering, densification and grain growth. One of the distinct advantages of using this methodology as opposed to the more traditional processing techniques is that densification is often achieved at a much lower temperature.

The precursor sol can be either deposited on a substrate to form a film (e.g. by dip-coating or spin-coating), cast into a suitable container with the desired shape (e.g. to obtain a monolithic ceramics, glasses, fibers, membranes, aerogels), or used to synthesize powders (e.g. microspheres, nanospheres). The sol-gel approach is a cheap and low-temperature technique that allows for the fine control of the product's chemical composition. Even small quantities of dopants, such as organic dyes and rare earth metals, can be introduced in the sol and end up uniformly dispersed in the final product. It can be used in ceramics processing and manufacturing as an investment casting material, or as a means of producing very thin films of metal oxides for various purposes. Sol-gel derived materials have diverse applications in optics, electronics, energy, space, (bio)sensors, medicine (e.g. controlled drug release) and separation (e.g. chromatography) technology.

Colloids

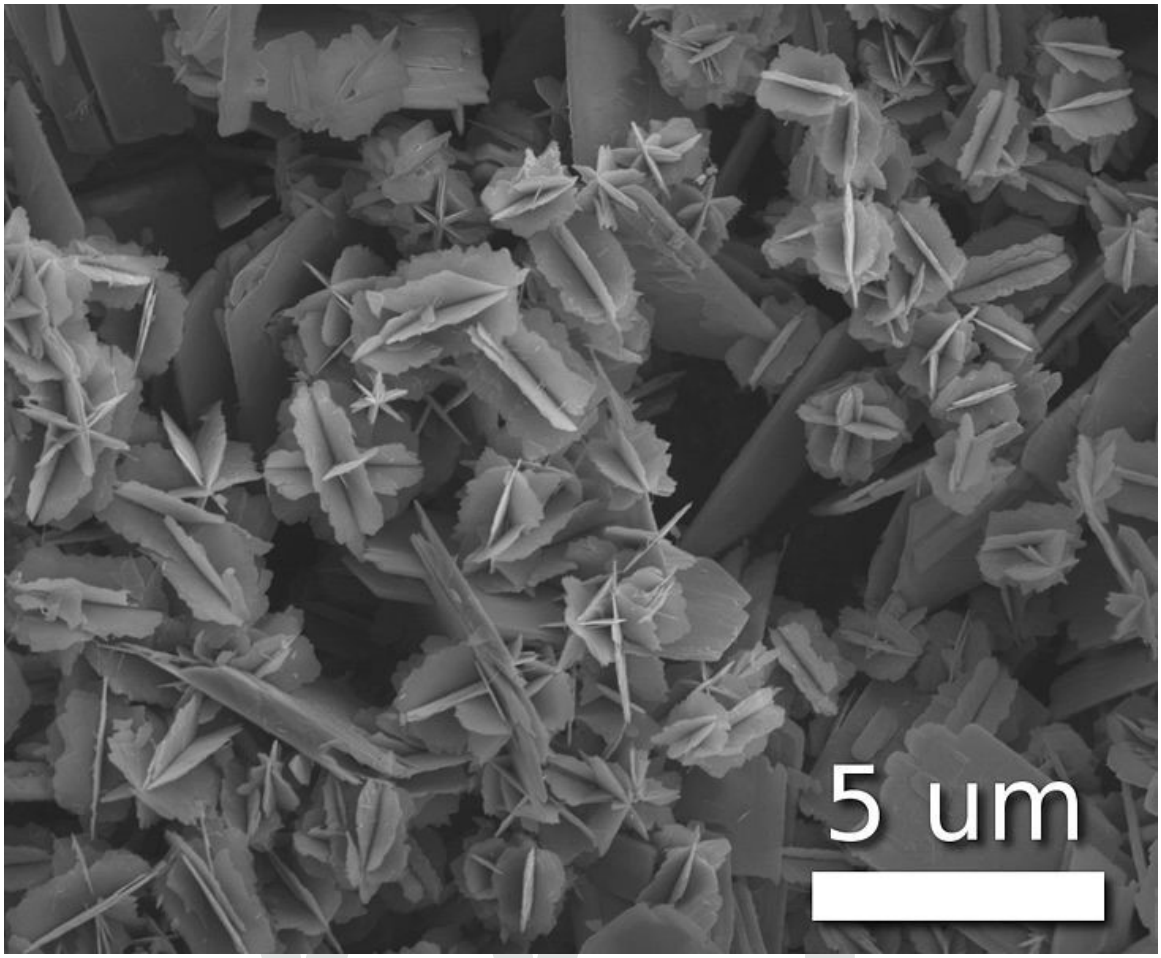

Nanostars of vanadium(IV) oxide

The term colloid is used primarily to describe a broad range of solid-liquid (and/or liquid-liquid) mixtures, all of which contain distinct solid (and/or liquid) particles which are dispersed to various degrees in a liquid medium. The term is specific to the size of the individual particles, which are larger than atomic dimensions but small enough to exhibit Brownian motion. If the particles are large enough, then their dynamic behavior in any given period of time in suspension would be governed by forces of gravity and sedimentation. But if they are small enough to be colloids, then their irregular motion in suspension can be attributed to the collective bombardment of a myriad of thermally agitated molecules in the liquid suspending medium, as described originally by Albert Einstein in his dissertation. Einstein proved the existence of water molecules by concluding that this erratic particle behavior could adequately be described using the theory of Brownian motion, with sedimentation being a possible long-term result. This critical size range (or particle diameter) typically ranges from nanometers (10^{-9} m) to micrometers (10^{-6} m).

Morphology

Scientists have taken to naming their particles after the real world shapes that they might represent. Nanospheres , nanoreefs , nanoboxes and more have appeared in the literature. These morphologies sometimes arise spontaneously as an effect of a templating or directing agent present in the synthesis such as miscellar emulsions or anodized alumina pores, or from the innate crystallographic growth patterns of the materials themselves. Some of these morphologies may serve a purpose, such as long carbon nanotubes being used to bridge an electrical junction, or just a scientific curiosity like the stars shown at right.

Amorphous particles usually adopt a spherical shape (due to their microstructural isotropy) – whereas the shape of anisotropic microcrystalline whiskers corresponds to their particular crystal habit. At the small end of the size range, nanoparticles are often referred to as clusters. Spheres, rods, fibers, and cups are just a few of the shapes that have been grown. The study of fine particles is called micromeritics.

Characterization

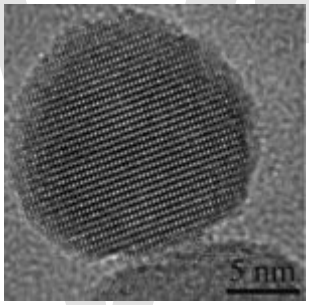

TEM image of magnetic Fe_3O_4 nanoparticle.

Nanoparticle characterization is necessary to establish understanding and control of nanoparticle synthesis and applications. Characterization is done by using a variety of different techniques, mainly drawn from materials science. Common techniques are electron microscopy (TEM, SEM), atomic force microscopy (AFM), dynamic light scattering (DLS), x-ray photoelectron spectroscopy (XPS), powder X-ray diffraction (XRD), Fourier transform infrared spectroscopy (FTIR), matrix-assisted laser desorption/ionization time-of-flight mass spectrometry (MALDI-TOF), ultraviolet-visible spectroscopy, dual polarisation interferometry and nuclear magnetic resonance (NMR).

Whilst the theory has been known for over a century, the technology for Nanoparticle tracking analysis (NTA) allows direct tracking of the Brownian motion and this method therefore allows the sizing of individual nanoparticles in solution.

Functionalization

The surface coating of nanoparticles is crucial to determining their properties. In particular, the surface coating can regulate stability, solubility and targeting. A coating

that is multivalent or polymeric confers high stability. For biological applications, the surface coating should be polar to give high aqueous solubility and prevent nanoparticle aggregation. In serum or on the cell surface, highly charged coatings promote non-specific binding, while polyethylene glycol linked to terminal hydroxyl or methoxy groups repel non-specific interactions. Nanoparticles can be linked to biological molecules which can act as address tags, to direct the nanoparticles to specific sites within the body, specific organelles within the cell, or to follow specifically the movement of individual protein or RNA molecules in living cells. Common address tags are monoclonal antibodies, aptamers, streptavidin or peptides. These targeting agents should ideally be covalently linked to the nanoparticle and should be present in a controlled number per nanoparticle. Multivalent nanoparticles, bearing multiple targeting groups, can cluster receptors, which can activate cellular signaling pathways, and give stronger anchoring. Monovalent nanoparticles, bearing a single binding site, avoid clustering and so are preferable for tracking the behavior of individual proteins.

Safety

Nanoparticles present possible dangers, both medically and environmentally. Most of these are due to the high surface to volume ratio, which can make the particles very reactive or catalytic. They are also able to pass through cell membranes in organisms, and their interactions with biological systems are relatively unknown. A recent study looking at the effects of ZnO nanoparticles on human immune cells has found varying levels of susceptibility to cytotoxicity. Smaller nanoparticles evinced increased cytotoxicity. Lymphocytes (especially naive T cells) were found to be more resistant to nanoparticle cytotoxicity than monocytes, likely due to the capacity of the latter to produce higher levels of reactive oxygen species in response to internalized nanoparticles. Previously activated memory T cells were more susceptible than naive T cells, implying a relationship between cell-cycle and nanoparticle susceptibility. In addition, nanoparticle concentrations below those causing appreciable cell death nonetheless induced the production of proinflammatory cytokines, such as IFN-γ and TNF. Despite these laboratory findings, free nanoparticles in the environment may rapidly agglomerate and thus leave the nano-regime . Nature itself presents many nanoparticles to which organisms on earth may have evolved immunity (such as salt particulates from ocean aerosols, terpenes from plants, or dust from volcanic eruptions) .

According to the *San Francisco Chronicle*, "Animal studies have shown that some nanoparticles can penetrate cells and tissues, move through the body and brain and cause biochemical damage they also have shown to cause a risk factor in men for testicular cancer. But whether cosmetics and sunscreens containing nanomaterials pose health risks remains largely unknown, pending completion of long-range studies recently begun by the FDA and other agencies." Diesel nanoparticles have been found to damage the cardiovascular system in a mouse model.

Chapter- 2

Quantum Dot

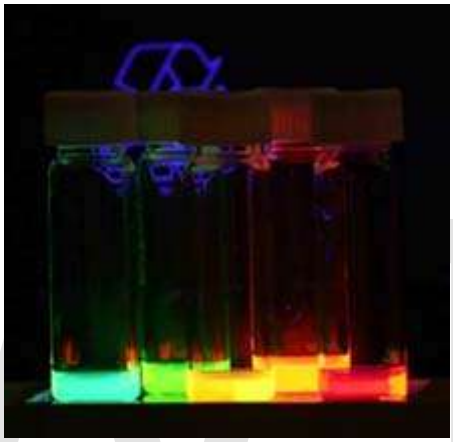

Colloidal quantum dots irradiated with a UV light. Different sized quantum dots emit different color light due to quantum confinement.

A **quantum dot** is a semiconductor whose excitons are confined in all three spatial dimensions. Consequently, such materials have electronic properties intermediate between those of bulk semiconductors and those of discrete molecules. They were discovered at the beginning of the 1980s by Alexei Ekimov in a glass matrix and by Louis E. Brus in colloidal solutions. The term "Quantum Dot" was coined by Mark Reed.

Researchers have studied quantum dots in transistors, solar cells, LEDs, and diode lasers. They have also investigated quantum dots as agents for medical imaging and hope to use them as qubits.

Stated simply, quantum dots are semiconductors whose electronic characteristics are closely related to the size and shape of the individual crystal. Generally, the smaller the size of the crystal, the larger the band gap, the greater the difference in energy between the highest valence band and the lowest conduction band becomes, therefore more energy is needed to excite the dot, and concurrently, more energy is released when the crystal returns to its resting state. For example, in fluorescent dye applications, this equates to higher frequencies of light emitted after excitation of the dot as the crystal size grows smaller, resulting in a color shift from red to blue in the light emitted. In addition to such tuning, a main advantage with quantum dots is that, because of the high level of control

possible over the size of the crystals produced, it is possible to have very precise control over the conductive properties of the material. Quantum dots of different sizes can be assembled into a gradient multi-layer nanofilm.

Quantum confinement in semiconductors

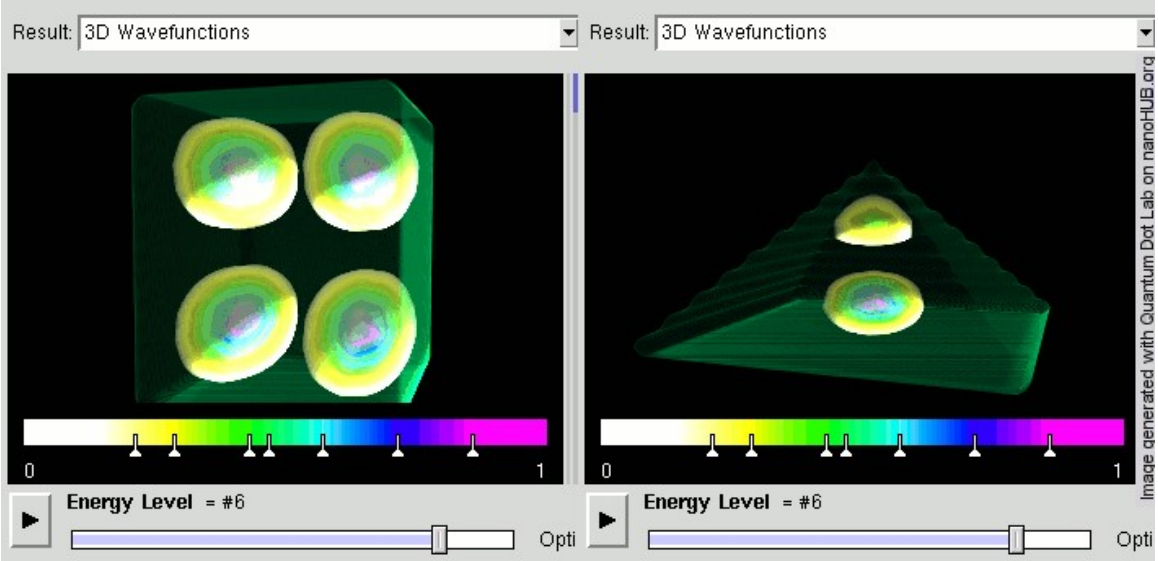

3D confined electron wave functions in a Quantum Dot. Here, rectangular and triangular-shaped quantum dots are shown. Energy states in rectangular dots are more 's-type' and 'p-type'. However, in a triangular dot the wave functions are mixed due to confinement symmetry.

In an unconfined (bulk) semiconductor, an electron-hole pair is typically bound within a characteristic length, called the exciton Bohr radius. This is estimated by replacing the positively charged atomic core with the hole in the Bohr formula. If the electron and hole are constrained further, then properties of the semiconductor change. This effect is a form of quantum confinement, and it is a key feature in many emerging electronic structures.

Besides confinement in all three dimensions i.e. Quantum Dot - other quantum confined semiconductors include:

- quantum wires, which confine electrons or holes in two spatial dimensions and allow free propagation in the third.
- quantum wells, which confine electrons or holes in one dimension and allow free propagation in two dimensions.

Production

There are several ways to confine excitons in semiconductors, resulting in different methods to produce quantum dots. In general, quantum wires, wells and dots are grown

by advanced epitaxial techniques in nanocrystals produced by chemical methods or by ion implantation, or in nanodevices made by state-of-the-art lithographic techniques.

Colloidal synthesis

Colloidal semiconductor nanocrystals are synthesized from precursor compounds dissolved in solutions, much like traditional chemical processes. The synthesis of colloidal quantum dots is based on a three-component system composed of: precursors, organic surfactants, and solvents. When heating a reaction medium to a sufficiently high temperature, the precursors chemically transform into monomers. Once the monomers reach a high enough supersaturation level, the nanocrystal growth starts with a nucleation process. The temperature during the growth process is one of the critical factors in determining optimal conditions for the nanocrystal growth. It must be high enough to allow for rearrangement and annealing of atoms during the synthesis process while being low enough to promote crystal growth. Another critical factor that has to be stringently controlled during nanocrystal growth is the monomer concentration. The growth process of nanocrystals can occur in two different regimes, “focusing” and “defocusing”. At high monomer concentrations, the critical size (the size where nanocrystals neither grow nor shrink) is relatively small, resulting in growth of nearly all particles. In this regime, smaller particles grow faster than large ones (since larger crystals need more atoms to grow than small crystals) resulting in “focusing” of the size distribution to yield nearly monodisperse particles. The size focusing is optimal when the monomer concentration is kept such that the average nanocrystal size present is always slightly larger than the critical size. When the monomer concentration is depleted during growth, the critical size becomes larger than the average size present, and the distribution “defocuses” as a result of Ostwald ripening.

There are colloidal methods to produce many different semiconductors. Typical dots are made of binary alloys such as cadmium selenide, cadmium sulfide, indium arsenide, and indium phosphide. Although, dots may also be made from ternary alloys such as cadmium selenide sulfide. These quantum dots can contain as few as 100 to 100,000 atoms within the quantum dot volume, with a diameter of 10 to 50 atoms. This corresponds to about 2 to 10 nanometers, and at 10 nm in diameter, nearly 3 million quantum dots could be lined up end to end and fit within the width of a human thumb.

Large batches of quantum dots may be synthesized via colloidal synthesis. Due to this scalability and the convenience of benchtop conditions, colloidal synthetic methods are promising for commercial applications. It is acknowledged to be the least toxic of all the different forms of synthesis.

Fabrication

- Self-assembled quantum dots are typically between 5 and 50 nm in size. Quantum dots defined by lithographically patterned gate electrodes, or by etching on two-dimensional electron gases in semiconductor heterostructures can have lateral dimensions exceeding 100 nm.

- Some quantum dots are small regions of one material buried in another with a larger band gap. These can be so-called core-shell structures, e.g., with CdSe in the core and ZnS in the shell or from special forms of silica called ormosil.
- Quantum dots sometimes occur spontaneously in quantum well structures due to monolayer fluctuations in the well's thickness.
- Self-assembled quantum dots nucleate spontaneously under certain conditions during molecular beam epitaxy (MBE) and metallorganic vapor phase epitaxy (MOVPE), when a material is grown on a substrate to which it is not lattice matched. The resulting strain produces coherently strained islands on top of a two-dimensional "wetting-layer." This growth mode is known as Stranski–Krastanov growth. The islands can be subsequently buried to form the quantum dot. This fabrication method has potential for applications in quantum cryptography (i.e. single photon sources) and quantum computation. The main limitations of this method are the cost of fabrication and the lack of control over positioning of individual dots.
- Individual quantum dots can be created from two-dimensional electron or hole gases present in remotely doped quantum wells or semiconductor heterostructures called lateral quantum dots. The sample surface is coated with a thin layer of resist. A lateral pattern is then defined in the resist by electron beam lithography. This pattern can then be transferred to the electron or hole gas by etching, or by depositing metal electrodes (lift-off process) that allow the application of external voltages between the electron gas and the electrodes. Such quantum dots are mainly of interest for experiments and applications involving electron or hole transport, i.e., an electrical current.
- The energy spectrum of a quantum dot can be engineered by controlling the geometrical size, shape, and the strength of the confinement potential. Also, in contrast to atoms, it is relatively easy to connect quantum dots by tunnel barriers to conducting leads, which allows the application of the techniques of tunneling spectroscopy for their investigation.

The quantum dot absorption features correspond to transitions between discrete,three-dimensional particle in a box states of the electron and the hole, both confined to the same nanometer-size box.These discrete transitions are reminiscent of atomic spectra and have resulted in quantum dots also being called *artificial atoms*.

- Confinement in quantum dots can also arise from electrostatic potentials (generated by external electrodes, doping, strain, or impurities).

Viral assembly

Lee et al. (2002) reported using genetically engineered M13 bacteriophage viruses to create quantum dot biocomposite structures. As a background to this work, it has previously been shown that genetically engineered viruses can recognize specific semiconductor surfaces through the method of selection by combinatorial phage display. Additionally, it is known that liquid crystalline structures of wild-type viruses (Fd, M13, and TMV) are adjustable by controlling the solution concentrations, solution ionic

strength, and the external magnetic field applied to the solutions. Consequently, the specific recognition properties of the virus can be used to organize inorganic nanocrystals, forming ordered arrays over the length scale defined by liquid crystal formation. Using this information, Lee et al. (2000) were able to create self-assembled, highly oriented, self-supporting films from a phage and ZnS precursor solution. This system allowed them to vary both the length of bacteriophage and the type of inorganic material through genetic modification and selection.

Electrochemical assembly

Highly ordered arrays of quantum dots may also be self-assembled by electrochemical techniques. A template is created by causing an ionic reaction at an electrolyte-metal interface which results in the spontaneous assembly of nanostructures, including quantum dots, onto the metal which is then used as a mask for mesa-etching these nanostructures on a chosen substrate.

Bulk-manufacture

Conventional, small-scale quantum dot manufacturing relies on a process called “high temperature dual injection” which is impractical for most commercial applications that require large quantities of quantum dots.

A reproducible method for creating larger quantities of consistent, high-quality quantum dots involves producing nanoparticles from chemical precursors in the presence of a molecular cluster compound under conditions whereby the integrity of the molecular cluster is maintained and acts as a prefabricated seed template. Individual molecules of a cluster compound act as a seed or nucleation point upon which nanoparticle growth can be initiated. In this way, a high temperature nucleation step is not necessary to initiate nanoparticle growth because suitable nucleation sites are already provided in the system by the molecular clusters. A significant advantage of this method is that it is highly scalable.

Cadmium-free quantum dots

Cadmium-free quantum dots are also called “CFQD”. In many regions of the world there is now a restriction or ban on the use of heavy metals in many household goods which means that most cadmium based quantum dots are unusable for consumer-goods applications.

For commercial viability, a range of restricted, heavy metal-free quantum dots has been developed showing bright emissions in the visible and near infra-red region of the spectrum and have similar optical properties to those of CdSe quantum dots.

Cadmium and other restricted heavy metals used in conventional quantum dots is of a major concern in commercial applications. For Quantum Dots to be commercially viable in many applications they must not contain cadmium or other restricted metal elements.

A new type of CFQD can be made from rare earth (RE) doped oxide colloidal phosphor nanoparticles. Unlike semiconductor nanoparticles, excitation was due to UV absorption of host material, which is same for different RE doped materials using same host. Multiplexing applications can be thus realized. The emission depends on the type of RE, which enables very large stokes shift and is narrower than CdSe QDs. The synthesis is aqueous based, which eliminated issues of water solubility for biological applications. The oxide surface might be easier for chemical functionalizion more and chemically stable in various environments. Some reports exist concerning the use of such phosphor nanoparticles on biological targeting and imaging.

Optical properties

An immediate optical feature of colloidal quantum dots is their coloration. While the material which makes up a quantum dot defines its intrinsic energy signature, the nanocrystal's quantum confined size is more significant at energies near the band gap. Thus quantum dots of the same material, but with different sizes, can emit light of different colors. The physical reason is the quantum confinement effect.

The larger the dot, the redder (lower energy) its fluorescence spectrum. Conversely, smaller dots emit bluer (higher energy) light. The coloration is directly related to the energy levels of the quantum dot. Quantitatively speaking, the bandgap energy that determines the energy (and hence color) of the fluorescent light is inversely proportional to the size of the quantum dot. Larger quantum dots have more energy levels which are also more closely spaced. This allows the quantum dot to absorb photons containing less energy, i.e., those closer to the red end of the spectrum. Recent articles in nanotechnology and in other journals have begun to suggest that the shape of the quantum dot may be a factor in the coloration as well, but as yet not enough information is available. Furthermore, it was shown that the lifetime of fluorescence is determined by the size of the quantum dot. Larger dots have more closely spaced energy levels in which the electron-hole pair can be trapped. Therefore, electron-hole pairs in larger dots live longer causing larger dots to show a longer lifetime.

As with any crystalline semiconductor, a quantum dot's electronic wave functions extend over the crystal lattice. Similar to a molecule, a quantum dot has both a quantized energy spectrum and a quantized density of electronic states near the edge of the band gap.

Qdots can be synthesized with larger(thicker) shells (CdSe qdots with CdS shells). The shell thickness has shown direct correlation to the lifetime and emission intensity.

Applications

Quantum dots are particularly significant for optical applications due to their high extinction co-efficient . In electronic applications they have been proven to operate like a single-electron transistor and show the Coulomb blockade effect. Quantum dots have also been suggested as implementations of qubits for quantum information processing.

The ability to tune the size of quantum dots is advantageous for many applications. For instance, larger quantum dots have a greater spectrum-shift towards red compared to smaller dots, and exhibit less pronounced quantum properties. Conversely, the smaller particles allow one to take advantage of more subtle quantum effects.

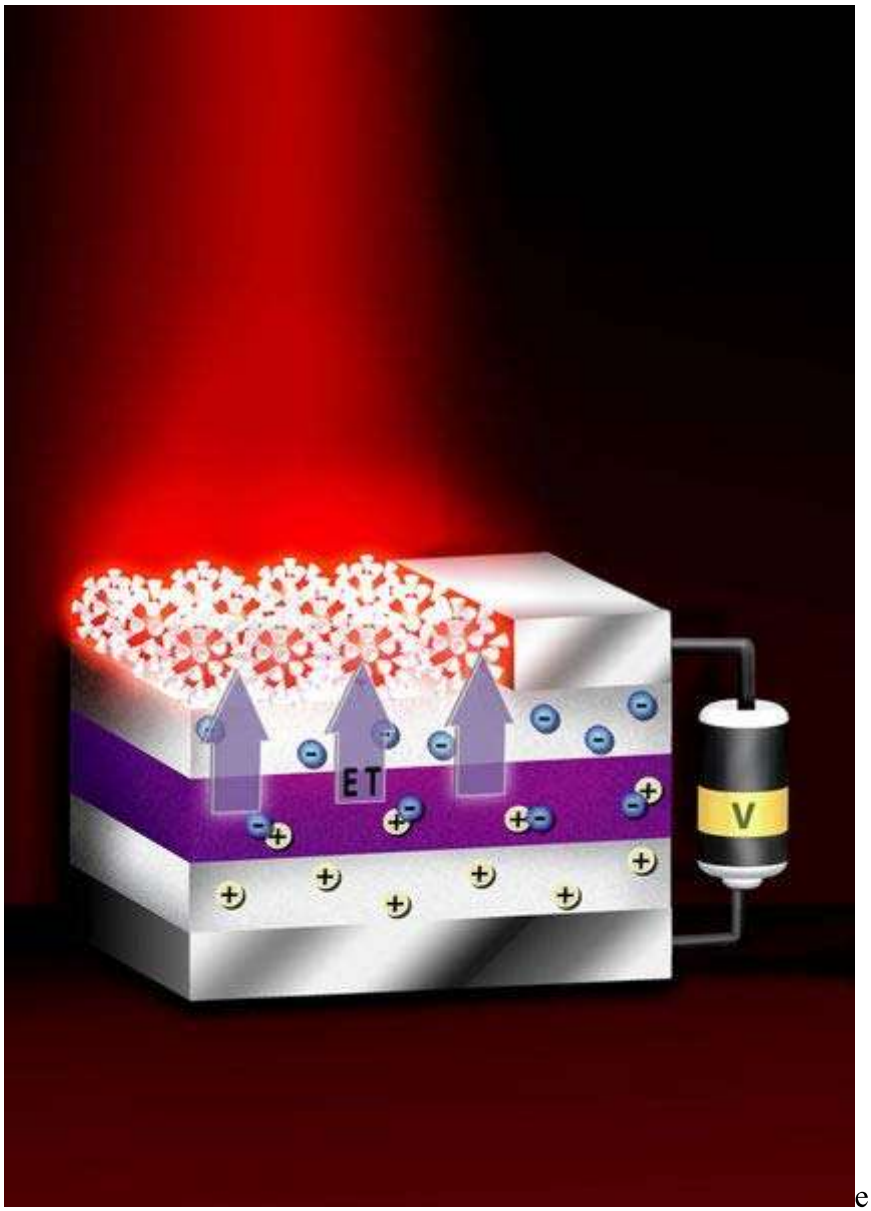

e

Researchers at Los Alamos National Laboratory have developed a wireless device that efficiently produces visible light, through energy transfer from thin layers of quantum wells to crystals above the layers.

Being zero dimensional, quantum dots have a sharper density of states than higher-dimensional structures. As a result, they have superior transport and optical properties, and are being researched for use in diode lasers, amplifiers, and biological sensors. Quantum dots may be excited within the locally enhanced electromagnetic field produced

by the gold nanoparticles, which can then be observed from the surface Plasmon resonance in the photoluminescent excitation spectrum of (CdSe)ZnS nanocrystals. High-quality quantum dots are well suited for optical encoding and multiplexing applications due to their broad excitation profiles and narrow/symmetric emission spectra. The new generations of quantum dots have far-reaching potential for the study of intracellular processes at the single-molecule level, high-resolution cellular imaging, long-term in vivo observation of cell trafficking, tumor targeting, and diagnostics.

Computing

Quantum dot technology is one of the most promising candidates for use in solid-state quantum computation. By applying small voltages to the leads, the flow of electrons through the quantum dot can be controlled and thereby precise measurements of the spin and other properties therein can be made. With several entangled quantum dots, or qubits, plus a way of performing operations, quantum calculations and the computers that would perform them might be possible.

Biology

In modern biological analysis, various kinds of organic dyes are used. However, with each passing year, more flexibility is being required of these dyes, and the traditional dyes are often unable to meet the expectations. To this end, quantum dots have quickly filled in the role, being found to be superior to traditional organic dyes on several counts, one of the most immediately obvious being brightness (owing to the high extinction co-efficient combined with a comparable quantum yield to fluorescent dyes) as well as their stability (allowing much less photobleaching). It has been estimated that quantum dots are 20 times brighter and 100 times more stable than traditional fluorescent reporters. For single-particle tracking, the irregular blinking of quantum dots is a minor drawback.

The usage of quantum dots for highly sensitive cellular imaging has seen major advances over the past decade. The improved photostability of quantum dots, for example, allows the acquisition of many consecutive focal-plane images that can be reconstructed into a high-resolution three-dimensional image. Another application that takes advantage of the extraordinary photostability of quantum dot probes is the real-time tracking of molecules and cells over extended periods of time. Antibodies, streptavidin, peptides, nucleic acid aptamers, or small-molecule ligands can be used to target quantum dots to specific proteins on cells. Researchers were able to observe quantum dots in lymph nodes of mice for more than 4 months.

Semiconductor quantum dots have also been employed for in vitro imaging of pre-labeled cells. The ability to image single-cell migration in real time is expected to be important to several research areas such as embryogenesis, cancer metastasis, stem-cell therapeutics, and lymphocyte immunology.

Scientists have proven that quantum dots are dramatically better than existing methods for delivering a gene-silencing tool, known as siRNA, into cells.

First attempts have been made to use quantum dots for tumor targeting under in vivo conditions. There exist two basic targeting schemes: active targeting and passive targeting. In the case of active targeting, quantum dots are functionalized with tumor-specific binding sites to selectively bind to tumor cells. Passive targeting utilizes the enhanced permeation and retention of tumor cells for the delivery of quantum dot probes. Fast-growing tumor cells typically have more permeable membranes than healthy cells, allowing the leakage of small nanoparticles into the cell body. Moreover, tumor cells lack an effective lymphatic drainage system, which leads to subsequent nanoparticle-accumulation.

One of the remaining issues with quantum dot probes is their potential in vivo toxicity. For example, CdSe nanocrystals are highly toxic to cultured cells under UV illumination. The energy of UV irradiation is close to that of the covalent chemical bond energy of CdSe nanocrystals. As a result, semiconductor particles can be dissolved, in a process known as photolysis, to release toxic cadmium ions into the culture medium. In the absence of UV irradiation, however, quantum dots with a stable polymer coating have been found to be essentially nontoxic. Then again, only little is known about the excretion process of quantum dots from living organisms. These and other questions must be carefully examined before quantum dot applications in tumor or vascular imaging can be approved for human clinical use.

Another potential cutting-edge application of quantum dots is being researched, with quantum dots acting as the inorganic fluorophore for intra-operative detection of tumors using fluorescence spectroscopy.

Photovoltaic devices

Quantum dots may be able to increase the efficiency and reduce the cost of today's typical silicon photovoltaic cells. According to an experimental proof from 2006 (controversial results), quantum dots of lead selenide can produce as many as seven excitons from one high energy photon of sunlight (7.8 times the bandgap energy). This compares favorably to today's photovoltaic cells which can only manage one exciton per high-energy photon, with high kinetic energy carriers losing their energy as heat. This would not result in a 7-fold increase in final output however, but could boost the maximum theoretical efficiency from 31% to 42%. Quantum dot photovoltaics would theoretically be cheaper to manufacture, as they can be made "using simple chemical reactions." The generation of more than one exciton by a single photon is called multiple exciton generation (MEG) or carrier multiplication.

Light emitting devices

There are several inquiries into using quantum dots as light-emitting diodes to make displays and other light sources, such as "QD-LED" displays, and "QD-WLED" (White LED). In June, 2006, QD Vision announced technical success in making a proof-of-concept quantum dot display and show a bright emission in the visible and near infra-red region of the spectrum. Quantum dots are valued for displays, because they emit light in

very specific gaussian distributions. This can result in a display that more accurately renders the colors that the human eye can perceive. Quantum dots also require very little power since they are not color filtered. Additionally, since the discovery of "white-light emitting" QD, general solid-state lighting applications appear closer than ever. A color liquid crystal display (LCD), for example, is usually powered by a single fluorescent lamp (or occasionally, conventional white LEDs) that is color filtered to produce red, green, and blue pixels. Displays that intrinsically produce monochromatic light can be more efficient, since more of the light produced reaches the eye.

WT

Chapter- 3

Nanostructure

A **nanostructure** is an object of intermediate size between molecular and microscopic (micrometer-sized) structures.

In describing nanostructures it is necessary to differentiate between the number of dimensions on the nanoscale. Nanotextured surfaces have **one dimension** on the nanoscale, i.e., only the thickness of the surface of an object is between 0.1 and 100 nm. Nanotubes have **two dimensions** on the nanoscale, i.e., the diameter of the tube is between 0.1 and 100 nm; its length could be much greater. Finally, spherical nanoparticles have **three dimensions** on the nanoscale, i.e., the particle is between 0.1 and 100 nm in each spatial dimension. The terms nanoparticles and ultrafine particles (UFP) often are used synonymously although UFP can reach into the micrometre range. The term 'nanostructure' is often used when referring to magnetic technology.

List of nanostructures

Gradient Multi-Layer nanofilm

Gradient Multi-Layer (GML)' nano-film is an assembly of Quantum Dot layers with a built-in gradient of nanoparticle size, composition or density.

Properties of such nanostructure are finding its applications in design of solar cells and energy storage devices .

The GML nano-structure can be embedded in the organic material (polymer), or can include Quantum Dots made of two or more types of material.

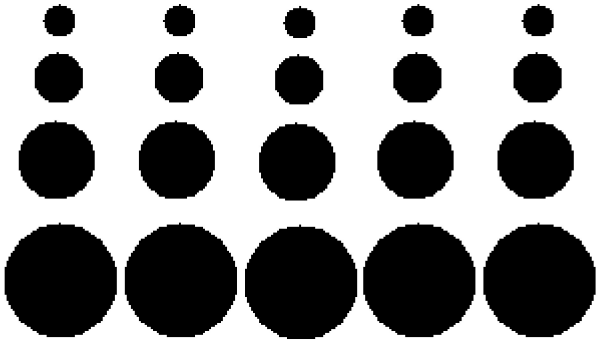

Schema of Gradient Multi-Layer (GML) nanofilm

Photovoltaic applications

The GML nanofilm only 100 nanometers thick can absorb the entire Sun spectrum (0.3-2.0+ eV). At the same time, gradient of the quantum dots size can create a gradient of the electro-chemical potential, acting as an equivalent of built-in electric field inside a nanofilm. This enhances transport of electrons and holes, and improves internal quantum efficiency (IQE) and photocurrent.

Manufacturing

The industrial manufacturing of GML nanofilms represents a challenge. Traditional methods of building nanostructured materials (like spin coating) can't form GML nanostructures, while more effective methods like Atomic Layer Deposition (ALD) or Langmuir-Blodget "microchemical" method. are expensive.

The cost-efficient alternative for manufacturing GML nano films is FP ("Flying Particles") method.

Nanocages

Inorganic Nanocages are hollow porous gold nanoparticles ranging in size from 10 to over 150 nm. They are created by reacting silver nanoparticles with chloroauric acid ($HAuCl_4$) in boiling water. While gold nanoparticles absorb light in the visible spectrum of light (at about 550 nm), gold nanocages absorb light in the near-infrared, where biological tissues absorb the least light. Because they are also biocompatible, gold nanocages are promising as a contrast agent for optical coherence tomography, which uses light scattering in a way analogous to ultrasound to produce in-vivo images of tissue with resolution approaching a few micrometres. A contrast agent is required if this technique will be able to image cancers at an early, more treatable stage. Gold nanocages also absorb light and heat up, killing surrounding cancer cells. The Xia group at Washington University, the original inventors of the nanocages, has functionalized nanocages with cancer-specific antibodies so they specifically attach to cancer cells.

Nanocomposite

A **nanocomposite** is as a multiphase solid material where one of the phases has one, two or three dimensions of less than 100 nanometers (nm), or structures having nano-scale repeat distances between the different phases that make up the material. In the broadest sense this definition can include porous media, colloids, gels and copolymers, but is more usually taken to mean the solid combination of a bulk matrix and nano-dimensional phase(s) differing in properties due to dissimilarities in structure and chemistry. The mechanical, electrical, thermal, optical, electrochemical, catalytic properties of the nanocomposite will differ markedly from that of the component materials. Size limits for these effects have been proposed , <5 nm for catalytic activity, <20 nm for making a hard magnetic material soft, <50 nm for refractive index changes, and <100 nm for achieving superparamagnetism, mechanical strengthening or restricting matrix dislocation movement.

Nanocomposites are found in nature, for example in the structure of the abalone shell and bone. The use of nanoparticle-rich materials long predates the understanding of the physical and chemical nature of these materials. Jose-Yacaman *et al.* investigated the origin of the depth of colour and the resistance to acids and bio-corrosion of Maya blue paint, attributing it to a nanoparticle mechanism. From the mid 1950s nanoscale organo-clays have been used to control flow of polymer solutions (e.g. as paint viscosifiers) or the constitution of gels (e.g. as a thickening substance in cosmetics, keeping the preparations in homogeneous form). By the 1970s polymer/clay composites were the topic of textbooks , although the term "nanocomposites" was not in common use.

In mechanical terms, nanocomposites differ from conventional composite materials due to the exceptionally high surface to volume ratio of the reinforcing phase and/or its exceptionally high aspect ratio. The reinforcing material can be made up of particles (e.g. minerals), sheets (e.g. exfoliated clay stacks) or fibres (e.g. carbon nanotubes or electrospun fibres). The area of the interface between the matrix and reinforcement phase(s) is typically an order of magnitude greater than for conventional composite materials. The matrix material properties are significantly affected in the vicinity of the reinforcement. Ajayan *et al.* note that with polymer nanocomposites, properties related to local chemistry, degree of thermoset cure, polymer chain mobility, polymer chain conformation, degree of polymer chain ordering or crystallinity can all vary significantly and continuously from the interface with the reinforcement into the bulk of the matrix.

This large amount of reinforcement surface area means that a relatively small amount of nanoscale reinforcement can have an observable effect on the macroscale properties of the composite. For example, adding carbon nanotubes improves the electrical and thermal conductivity. Other kinds of nanoparticulates may result in enhanced optical properties, dielectric properties, heat resistance or mechanical properties such as stiffness, strength and resistance to wear and damage. In general, the nano reinforcement is dispersed into the matrix during processing. The percentage by weight (called *mass fraction*) of the nanoparticulates introduced can remain very low (on the order of 0.5% to 5%) due to the low filler percolation threshold, especially for the most commonly used non-spherical,

high aspect ratio fillers (e.g. nanometer-thin platelets, such as clays, or nanometer-diameter cylinders, such as carbon nanotubes).

Ceramic-matrix nanocomposites

In this group of composites the main part of the volume is occupied by a ceramic, i.e. a chemical compound from the group of oxides, nitrides, borides, silicides etc.. In most cases, ceramic-matrix nanocomposites encompass a metal as the second component. Ideally both components, the metallic one and the ceramic one, are finely dispersed in each other in order to elicit the particular nanoscopic properties. Nanocomposite from these combinations were demonstrated in improving their optical, electrical and magnetic properties as well as tribological, corrosion-resistance and other protective properties .

The binary phase diagram of the mixture should be considered in designing ceramic-metal nanocomposites and measures have to be taken to avoid a chemical reaction between both components. The last point mainly is of importance for the metallic component that may easily react with the ceramic and thereby loose its metallic character. This is not an easily obeyed constraint, because the preparation of the ceramic component generally requires high process temperatures. The most safe measure thus is to carefully choose immiscible metal and ceramic phases. A good example for such a combination is represented by the ceramic-metal composite of TiO_2 and Cu, the mixtures of which were found immiscible over large areas in the Gibbs' triangle of Cu-O-Ti .

The concept of ceramic-matrix nanocomposites was also applied to thin films that are solid layers of a few nm to some tens of µm thickness deposited upon an underlying substrate and that play an important role in the functionalization of technical surfaces. Gas flow sputtering by the hollow cathode technique turned out as a rather effective technique for the preparation of nanocomposite layers. The process operates as a vacuum-based deposition technique and is associated with high deposition rates up to some µm/s and the growth of nanoparticles in the gas phase. Nanocomposite layers in the ceramics range of composition were prepared from TiO_2 and Cu by the hollow cathode technique that showed a high mechanical hardness, small coefficients of friction and a high resistance to corrosion.

Metal-matrix nanocomposites

Another kind of nanocomposite is the energetic nanocomposite, generally as a hybrid sol–gel with a silica base, which, when combined with metal oxides and nano-scale aluminium powder, can form *superthermite* materials.

Polymer-matrix nanocomposites

Definitions: In the simplest case, appropriately adding nanoparticulates to a polymer matrix can enhance its performance, often in very dramatic degree, by simply capitalizing on the nature and properties of the nanoscale filler (these materials are better described

by the term ***nanofilled polymer composites***). This strategy is particularly effective in yielding high performance composites, when good dispersion of the filler is achieved and the properties of the nanoscale filler are substantially different or better than those of the matrix, for example, reinforcing a polymer matrix by much stiffer nanoparticles of ceramics, clays, or carbon nanotubes. Alternatively, the enhanced properties of high performance nanocomposites may be mainly due to the high aspect ratio and/or the high surface area of the fillers, since nanoparticulates have extremely high surface area to volume ratios when good dispersion is achieved.

Nanoscale dispersion of filler or controlled nanostructures in the composite can introduce new physical properties and novel behaviours that are absent in the unfilled matrices, effectively changing the nature of the original matrix (such composite materials can be better described by the term ***genuine nanocomposites*** or ***hybrids***). Some examples of such new properties are fire resistance or flame retardancy and accelerated biodegradability.

Nanofabrics

Nanofabrics is an emerging nanotechnology that deals with building specialized fabrics. Active Camouflage is a costume that hides the wearer by redirecting light from one side to the other.

WT

Nanofiber

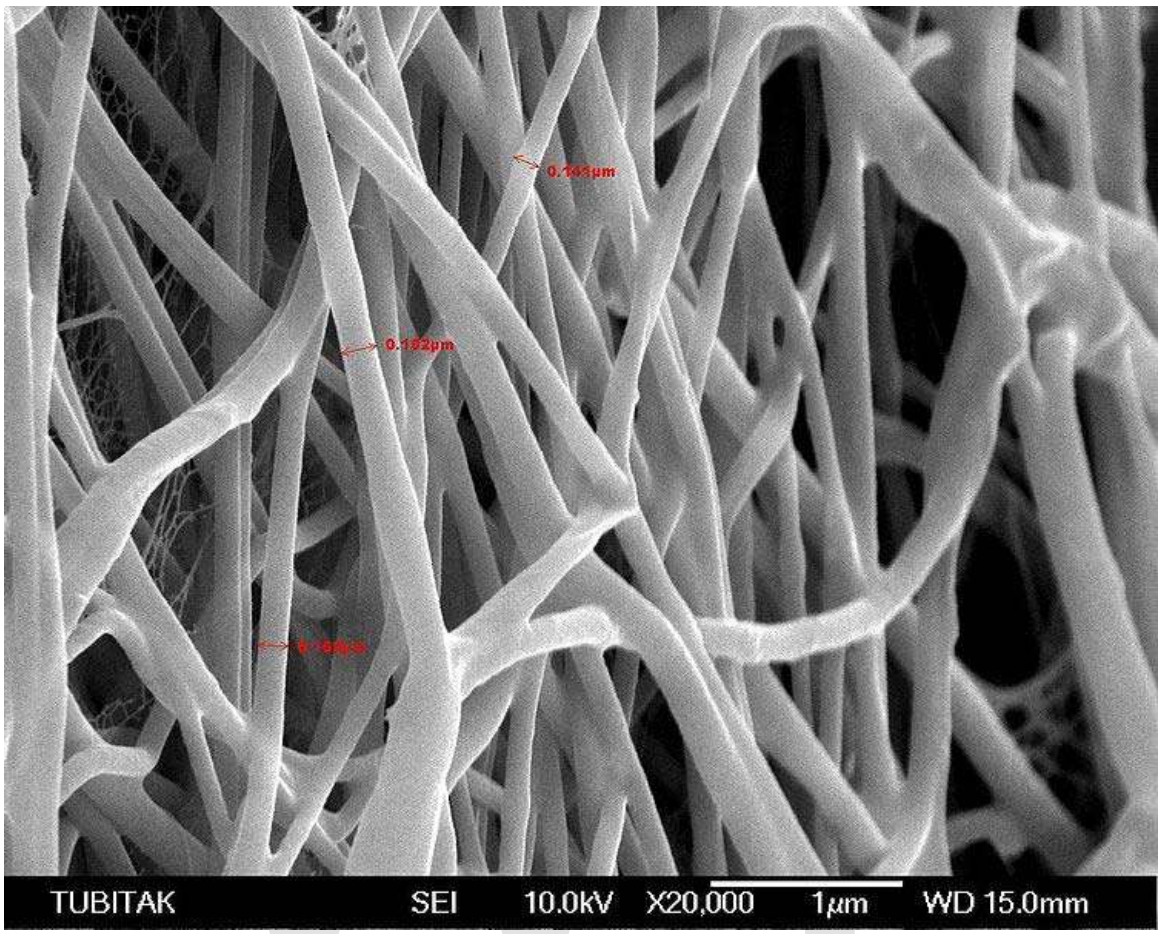

SEM image of nanofibers by Nano FMG.

Nanofibers are defined as fibers with diameters less than 1000 nm nanometers. They can be produced by interfacial polymerization and electrospinning. Carbon nanofibers are graphitized fibers produced by catalytic synthesis.

Synthesis

Inorganic nanofibers (sometimes called ceramic nanofibers) can be prepared from various kinds of inorganic substances by electrospinning technique. The most frequently mentioned ceramic materials with nanofiber morphology are titanium dioxide (TiO_2), silicon dioxide (SiO_2), zirconium dioxide (ZrO_2), aluminum oxide (Al_2O_3), lithium titanate ($Li_4Ti_5O_{12}$), titanium nitride (TiN) or platinum (Pt). The synthesis usually consists of two main steps. In the first step, the polymer (organic) nanofibers are created by conventional electrospinning technique. As prepared, polymer nanofibers made of inorganic salts or organometallic compounds are subsequently transformed to ceramics by heat treatment.

Potential applications

- Medical: Artificial organ components, Tissue engineering, Implant material, Drug delivery, Wound dressing, Medical textile materials.
- Protective materials: Sound absorption materials, Protective clothings against chemical and biological warfare agents, Sensor applications for detecting chemical agents.
- Textile: Sport Apparels, Sport Shoes, Climbing, Rainwear, Outerwear Garments, Baby Diapers.
- Filtration: HVAC system filters, HEPA, ULPA High efficient filters, Air, oil, fuel filters for automotive, Filters for beverage, pharmacy, medical applications.
- In one study, combined neural stem cells with carbon nanofibers triggered neural tissue regeneration in the brains of rats that had suffered a simulated stroke. On their own, neither nanofibers nor stem cells could heal the rats.
- Napkins with nanofibers contain antibodies against numerous biohazards and chemicals that signal by changing color (potentially useful in identifying bacteria in kitchens).
- In wound healing nanofibers assemble at the injury site and stay put, drawing the body's own growth factors to the injury site.
- Donaldson develops nanofiber filter media for new air and liquid filtration applications, such as vacuum cleaners.
- Dye-sensitized solar cell
- Pigments for cosmetics
- Energy: Li-ion batteries, Photovoltaic cells, Membrane Fuel Cells.
- Carrier materials for various catalysts
- Photocatalytic air/water purification
- Micropower to operate personal electronic devices via piezoelectric nanofibers woven into clothing.

Self-twisting

Nanofibers that self-braid have been studied at Harvard University. The effect is related to a balance between flexibility, adhesion, and evaporation of solvent. Potential applications include:

- Substances that can change optical properties on demand
- Molecule capture and release for e.g. timed drug delivery
- Energy storage
- Adhesives

Nanoflower

A **nanoflower**, in chemistry, refers to a compound of certain elements that results in formations which in microscopic view resemble flowers or, in some cases, trees that are

called nanobouquets or nanotrees. These formations are nanometers long and thick so they can only be observed using electron microscopy.

Production

Several ways to produce nanoflowers are known:

- A process similar to the making of a carbon nanotube using a hydrocarbon gas.
- Heating gallium (Ga) and then flowing methane (CH_4) over, under specific pressure and heat. This forms flower-shaped silicon carbide (SiC) structures.
- Heating a molybdenum dioxide (MoO_2) thin film on a piece of molybdenum foil surrounded by sulfur vapour.

Nanomeadow

In supercapacitors, energy is stored because the electrodes are coated with a porous material that soaks up ions like a sponge, usually activated carbon. Nanomeadow supercapacitors store ions in manganese oxide (MnO), a material with a much greater capacity for ions than activated carbon.

Scientists at Research Institute of Chemical Defence (Beijing, China) and Peking University created a nanomeadow of microscopic structures, fuzzy flowers of MnO each about 100 nanometres across on a field of messy carbon nanotube grass grown on a tantalum metal foil. Nanomeadows perform 10 times better than MnO alone and can store twice as much charge as the carbon-based electrodes in existing ultracapacitors.

Nanomesh

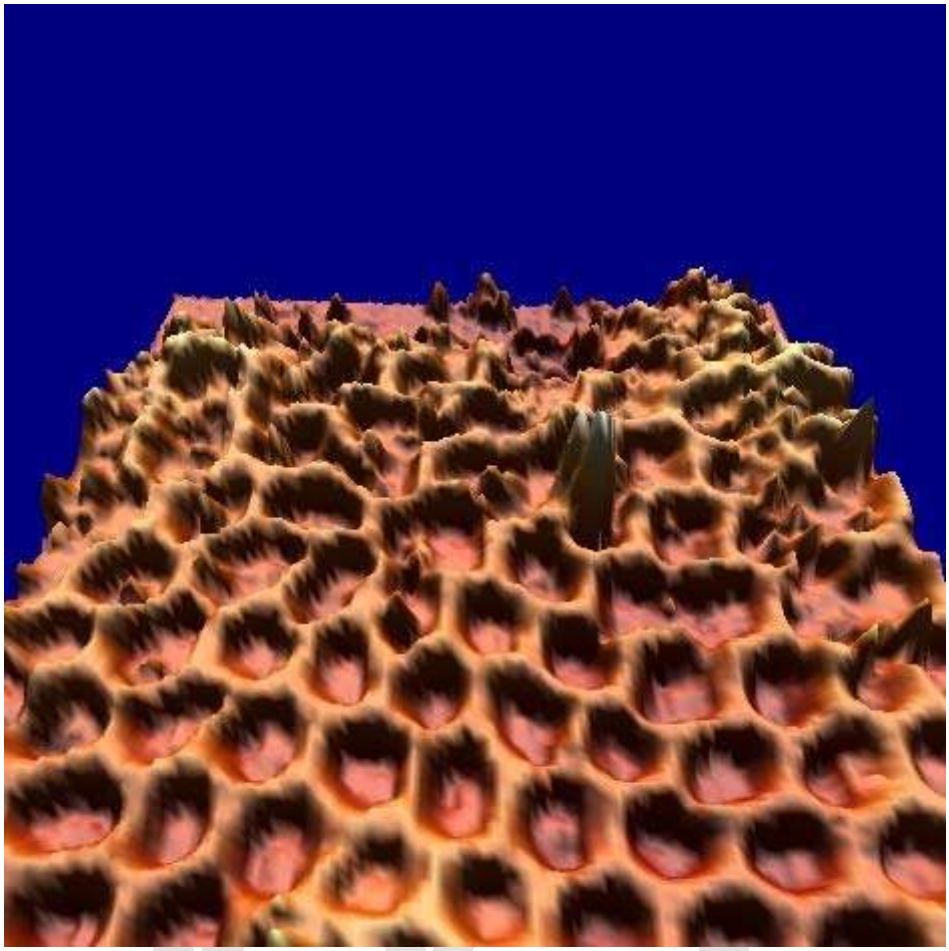

Perspective view of nanomesh, whose structure ends at the back of the figure. The distance between two pore centers is 3.2nm, and the pores are 0.05nm deep.

The **nanomesh** is a new inorganic nanostructured two-dimensional material, similar to graphene. It was discovered in 2003 at the University of Zurich, Switzerland .

It consists of a single layer of boron (B) and nitrogen (N) atoms, which forms by self-assembly a highly regular mesh after high-temperature exposure of a clean rhodium or ruthenium surface to borazine under ultra-high vacuum.

The nanomesh looks like an assembly of hexagonal pores at the nanometer (nm) scale. The distance between 2 pore centers is only of 3.2 nm, whereas each pore has a diameter of about 2 nm and is 0.05 nm deep. The lowest regions bind strongly to the underlying metal, while the wires (highest regions) are only bound to the surface through strong cohesive forces within the layer itself.

The boron nitride nanomesh is not only stable under vacuum , air and some liquids , but also up to temperatures of 796^{o}C (1070 K) . In addition it shows the extraordinary ability to trap molecules and metallic clusters , which have similar sizes to the nanomesh pores, forming a well-ordered array. These characteristics promise interesting applications of

the nanomesh in areas like nanocatalysis, surface functionalisation, spintronics, quantum computing and data storage media like hard drives.

Structure

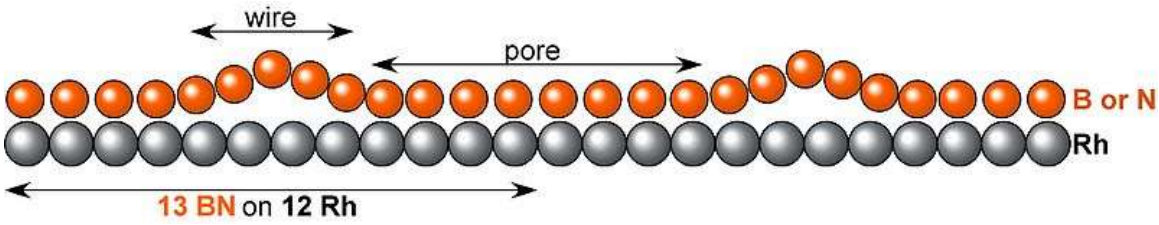

Cross-section of nanomesh on rhodium showing pore and wire regions.

h-BN nanomesh is a single sheet of hexagonal boron nitride, which forms on substrates like rhodium Rh(111) or ruthenium Ru(0001) crystals by a self-assembly process.

The unit cell of the h-BN nanomesh consists of 13x13 BN or 12x12 Rh atoms with a lattice constant of 3.2 nm. In a cross-section it means that 13 boron or nitrogen atoms are sitting on 12 rhodium atoms. This implies a modification of the relative positions of each BN towards the substrate atoms within a unit cell, where some bonds are more attractive or repulsive than other (site selective bonding), what induces the corrugation of the nanomesh.

The nanomesh corrugation amplitude of 0.05 nm causes a strong effect on the electronic structure, where two distinct BN regions are observed. They are easily recognized in the lower right image, which is a scanning tunneling microscopy (STM) measurement, as well as in the lower left image representing a theoretical calculation of the same area. A strongly bounded region assigned to the pores is visible in blue in the left image below (center of bright rings in the right image) and a weakly bound region assigned to the wires appears yellow-red in the left image below (area in-between rings in the right image).

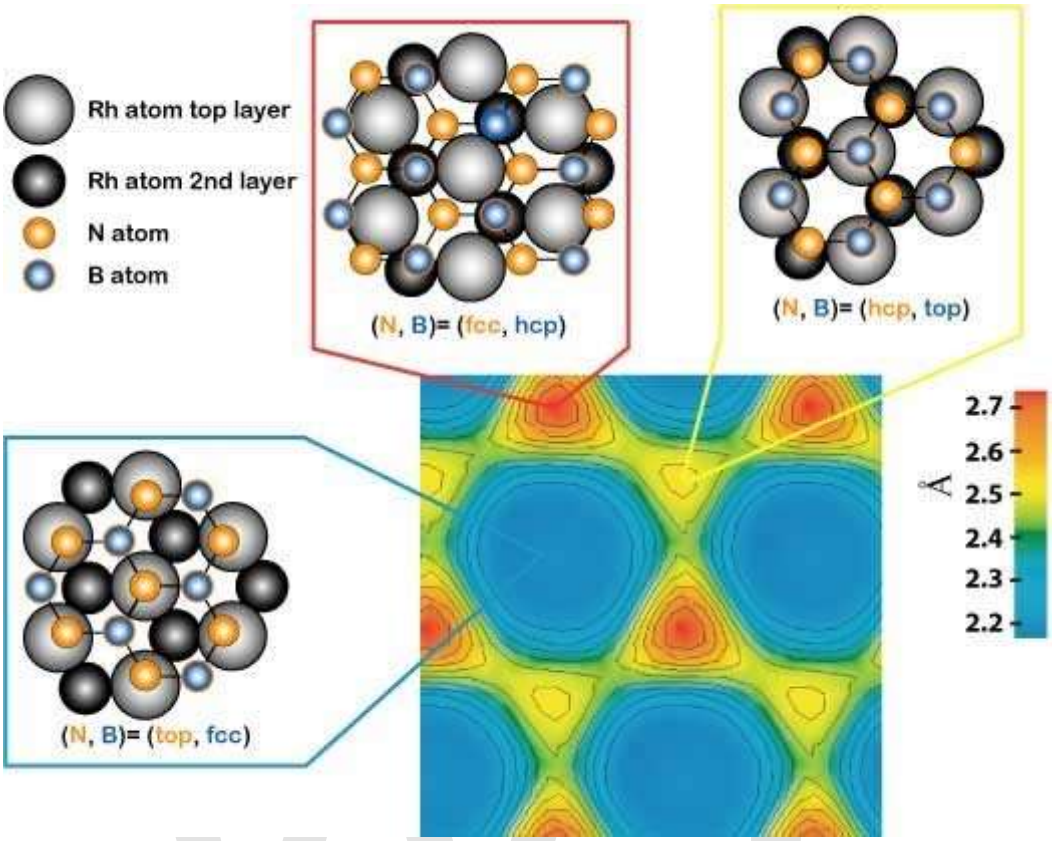

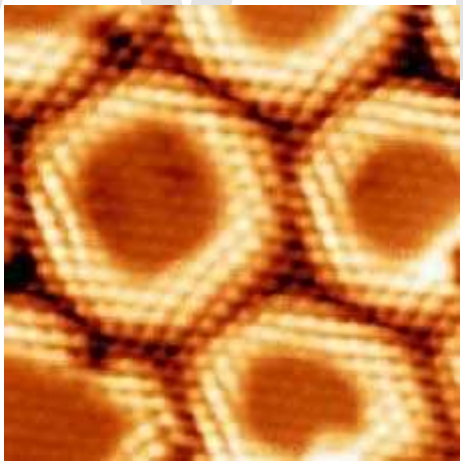

The right image shows the boron nitride nanomesh measured by STM at 77K, where each "ball" represents one N atom. The center of each ring corresponds to the center of the pores.

The left image is the theoretical calculation of the same area, where the N height relative to the underlying substrate is given. The exact arrangement of Rh, N and B atoms is given for three different areas (blue: pores, yellow-red: wires).

Properties

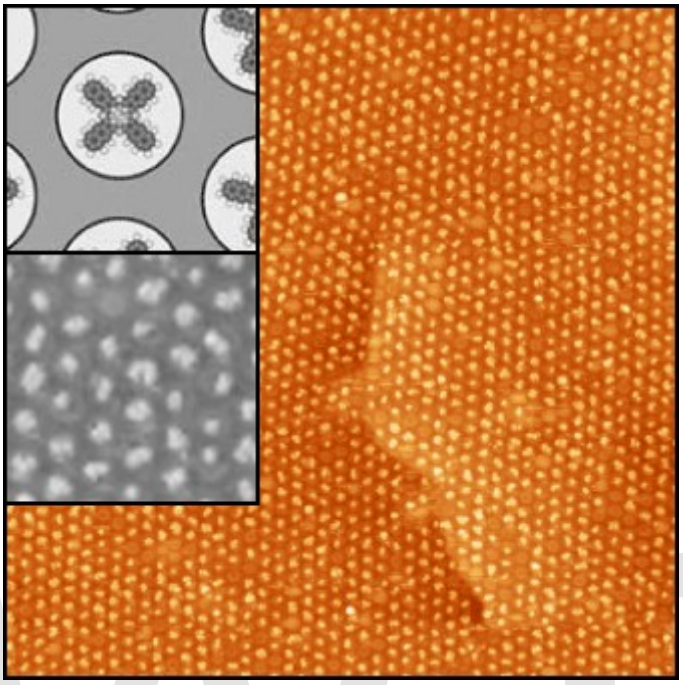

Naphthalocyanine molecules evaporated onto the nanomesh. They only adsorb in pores, forming a well-defined pattern.

The nanomesh is stable under a wide range of environments like air, water and electrolytes among others. It is also temperature resistant since it doesn't decompose up to 1275K under vacuum. In addition to these exceptional stabilities, the nanomesh shows the extraordinary ability to act as a scaffold for metallic nanoclusters and to trap molecules forming a well-ordered array.

In the case of gold (Au), its evaporation on the nanomesh leads to formation of well-defined round Au nanoparticles, which are centered at the nanomesh pores.

The STM figure on the right shows Naphthalocyanine (Nc) molecules, which were vapor-deposited onto the nanomesh. These planar molecules have a diameter of about 2 nm, whose size is comparable to that of the nanomesh pores. It is spectacularly visible how the molecules form a well-ordered array with the periodicity of the nanomesh (3.22 nm). The lower inset shows a region of this substrate with higher resolution, where individual molecules are trapped inside the pores. In addition, the molecules seem to keep their native conformation, what means that their functionality is kept, which is nowadays a challenge in nanoscience.

Such systems with wide spacing between individual molecules/clusters and negligible intermolecular interactions might be interesting for applications such as molecular electronics and memory elements, in photochemistry or in optical devices.

Preparation and analysis

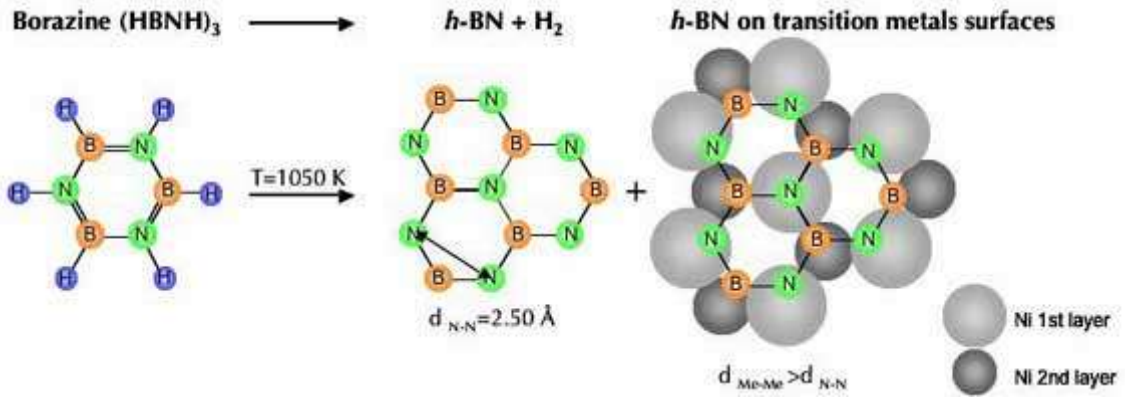

Decomposition of borazine on transition metal surfaces.

Well-ordered nanomeshes are grown by thermal decomposition of borazine $(HBNH)_3$, a colorless substance that is liquid at room temperature. The nanomesh results after exposing the atomically clean Rh(111) or Ru(0001) surface to borazine by chemical vapor deposition (CVD).

The substrate is kept at a temperature of 796°C (1070 K) when borazine is introduced in the vacuum chamber at a dose of about 40 L (1 Langmuir = 10^{-6} torr sec). A typical borazine vapor pressure inside the ultrahigh vacuum chamber during the exposure is $3x10^{-7}$ mbar.

After cooling down to room temperature, the regular mesh structure is observed using different experimental techniques. Scanning tunneling microscopy (STM) gives a direct look on the local real space structure of the nanomesh, while low energy electron diffraction (LEED) gives information about the surface structures ordered over the whole sample. Ultraviolet photoelectron spectroscopy (UPS) gives information about the electronic states in the outermost atomic layers of a sample, i.e. electronic information of the top substrate layers and the nanomesh.

Other forms

CVD of borazine on other substrates didn't led so far to the formation of a corrugated nanomesh. A flat BN layer is observed on nickel and palladium , whereas stripped structures appear on molybdenum instead.

Nanorod

In nanotechnology, **nanorods** are one morphology of nanoscale objects. Each of their dimensions range from 1–100 nm. They may be synthesized from metals or semiconducting materials. Standard aspect ratios (length divided by width) are 3-5.

Nanorods are produced by direct chemical synthesis. A combination of ligands act as shape control agents and bond to different facets of the nanorod with different strengths. This allows different faces of the nanorod to grow at different rates, producing an elongated object.

The applications of nanorods are diverse, ranging from display technologies (the reflectivity of the rods can be changed by changing their orientation with an applied electric field) to microelectromechanical systems (MEMS).

Nanorods based on semiconducting materials have also been investigated for application as energy harvesting and light emitting devices. In 2006, Ramanathan et. al. demonstrated[1] electric-field mediated tunable photoluminescence from ZnO nanorods, with potential for application as novel sources of near-ultraviolet radiation.

Quantum heterostructure

Quantum heterostructure is a heterostructure in a substrate (usually a semiconductor material), where size restricts the movements of the charge carriers forcing them into a quantum confinement. This leads to the formation of a set of discrete energy levels at which the carriers can exist. Quantum heterostructures have sharper density of states than structures of more conventional sizes.

Quantum heterostructures are important for fabrication of short-wavelength light-emitting diodes and diode lasers, and for other optoelectronic applications, eg. high-efficiency photovoltaic cells.

WT

Chapter- 4

Silver, Iron and Platinum Nanoparticles

Silver nanoparticles

Silver nanoparticles are nanoparticles of silver, i.e. silver particles of between 1 nm and 100 nm in size. While frequently described as being 'silver' some are composed of a large percentage of silver oxide due to their large ratio of surface to bulk silver atoms.

Synthesis

There are many different synthetic routes to silver nanoparticles. They can be divided into three broad categories: physical vapor deposition, ion implantation, or wet chemistry.

Ion implantation

Although it may seem counter-intuitive, ion implantation has been used to create silver nanoparticles. This process has been shown to produce silver particles embedded in polyurethane, silicone, polyethylene, and polymethylmethacrylate. The particles grow in the substrate with the bombardment of ions. The existence of nanoparticles is proven with optical absorbance, though the exact nature of the particles created with this method is not known.

Wet chemistry

There are several wet chemical methods for creating silver nanoparticles. Typically, they involve the reduction of a silver salt such as silver nitrate with a reducing agent like sodium borohydride in the presence of a colloidal stabilizer. Sodium borohydride has been used with polyvinyl alcohol, poly(vinylpyrrolidone), bovine serum albumin (BSA), citrate and cellulose as stabilizing agents. In the case of BSA, the sulfur-, oxygen- and nitrogen-bearing groups mitigate the high surface energy of the nanoparticles during the reduction. The hydroxyl groups on the cellulose are reported to help stabilize the particles. Polydopamine coated magnetic-bacterial cellulose contains multifunctional groups, which acts as a reducing agent for in situ preparation of reusable antibacterial Ag-nanocomposites Article . Citrate and cellulose have been used to create silver nanoparticles independent of a reducing agent as well. An additional novel wet chemistry

method used to create silver nanoparticles took advantage of ß-D-glucose as a reducing sugar and a starch as the stabilizer.

Also, it is important to note, not all nanoparticles are created equal. The size and shape have been shown to have an impact on its efficacy. Additionally, crystal facet size, oxide content and several other factors could also affect the antimicrobial properties.

Uses

Over the last decades silver nanoparticles have found applications in catalysis, optics, electronics and other areas due to their unique size-dependent optical, electrical and magnetic properties. Currently most of the applications of silver nanoparticles are in antibacterial/antifungal agents in biotechnology and bioengineering, textile engineering, water treatment, and silver-based consumer products.

There is also an effort to incorporate silver nanoparticles into a wide range of medical devices, including but not limited to

- bone cement,
- surgical instruments,
- surgical masks,
- wound dressings.

Samsung has created and marketed a material called Silver Nano, that includes silver nanoparticles on the surfaces of household appliances.

Silver nanoparticles have been used as the cathode in a silver-oxide battery.

Health concerns

Ionic silver has a long history of use in topical medical applications, and it has been shown that ionic silver, in the right quantities, is suitable in treating wounds. The US Food and Drug Administration has approved the use of a range of different silver-impregnated wound dressings. Silver nanoparticles are now replacing silver sulfadiazine as an effective agent in the treatment of wounds.

- Allergic reaction: While there is anecdotal evidence suggesting the possibility of a silver allergy, an extensive review of the medical literature does not lend any credence to this possibility. Some silver alloys that include nickel do elicit an allergic reaction.

- Argyria and staining: Ingested silver or silver compounds, including colloidal silver, can cause a condition called argyria, a discoloration of the skin and organs.In 2006, there was a case study of a 17-year-old man, who sustained burns to 30% of his body, and experienced a temporary bluish-grey hue after several

days of treatment with Acticoat, a brand of wound dressing containg silver nanoparticles. Argyria is the deposition of silver in deep tissues, a condition that cannot happen on a temporary basis, raising the question of whether the cause of the man's discoloration was argyria or even a result of the silver treatment. . Silver dressings are known to cause a "transient discoloration" that dissipates in 2–14 days, but not a permanent discoloration.

- Silzone heart valve: St. Jude Medical released a mechanical heart valve with a silver coated sewing cuff (coated using ion beam-assisted deposition) in 1997. The valve was designed to reduce the instances of endocarditis. The valve was approved for sale in Canada, Europe, the United States, and most other markets around the world. In a post-commercialization study, researchers showed that the valve prevented tissue ingrowth, created paravalvular leakage, valve loosening, and in the worst cases explantation. After 3 years on the market and 36,000 implants, St. Jude discontinued and voluntarily recalled the valve.

Nanoscale iron particles

Nanoscale iron particles are sub-micrometer particles of iron metal. They are highly reactive because of their large surface area. In the presence of oxygen and water, they rapidly oxidize to form free iron ions. They are widely used in medical and laboratory applications and have also been studied for remediation of industrial sites contaminated with chlorinated organic compounds.

Chemistry

Synthesis

Reactivity

When exposed to oxygen and water, iron oxidizes. This redox process can occur under either acidic or neutral/basic conditions:

$$2\ Fe^0(s) + 4\ H^+(aq) + O_2(aq) \rightarrow 2\ Fe^{2+}(aq) + 2\ H_2O(l)$$
$$Fe^0(s) + 2\ H_2O\ (aq) \rightarrow Fe^{2+}(aq) + H_2(g) + 2\ OH^-(aq)$$

Research

Research has shown that nanoscale iron particles can be effectively used to treat several forms of ground contamination, including grounds contaminated by polychlorinated biphenyls (PCBs), chlorinated organic solvents, and organochlorine pesticides. Nanoscale

iron particle are easily transportable through ground water, allowing for in situ treatment. Additionally, the nanoparticle-water slurry can be injected into the contaminated area and stay there for long periods of time . These factors combine to make this method of cheaper than most currently used alternative.

Researchers have found that although metallic iron nanoparticles remediate contaminants well, they tend to agglomerate on the soil surfaces. In response, carbon nanoparticles and water-soluble polyelectrolytes have been used as supports to the metallic iron nanoparticles. The hydrophobic contaminants adsorb to these supports, improving permeability in sand and soil.

In field tests have generally confirmed lab findings. However, research is still ongoing and nanoscale iron particles are not yet commonly used for treating ground contamination.

Platinum nanoparticles

Platinum nanoparticles are usually in the form of a suspension or colloid of sub-micrometre-sized particles of platinum in a fluid, usually water. A colloid is technically defined as particles which remain suspended without forming an ionic, or dissolved solution. The broader commercial definition of "colloidal platinum" includes products that contain various concentrations of ionic platinum, platinum colloids, ionic platinum compounds or platinum nanoparticles in purified water.

The platinum nanoparticle sizes range between 2-3 nanometres (nm). Trillions of platinum nanoparticles are suspended in the brownish red or black colored colloidal solution. Nanoparticles come in wide variety of shapes including spheres, rods, cubes, and caps.

Due to the antioxidant properties of the platinum nanoparticles, they are the subject of substantial research with applications in a wide variety of areas, including nanotechnology, medicine and the synthesis of novel materials with unique properties.

Synthesis

Platinum nanoparticles are fabricated by reduction of hexachloroplatinate. After dissolving hexachloroplatinate, the solution is rapidly stirred while a reducing agent is added. This causes platinum ions to be reduced to neutral platinum atoms. As more and more of these platinum atoms form, the solution becomes supersaturated and platinum gradually starts to precipitate in the form of sub-nanometre particles. The rest of the platinum atoms that form stick to the existing particles, and, if the solution is stirred vigorously enough, the particles will be fairly uniform in size. Various procedures employed to attain platinum nanoparticles include heating, reflux, cooling, stirring,

filtration and filling, examinations & tests and packaging. To prevent the particles from aggregating, some sort of stabilizing agent or stabilizer that sticks to the nanoparticle surface is usually added. They can be functionalized with various organic ligands to create organic-inorganic hybrids with advanced functionality.

Biological effects

Research by Yusei Miyamoto at University of Tokyo, Japan, resulted in the use of platinum nanoparticles of the size 2-3 nm to increase the lifespan of the roundworm *Caenorhabditis elegans*.

Nanoparticles may present possible safety issues both medically and environmentally. Most of these issues usually arise due to the high surface to volume ratio, which can make the particles of some metals very reactive or catalytic. In particular, inhaled nanoparticles can pose health risks, and may cause inflammation and disease in the lung. They are able to pass through cell membranes in organisms and their interactions with biological systems are relatively unknown. However, free nanoparticles in the environment quickly tend to agglomerate and thus leave the nano-regime, and nature itself presents many nanoparticles to which organisms on earth may have evolved immunity (such as salt particulates from ocean aerosols, terpenes from plants, or dust from volcanic eruptions).

WT

Chapter- 5

Electron microscope

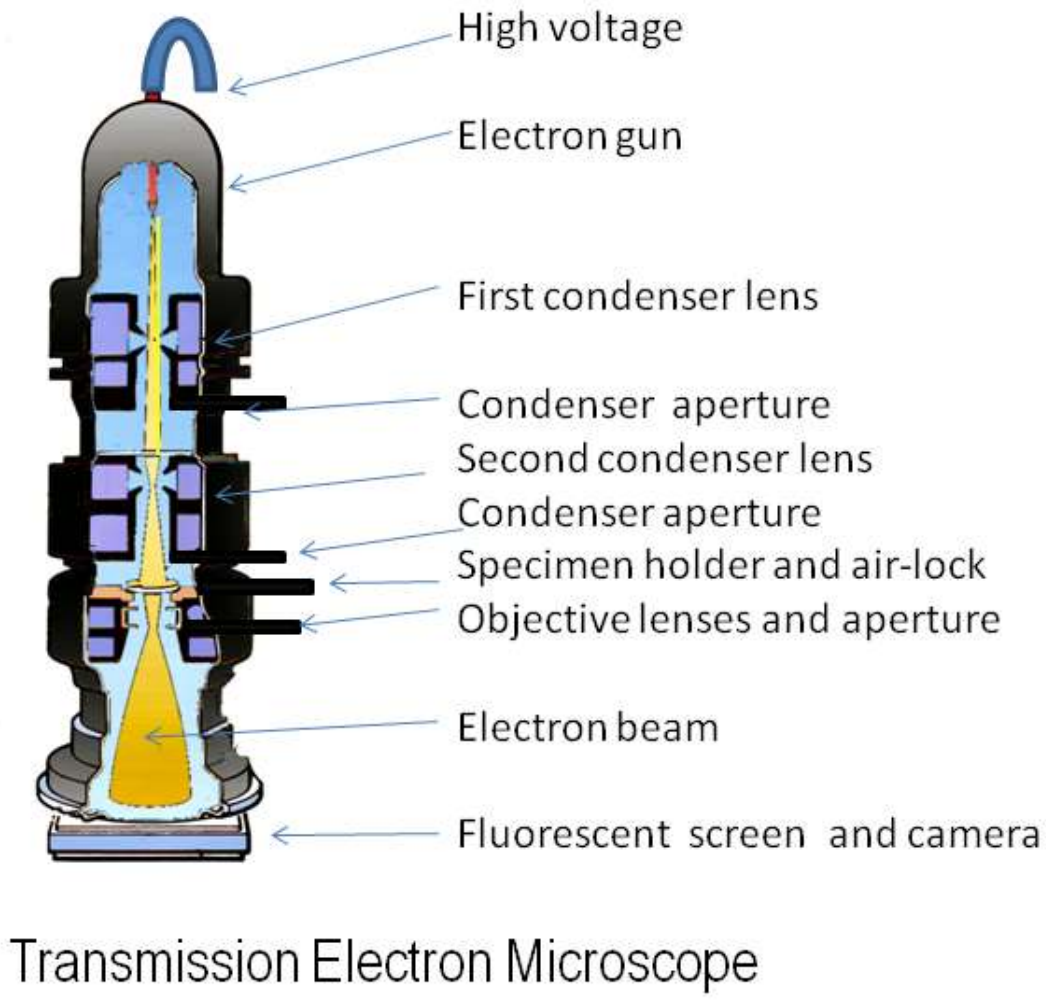

Diagram of a transmission electron microscope

A 1973 Siemens electron microscope, Musée des Arts et Métiers, Paris

An **electron microscope** is a type of microscope that produces an electronically-magnified image of a specimen for detailed observation. The electron microscope (EM) uses a particle beam of electrons to illuminate the specimen and create a magnified image of it. The microscope has a greater resolving power than a light-powered optical microscope, because it uses electrons that have wavelengths about 100,000 times shorter than visible light (photons), and can achieve magnifications of up to 2,000,000x, whereas ordinary, non-confocal light microscopes are limited to 2000x magnification.

The electron microscope uses electrostatic and electromagnetic "lenses" to control the electron beam and focus it to form an image. These lenses are analogous to, but different from the glass lenses of an optical microscope that form a magnified image by focusing

light on or through the specimen. In transmission, the electron beam is first diffracted by the specimen, and then, the electron microscope “lenses" re-focus the beam into a Fourier-transformed image of the diffraction pattern for the selected area of investigation. The real image thus formed is a highly `magnified' image by a factor of several million, and can be then recorded on a special photographic plate, or viewed on a detecting screen. Electron microscopes are used to observe a wide range of biological and inorganic specimens including microorganisms, cells, large molecules, biopsy samples, metals, and crystals. Industrially, the electron microscope is primarily used for quality control and failure analysis in semiconductor device fabrication.

An electron microscope's advantages over X-ray crystallography are that the specimen need not be a single crystal or even a polycrystalline powder, and also that the Fourier transform reconstruction of the object's magnified structure occurs physically and thus avoids the need for solving the phase problem faced by the X-ray crystalographers after obatining their X-ray diffraction patterns of a single crystal or polycrystalline powder. The transmission electron microscope's major `disadvantage' is the need for extremely thin sections of the specimens, typically less than 10 nanometers. For biological specimens it also requires biological sample special `staining' with heavy atom labels in order to achieve the required contrast, and then chemical fixation as well as encasing with a polymer resin to stabilize the biological specimen which is thin sectioned.

History

Electron microscope constructed by Ernst Ruska in 1933

In 1931, the German physicist Ernst Ruska and German electrical engineer Max Knoll constructed the prototype electron microscope, capable of four-hundred-power magnification; the apparatus was a practical application of the principles of electron microscopy. Two years later, in 1933, Ruska built an electron microscope that exceeded the resolution attainable with an optical (lens) microscope. Moreover, Reinhold Rudenberg, the scientific director of Siemens-Schuckertwerke, obtained the patent for the electron microscope in May 1931. Family illness compelled the electrical engineer to devise an electrostatic microscope, because he wanted to make visible the poliomyelitis virus.

In 1937, the Siemens company financed the development work of Ernst Ruska and Bodo von Borries, and employed Helmut Ruska (Ernst's brother) to develop applications for the microscope, especially with biologic specimens. Also in 1937, Manfred von Ardenne pioneered the scanning electron microscope. The first *practical* electron microscope was constructed in 1938, at the University of Toronto, by Eli Franklin Burton and students Cecil Hall, James Hillier, and Albert Prebus; and Siemens produced the first *commercial* Transmission Electron Microscope (TEM) in 1939. Although contemporary electron microscopes are capable of two million-power magnification, as scientific instruments, they remain based upon Ruska's prototype.

Types

Transmission electron microscope (TEM)

The original form of electron microscope, the transmission electron microscope (TEM) uses a high voltage electron beam to create an image. The electrons are emitted by an electron gun, commonly fitted with a tungsten filament cathode as the electron source. The electron beam is accelerated by an anode typically at +100 keV (40 to 400 keV) with respect to the cathode, focused by electrostatic and electromagnetic lenses, and transmitted through the specimen that is in part transparent to electrons and in part scatters them out of the beam. When it emerges from the specimen, the electron beam carries information about the structure of the specimen that is magnified by the objective lens system of the microscope. The spatial variation in this information (the "image") is viewed by projecting the magnified electron image onto a fluorescent viewing screen coated with a phosphor or scintillator material such as zinc sulfide. The image can be photographically recorded by exposing a photographic film or plate directly to the electron beam, or a high-resolution phosphor may be coupled by means of a lens optical system or a fibre optic light-guide to the sensor of a CCD (charge-coupled device) camera. The image detected by the CCD may be displayed on a monitor or computer.

Resolution of the TEM is limited primarily by spherical aberration, but a new generation of aberration correctors have been able to partially overcome spherical aberration to increase resolution. Hardware correction of spherical aberration for the High Resolution TEM (HRTEM) has allowed the production of images with resolution below 0.5 Ångström (50 picometres) at magnifications above 50 million times. The ability to determine the positions of atoms within materials has made the HRTEM an important tool for nano-technologies research and development.

Scanning electron microscope (SEM)

An image of an ant in a scanning electron microscope

Unlike the TEM, where electrons of the high voltage beam carry the image of the specimen, the electron beam of the Scanning Electron Microscope (SEM) does not at any time carry a complete image of the specimen. The SEM produces images by probing the specimen with a focused electron beam that is scanned across a rectangular area of the specimen (raster scanning). At each point on the specimen the incident electron beam loses some energy, and that lost energy is converted into other forms, such as heat, emission of low-energy secondary electrons, light emission (cathodoluminescence) or x-ray emission. The display of the SEM maps the varying intensity of any of these signals into the image in a position corresponding to the position of the beam on the specimen when the signal was generated. In the SEM image of an ant shown at right, the image was constructed from signals produced by a secondary electron detector, the normal or conventional imaging mode in most SEMs.

Generally, the image resolution of an SEM is about an order of magnitude poorer than that of a TEM. However, because the SEM image relies on surface processes rather than transmission, it is able to image bulk samples up to many centimetres in size and

(depending on instrument design and settings) has a great depth of field, and so can produce images that are good representations of the three-dimensional shape of the sample.

Reflection electron microscope (REM)

In the **Reflection Electron Microscope** (REM) as in the TEM, an electron beam is incident on a surface, but instead of using the transmission (TEM) or secondary electrons (SEM), the reflected beam of elastically scattered electrons is detected. This technique is typically coupled with Reflection High Energy Electron Diffraction (RHEED) and *Reflection high-energy loss spectrum (RHELS)*. Another variation is Spin-Polarized Low-Energy Electron Microscopy (SPLEEM), which is used for looking at the microstructure of magnetic domains.

Scanning transmission electron microscope (STEM)

The STEM rasters a focused incident probe across a specimen that (as with the TEM) has been thinned to facilitate detection of electrons scattered *through* the specimen. The high resolution of the TEM is thus possible in STEM. The focusing action (and aberrations) occur before the electrons hit the specimen in the STEM, but afterward in the TEM. The STEMs use of SEM-like beam rastering simplifies annular dark-field imaging, and other analytical techniques, but also means that image data is acquired in serial rather than in parallel fashion.

Low voltage electron microscope (LVEM)

The low voltage electron microscope (LVEM) is a combination of SEM, TEM and STEM in one instrument, which operates at relatively low electron accelerating voltage of 5 kV. Low voltage increases image contrast which is especially important for biological specimens. This increase in contrast significantly reduces, or even eliminates the need to stain. Sectioned samples generally need to be thinner than they would be for conventional TEM (20-65 nm). Resolutions of a few nm are possible in TEM, SEM and STEM modes.

Sample preparation

An insect coated in gold for viewing with a scanning electron microscope.

Materials to be viewed under an electron microscope may require processing to produce a suitable sample. The technique required varies depending on the specimen and the analysis required:

- *Chemical fixation* for biological specimens aims to stabilize the specimen's mobile macromolecular structure by chemical crosslinking of proteins with aldehydes such as formaldehyde and glutaraldehyde, and lipids with osmium tetroxide.
- *Cryofixation* – freezing a specimen so rapidly, to liquid nitrogen or even liquid helium temperatures, that the water forms vitreous (non-crystalline) ice. This preserves the specimen in a snapshot of its solution state. An entire field called

cryo-electron microscopy has branched from this technique. With the development of cryo-electron microscopy of vitreous sections (CEMOVIS), it is now possible to observe samples from virtually any biological specimen close to its native state.

- *Dehydration* – freeze drying, or replacement of water with organic solvents such as ethanol or acetone, followed by critical point drying or infiltration with embedding resins.
- *Embedding, biological specimens* – after dehydration, tissue for observation in the transmission electron microscope is embedded so it can be sectioned ready for viewing. To do this the tissue is passed through a 'transition solvent' such as epoxy propane and then infiltrated with a resin such as Araldite epoxy resin; tissues may also be embedded directly in water-miscible acrylic resin. After the resin has been polymerised (hardened) the sample is thin sectioned (ultrathin sections) and stained - it is then ready for viewing.
- *Embedding, materials* - after embedding in resin, the specimen is usually ground and polished to a mirror-like finish using ultra-fine abrasives. The polishing process must be performed carefully to minimize scratches and other polishing artifacts that reduce image quality.
- *Sectioning* – produces thin slices of specimen, semitransparent to electrons. These can be cut on an ultramicrotome with a diamond knife to produce ultrathin slices about 60-90 nm thick. Disposable glass knives are also used because they can be made in the lab and are much cheaper.
- *Staining* – uses heavy metals such as lead, uranium or tungsten to scatter imaging electrons and thus give contrast between different structures, since many (especially biological) materials are nearly "transparent" to electrons (weak phase objects). In biology, specimens are can be stained "en bloc" before embedding and also later after sectioning. Typically thin sections are stained for several minutes with an aqueous or alcoholic solution of uranyl acetate followed by aqueous lead citrate.
- *Freeze-fracture or freeze-etch* – a preparation method particularly useful for examining lipid membranes and their incorporated proteins in "face on" view. The fresh tissue or cell suspension is frozen rapidly (cryofixed), then fractured by simply breaking or by using a microtome while maintained at liquid nitrogen temperature. The cold fractured surface (sometimes "etched" by increasing the temperature to about –100 °C for several minutes to let some ice sublime) is then shadowed with evaporated platinum or gold at an average angle of 45° in a high vacuum evaporator. A second coat of carbon, evaporated perpendicular to the average surface plane is often performed to improve stability of the replica coating. The specimen is returned to room temperature and pressure, then the extremely fragile "pre-shadowed" metal replica of the fracture surface is released from the underlying biological material by careful chemical digestion with acids, hypochlorite solution or SDS detergent. The still-floating replica is thoroughly washed from residual chemicals, carefully fished up on fine grids, dried then viewed in the TEM.
- *Ion Beam Milling* – thins samples until they are transparent to electrons by firing ions (typically argon) at the surface from an angle and sputtering material from

the surface. A subclass of this is Focused ion beam milling, where gallium ions are used to produce an electron transparent membrane in a specific region of the sample, for example through a device within a microprocessor. Ion beam milling may also be used for cross-section polishing prior to SEM analysis of materials that are difficult to prepare using mechanical polishing.

- *Conductive Coating* – an ultrathin coating of electrically-conducting material, deposited either by high vacuum evaporation or by low vacuum sputter coating of the sample. This is done to prevent the accumulation of static electric fields at the specimen due to the electron irradiation required during imaging. Such coatings include gold, gold/palladium, platinum, tungsten, graphite etc. and are especially important for the study of specimens with the scanning electron microscope. Another reason for coating, even when there is more than enough conductivity, is to improve contrast, a situation more common with the operation of a FESEM (field emission SEM).

Disadvantages

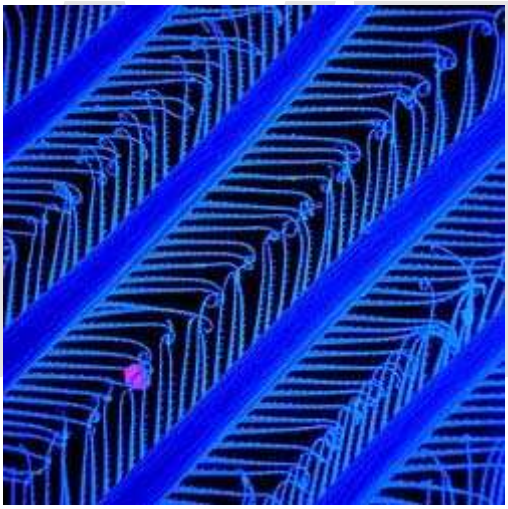

False-color SEM image of the filter setae of an Antarctic krill. (Raw electron microscope images carry no color information.)
Pictured: First degree filter setae with V-shaped second degree setae pointing towards the inside of the feeding basket. The purple ball is 1 μm in diameter.

Electron microscopes are expensive to build and maintain, but the capital and running costs of confocal light microscope systems now overlaps with those of basic electron microscopes. They are dynamic rather than static in their operation, requiring extremely stable high-voltage supplies, extremely stable currents to each electromagnetic coil/lens, continuously-pumped high- or ultra-high-vacuum systems, and a cooling water supply circulation through the lenses and pumps. As they are very sensitive to vibration and external magnetic fields, microscopes designed to achieve high resolutions must be housed in stable buildings (sometimes underground) with special services such as magnetic field cancelling systems. Some desktop low voltage electron microscopes have

TEM capabilities at very low voltages (around 5 kV) without stringent voltage supply, lens coil current, cooling water or vibration isolation requirements and as such are much less expensive to buy and far easier to install and maintain, but do not have the same ultra-high (atomic scale) resolution capabilities as the larger instruments.

The samples largely have to be viewed in vacuum, as the molecules that make up air would scatter the electrons. One exception is the environmental scanning electron microscope, which allows hydrated samples to be viewed in a low-pressure (up to 20 Torr/2.7 kPa), wet environment.

Scanning electron microscopes usually image conductive or semi-conductive materials best. Non-conductive materials can be imaged by an environmental scanning electron microscope. A common preparation technique is to coat the sample with a several-nanometer layer of conductive material, such as gold, from a sputtering machine; however, this process has the potential to disturb delicate samples.

Small, stable specimens such as carbon nanotubes, diatom frustules and small mineral crystals (asbestos fibres, for example) require no special treatment before being examined in the electron microscope. Samples of hydrated materials, including almost all biological specimens have to be prepared in various ways to stabilize them, reduce their thickness (ultrathin sectioning) and increase their electron optical contrast (staining). These processes may result in *artifacts*, but these can usually be identified by comparing the results obtained by using radically different specimen preparation methods. It is generally believed by scientists working in the field that as results from various preparation techniques have been compared and that there is no reason that they should all produce similar artifacts, it is reasonable to believe that electron microscopy features correspond with those of living cells. In addition, higher-resolution work has been directly compared to results from X-ray crystallography, providing independent confirmation of the validity of this technique. Since the 1980s, analysis of cryofixed, vitrified specimens has also become increasingly used by scientists, further confirming the validity of this technique.

Chapter- 6

Atomic force microscopy (Technique for Nanoparticle Characterization)

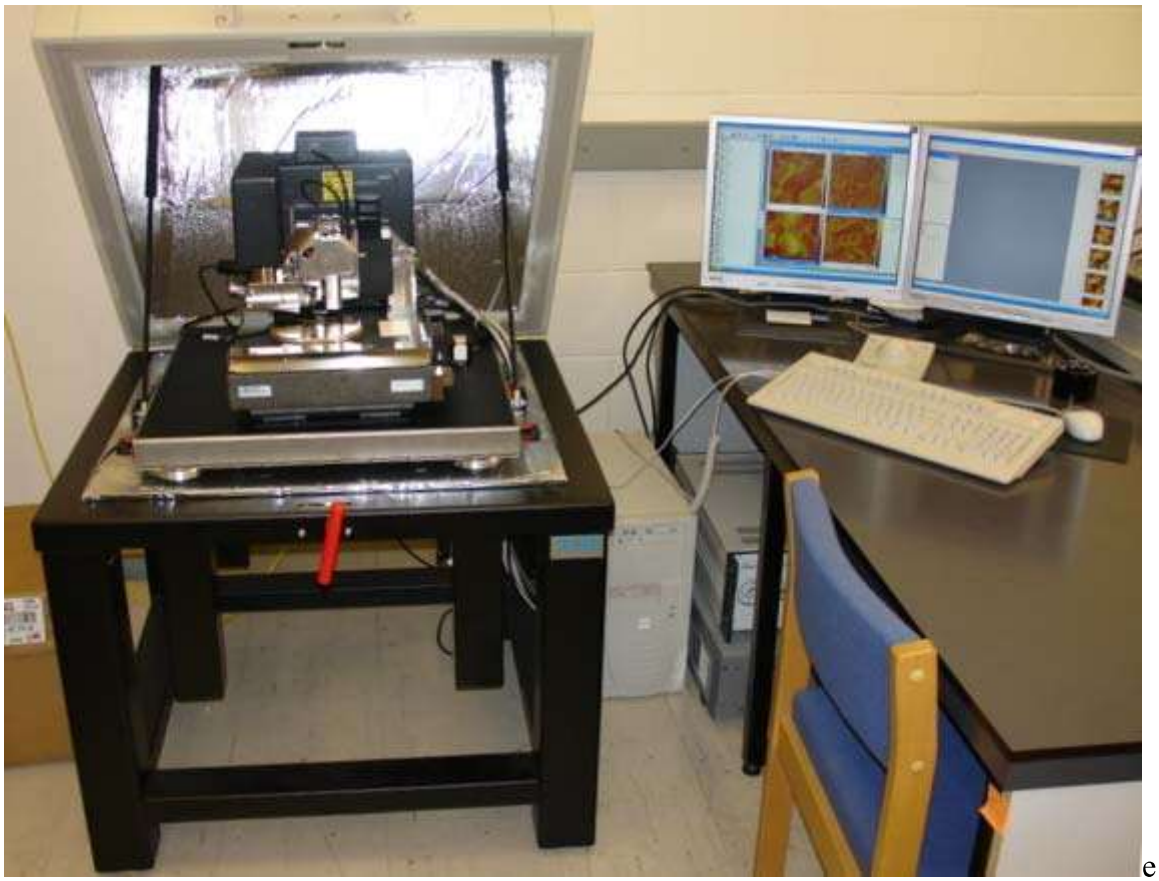
e

A commercial AFM setup

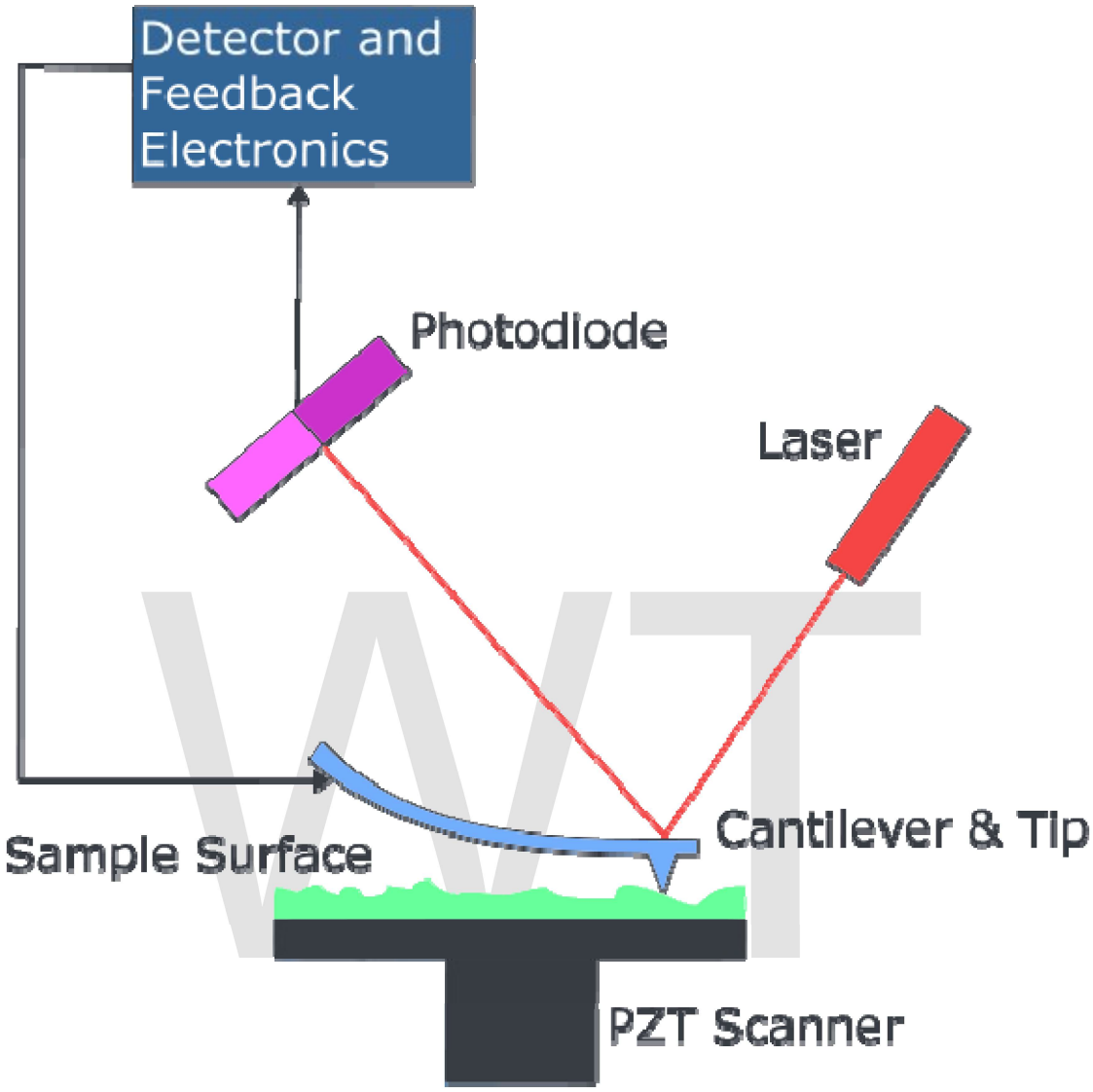

Block diagram of atomic force microscope

Atomic force microscopy (AFM) or scanning force microscopy (SFM) is a very high-resolution type of scanning probe microscopy, with demonstrated resolution on the order of fractions of a nanometer, more than 1000 times better than the optical diffraction limit. The precursor to the AFM, the scanning tunneling microscope, was developed by Gerd Binnig and Heinrich Rohrer in the early 1980s at IBM Research - Zurich, a development that earned them the Nobel Prize for Physics in 1986. Binnig, Quate and Gerber invented the first atomic force microscope (also abbreviated as AFM) in 1986. The first commercially available atomic force microscope was introduced in 1989. The AFM is one of the foremost tools for imaging, measuring, and manipulating matter at the nanoscale. The information is gathered by "feeling" the surface with a mechanical probe. Piezoelectric elements that facilitate tiny but accurate and precise movements on

(electronic) command enable the very precise scanning. In some variations, electric potentials can also be scanned using conducting cantilevers. In newer more advanced versions, currents can even be passed through the tip to probe the electrical conductivity or transport of the underlying surface, but this is much more challenging with very few groups reporting reliable data.

Basic principles

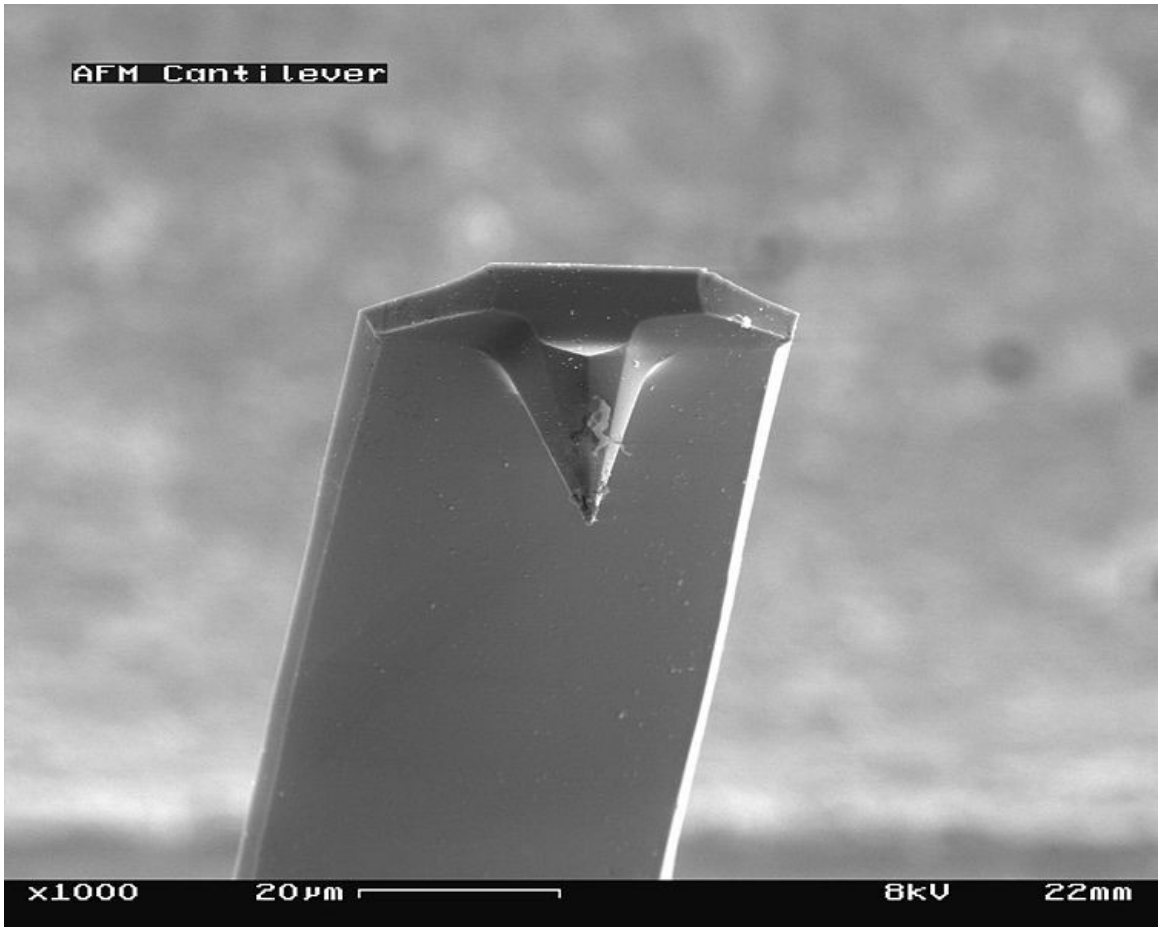

Electron micrograph of a used AFM cantilever image width ~100 micrometers...

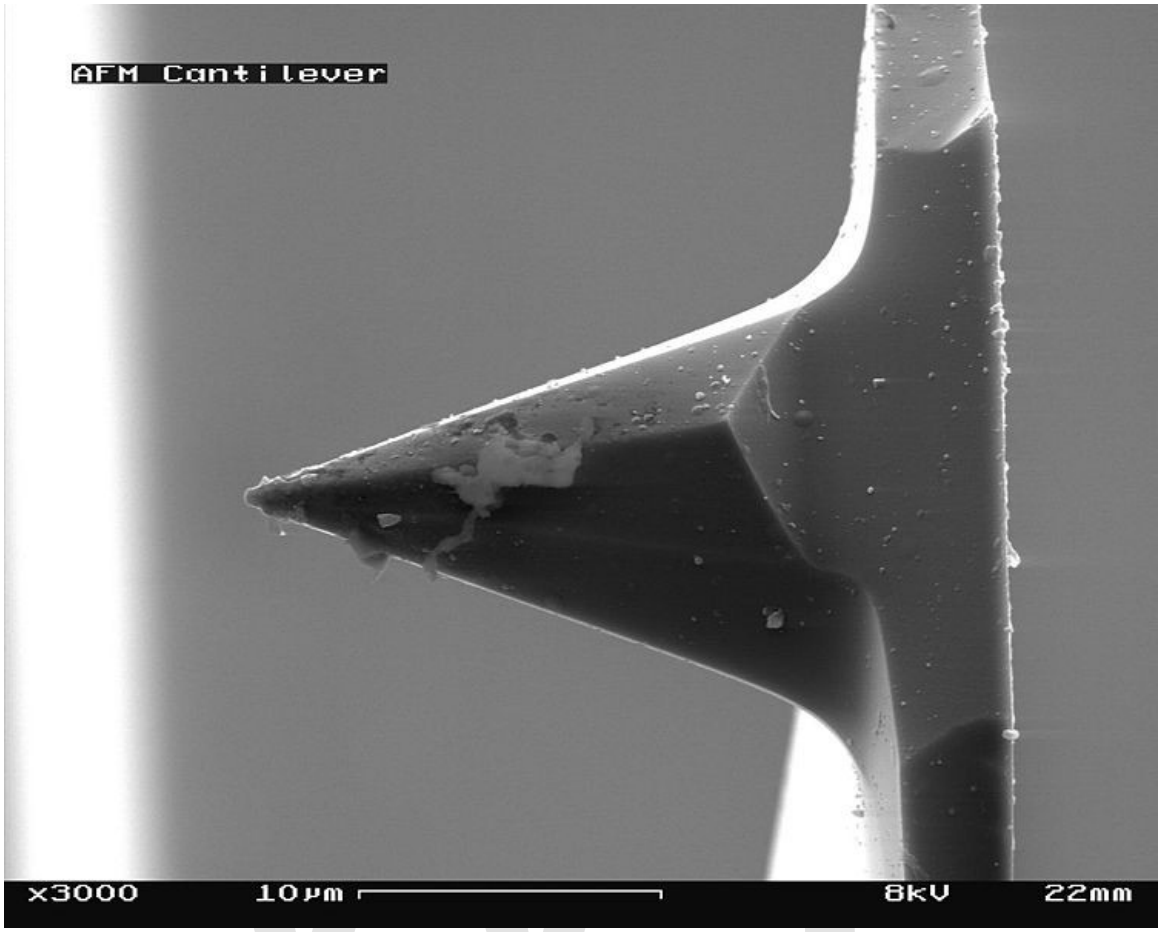

and ~30 micrometers

The AFM consists of a cantilever with a sharp tip (probe) at its end that is used to scan the specimen surface. The cantilever is typically silicon or silicon nitride with a tip radius of curvature on the order of nanometers. When the tip is brought into proximity of a sample surface, forces between the tip and the sample lead to a deflection of the cantilever according to Hooke's law. Depending on the situation, forces that are measured in AFM include mechanical contact force, van der Waals forces, capillary forces, chemical bonding, electrostatic forces, magnetic forces, Casimir forces, solvation forces, etc. Along with force, additional quantities may simultaneously be measured through the use of specialized types of probe. Typically, the deflection is measured using a laser spot reflected from the top surface of the cantilever into an array of photodiodes. Other methods that are used include optical interferometry, capacitive sensing or piezoresistive AFM cantilevers. These cantilevers are fabricated with piezoresistive elements that act as a strain gauge. Using a Wheatstone bridge, strain in the AFM cantilever due to deflection can be measured, but this method is not as sensitive as laser deflection or interferometry.

If the tip was scanned at a constant height, a risk would exist that the tip collides with the surface, causing damage. Hence, in most cases a feedback mechanism is employed to adjust the tip-to-sample distance to maintain a constant force between the tip and the sample. Traditionally, the sample is mounted on a piezoelectric tube, that can move the

sample in the *z* direction for maintaining a constant force, and the *x* and *y* directions for scanning the sample. Alternatively a 'tripod' configuration of three piezo crystals may be employed, with each responsible for scanning in the x,y and z directions. This eliminates some of the distortion effects seen with a tube scanner. In newer designs, the tip is mounted on a vertical piezo scanner while the sample is being scanned in X and Y using another piezo block. The resulting map of the area $s = f(x,y)$ represents the topography of the sample.

The AFM can be operated in a number of modes, depending on the application. In general, possible imaging modes are divided into static (also called *contact*) modes and a variety of dynamic (or non-contact) modes where the cantilever is vibrated.

Imaging modes

The primary modes of operation for an AFM are static mode and dynamic mode. In static mode, the cantilever is "dragged" across the surface of the sample and the contours of the surface are measured directly using the deflection of the cantilever. In the dynamic mode, the cantilever is externally oscillated at or close to its fundamental resonance frequency or a harmonic. The oscillation amplitude, phase and resonance frequency are modified by tip-sample interaction forces. These changes in oscillation with respect to the external reference oscillation provide information about the sample's characteristics.

Contact mode

In the static mode operation, the static tip deflection is used as a feedback signal. Because the measurement of a static signal is prone to noise and drift, low stiffness cantilevers are used to boost the deflection signal. However, close to the surface of the sample, attractive forces can be quite strong, causing the tip to "snap-in" to the surface. Thus static mode AFM is almost always done in contact where the overall force is repulsive. Consequently, this technique is typically called "contact mode". In contact mode, the force between the tip and the surface is kept constant during scanning by maintaining a constant deflection.

Non-contact mode

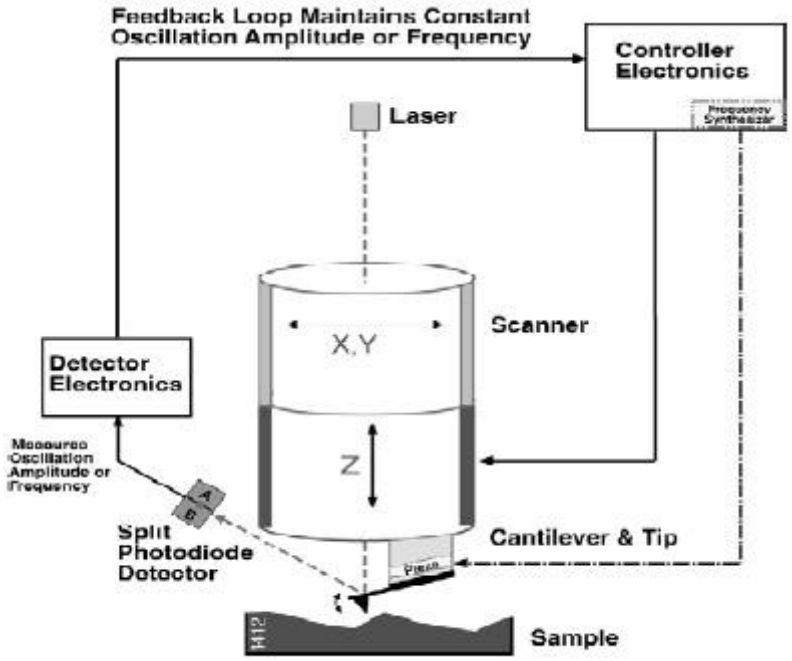

AFM - non-contact mode

In this mode, the tip of the cantilever does not contact the sample surface. The cantilever is instead oscillated at a frequency slightly above its resonance frequency where the amplitude of oscillation is typically a few nanometers (<10 nm). The van der Waals forces, which are strongest from 1 nm to 10 nm above the surface, or any other long range force which extends above the surface acts to decrease the resonance frequency of the cantilever. This decrease in resonance frequency combined with the feedback loop system maintains a constant oscillation amplitude or frequency by adjusting the average tip-to-sample distance. Measuring the tip-to-sample distance at each (x,y) data point allows the scanning software to construct a topographic image of the sample surface.

Non-contact mode AFM does not suffer from tip or sample degradation effects that are sometimes observed after taking numerous scans with contact AFM. This makes non-contact AFM preferable to contact AFM for measuring soft samples. In the case of rigid samples, contact and non-contact images may look the same. However, if a few monolayers of adsorbed fluid are lying on the surface of a rigid sample, the images may look quite different. An AFM operating in contact mode will penetrate the liquid layer to image the underlying surface, whereas in non-contact mode an AFM will oscillate above the adsorbed fluid layer to image both the liquid and surface.

Schemes for dynamic mode operation include frequency modulation and the more common amplitude modulation. In frequency modulation, changes in the oscillation frequency provide information about tip-sample interactions. Frequency can be measured with very high sensitivity and thus the frequency modulation mode allows for the use of very stiff cantilevers. Stiff cantilevers provide stability very close to the surface and, as a

result, this technique was the first AFM technique to provide true atomic resolution in ultra-high vacuum conditions.

In amplitude modulation, changes in the oscillation amplitude or phase provide the feedback signal for imaging. In amplitude modulation, changes in the phase of oscillation can be used to discriminate between different types of materials on the surface. Amplitude modulation can be operated either in the non-contact or in the intermittent contact regime. In dynamic contact mode, the cantilever is oscillated such that the separation distance between the cantilever tip and the sample surface is modulated.

Amplitude modulation has also been used in the non-contact regime to image with atomic resolution by using very stiff cantilevers and small amplitudes in an ultra-high vacuum environment.

Tapping mode

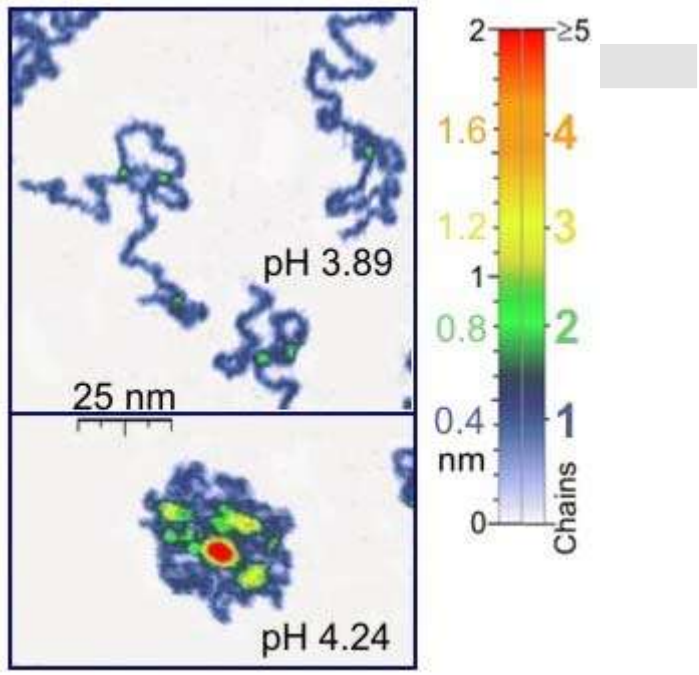

Single polymer chains (0.4 nm thick) recorded in a tapping mode under aqueous media with different pH.

In ambient conditions, most samples develop a liquid meniscus layer. Because of this, keeping the probe tip close enough to the sample for short-range forces to become detectable while preventing the tip from sticking to the surface presents a major problem for non-contact dynamic mode in ambient conditions. Dynamic contact mode (also called intermittent contact or tapping mode) was developed to bypass this problem.

In *tapping mode*, the cantilever is driven to oscillate up and down at near its resonance frequency by a small piezoelectric element mounted in the AFM tip holder similar to

non-contact mode. However, the amplitude of this oscillation is greater than 10 nm, typically 100 to 200 nm. Due to the interaction of forces acting on the cantilever when the tip comes close to the surface, Van der Waals force, dipole-dipole interaction, electrostatic forces, etc. cause the amplitude of this oscillation to decrease as the tip gets closer to the sample. An electronic servo uses the piezoelectric actuator to control the height of the cantilever above the sample. The servo adjusts the height to maintain a set cantilever oscillation amplitude as the cantilever is scanned over the sample. A *tapping AFM* image is therefore produced by imaging the force of the intermittent contacts of the tip with the sample surface.

This method of "tapping" lessens the damage done to the surface and the tip compared to the amount done in contact mode. Tapping mode is gentle enough even for the visualization of supported lipid bilayers or adsorbed single polymer molecules (for instance, 0.4 nm thick chains of synthetic polyelectrolytes) under liquid medium. With proper scanning parameters, the conformation of single molecules can remain unchanged for hours.

AFM cantilever deflection measurement

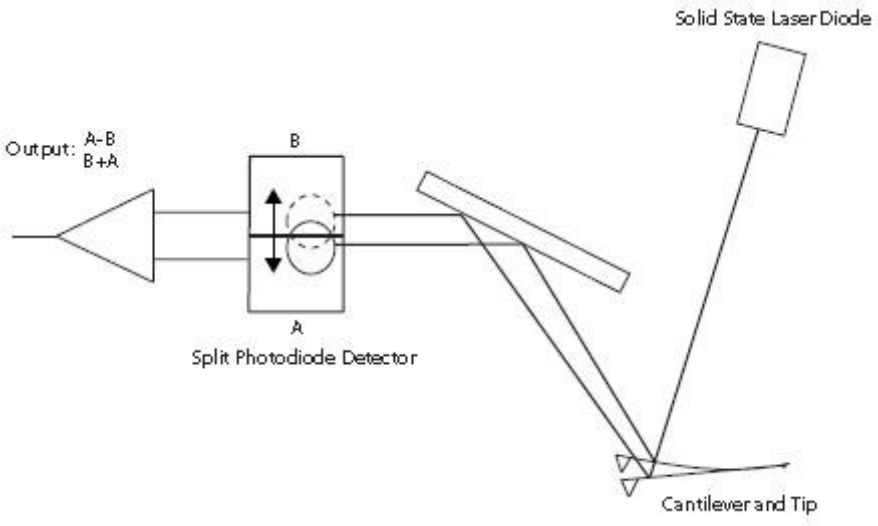

AFM beam deflection detection

Laser light from a solid state diode is reflected off the back of the cantilever and collected by a position sensitive detector (PSD) consisting of two closely spaced photodiodes whose output signal is collected by a differential amplifier. Angular displacement of cantilever results in one photodiode collecting more light than the other photodiode, producing an output signal (the difference between the photodiode signals normalized by their sum) which is proportional to the deflection of the cantilever. It detects cantilever deflections <10 nm (thermal noise limited). A long beam path (several centimeters) amplifies changes in beam angle.

Force spectroscopy

Another major application of AFM (besides imaging) is force spectroscopy, the direct measurement of tip-sample interaction forces as a function of the gap between the tip and sample (the result of this measurement is called a force-distance curve). For this method, the AFM tip is extended towards and retracted from the surface as the deflection of the cantilever is monitored as a function of piezoelectric displacement. These measurements have been used to measure nanoscale contacts, atomic bonding, Van der Waals forces, and Casimir forces, dissolution forces in liquids and single molecule stretching and rupture forces. Furthermore, AFM was used to measure in aqueous environment dispersion force due to polymer adsorbed on the substrate. Forces of the order of a few piconewtons can now be routinely measured with a vertical distance resolution of better than 0.1 nanometers. Force spectroscopy can be performed with either static or dynamic modes. In dynamic modes, information about the cantilever vibration is monitored in addition to the static deflection.

Problems with the technique include no direct measurement of the tip-sample separation and the common need for low stiffness cantilevers which tend to 'snap' to the surface. The snap-in can be reduced by measuring in liquids or by using stiffer cantilevers, but in the latter case a more sensitive deflection sensor is needed. By applying a small dither to the tip, the stiffness (force gradient) of the bond can be measured as well.

Identification of individual surface atoms

The AFM can be used to image and manipulate atoms and structures on a variety of surfaces. The atom at the apex of the tip "senses" individual atoms on the underlying surface when it forms incipient chemical bonds with each atom. Because these chemical interactions subtly alter the tip's vibration frequency, they can be detected and mapped. This principle was used to distinguish between atoms of silicon, tin and lead on an alloy surface, by comparing these 'atomic fingerprints' to values obtained from large-scale density functional theory (DFT) simulations.

The trick is to first measure these forces precisely for each type of atom expected in the sample, and then to compare with forces given by DFT simulations. The team found that the tip interacted most strongly with silicon atoms, and interacted 23% and 41% less strongly with tin and lead atoms, respectively. Thus, each different type of atom can be identified in the matrix as the tip is moved across the surface.

Such a technique has been used now in biology and extended recently to cell biology. Forces corresponding to (i) the unbinding of receptor ligand couples (ii) unfolding of proteins (iii) cell adhesion at single cell scale have been gathered.

Advantages and disadvantages

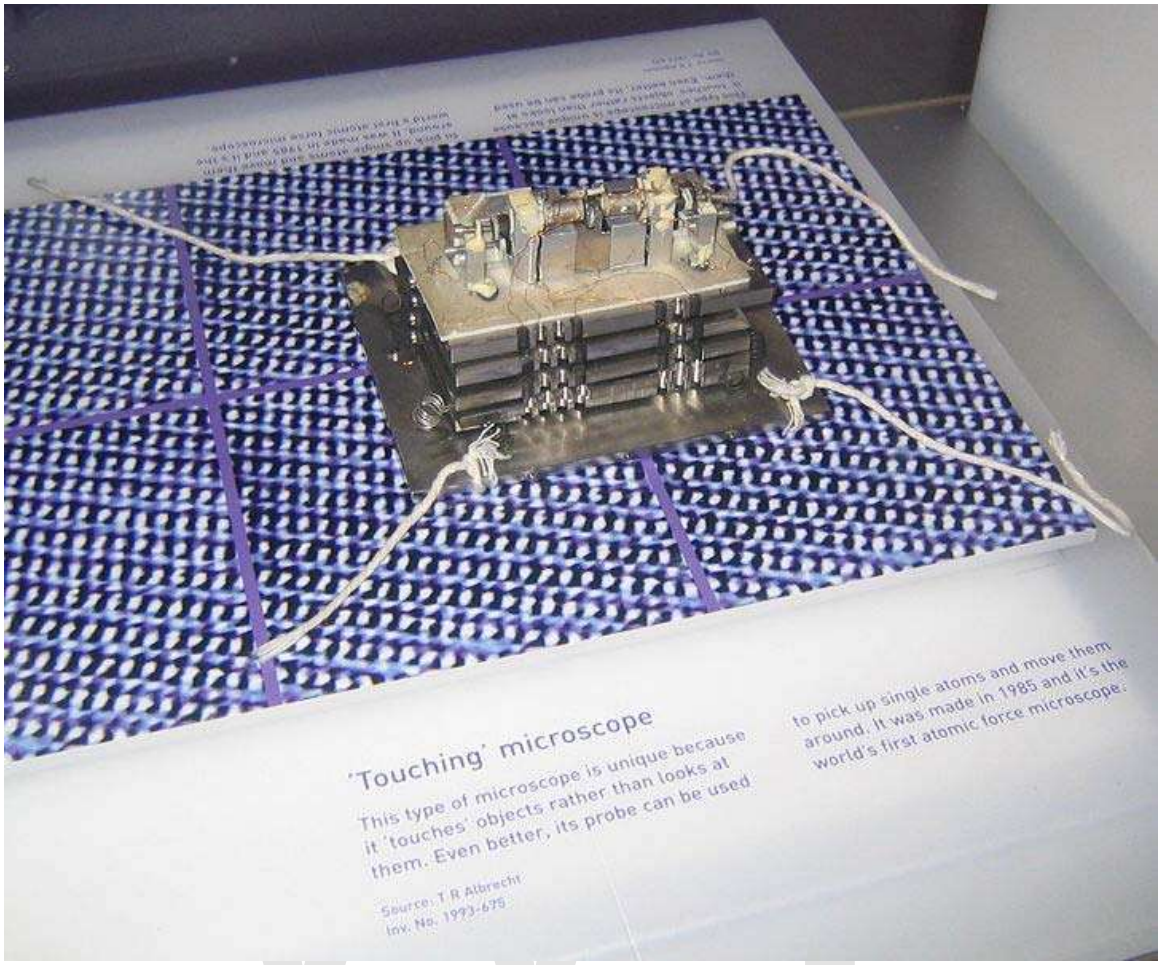

The first atomic force microscope

Just like any other tool, an AFM's usefulness has limitations. When determining whether or not analyzing a sample with an AFM is appropriate, there are various advantages and disadvantages that must be considered.

Advantages

AFM has several advantages over the scanning electron microscope (SEM). Unlike the electron microscope which provides a two-dimensional projection or a two-dimensional image of a sample, the AFM provides a three-dimensional surface profile. Additionally, samples viewed by AFM do not require any special treatments (such as metal/carbon coatings) that would irreversibly change or damage the sample. While an electron microscope needs an expensive vacuum environment for proper operation, most AFM modes can work perfectly well in ambient air or even a liquid environment. This makes it possible to study biological macromolecules and even living organisms. In principle, AFM can provide higher resolution than SEM. It has been shown to give true atomic resolution in ultra-high vacuum (UHV) and, more recently, in liquid environments. High

resolution AFM is comparable in resolution to scanning tunneling microscopy and transmission electron microscopy.

Disadvantages

A disadvantage of AFM compared with the scanning electron microscope (SEM) is the single scan image size. In one pass, the SEM can image an area on the order of square millimeters with a depth of field on the order of millimeters. Whereas the AFM can only image a maximum height on the order of 10-20 micrometers and a maximum scanning area of about 150×150 micrometers. One method of improving the scanned area size for AFM is by using parallel probes in a fashion similar to that of millipede data storage.

The scanning speed of an AFM is also a limitation. Traditionally, an AFM cannot scan images as fast as a SEM, requiring several minutes for a typical scan, while a SEM is capable of scanning at near real-time, although at relatively low quality. The relatively slow rate of scanning during AFM imaging often leads to thermal drift in the image making the AFM microscope less suited for measuring accurate distances between topographical features on the image. However, several fast-acting designs were suggested to increase microscope scanning productivity including what is being termed videoAFM (reasonable quality images are being obtained with videoAFM at video rate: faster than the average SEM). To eliminate image distortions induced by thermal drift, several methods have been introduced.

AFM images can also be affected by hysteresis of the piezoelectric material and cross-talk between the *x*, *y*, *z* axes that may require software enhancement and filtering. Such filtering could "flatten" out real topographical features. However, newer AFMs utilize closed-loop scanners which practically eliminate these problems. Some AFMs also use separated orthogonal scanners (as opposed to a single tube) which also serve to eliminate part of the cross-talk problems.

As with any other imaging technique, there is the possibility of image artifacts, which could be induced by an unsuitable tip, a poor operating environment, or even by the sample itself. These image artifacts are unavoidable however, their occurrence and effect on results can be reduced through various methods.

Due to the nature of AFM probes, they cannot normally measure steep walls or overhangs. Specially made cantilevers and AFMs can be used to modulate the probe sideways as well as up and down (as with dynamic contact and non-contact modes) to measure sidewalls, at the cost of more expensive cantilevers, lower lateral resolution and additional artifacts.

Piezoelectric scanners

AFM scanners are made from piezoelectric material, which expands and contracts proportionally to an applied voltage. Whether they elongate or contract depends upon the polarity of the voltage applied. The scanner is constructed by combining independently

operated piezo electrodes for X, Y, and Z into a single tube, forming a scanner which can manipulate samples and probes with extreme precision in 3 dimensions.

Scanners are characterized by their sensitivity which is the ratio of piezo movement to piezo voltage, i.e., by how much the piezo material extends or contracts per applied volt. Because of differences in material or size, the sensitivity varies from scanner to scanner. Sensitivity varies non-linearly with respect to scan size. Piezo scanners exhibit more sensitivity at the end than at the beginning of a scan. This causes the forward and reverse scans to behave differently and display hysteresis between the two scan directions. This can be corrected by applying a non-linear voltage to the piezo electrodes to cause linear scanner movement and calibrating the scanner accordingly.

The sensitivity of piezoelectric materials decreases exponentially with time. This causes most of the change in sensitivity to occur in the initial stages of the scanner's life. Piezoelectric scanners are run for approximately 48 hours before they are shipped from the factory so that they are past the point where they may have large changes in sensitivity. As the scanner ages, the sensitivity will change less with time and the scanner would seldom require recalibration.

WT

Chapter- 7

X-ray photoelectron spectroscopy (Technique for Nanoparticle Characterization)

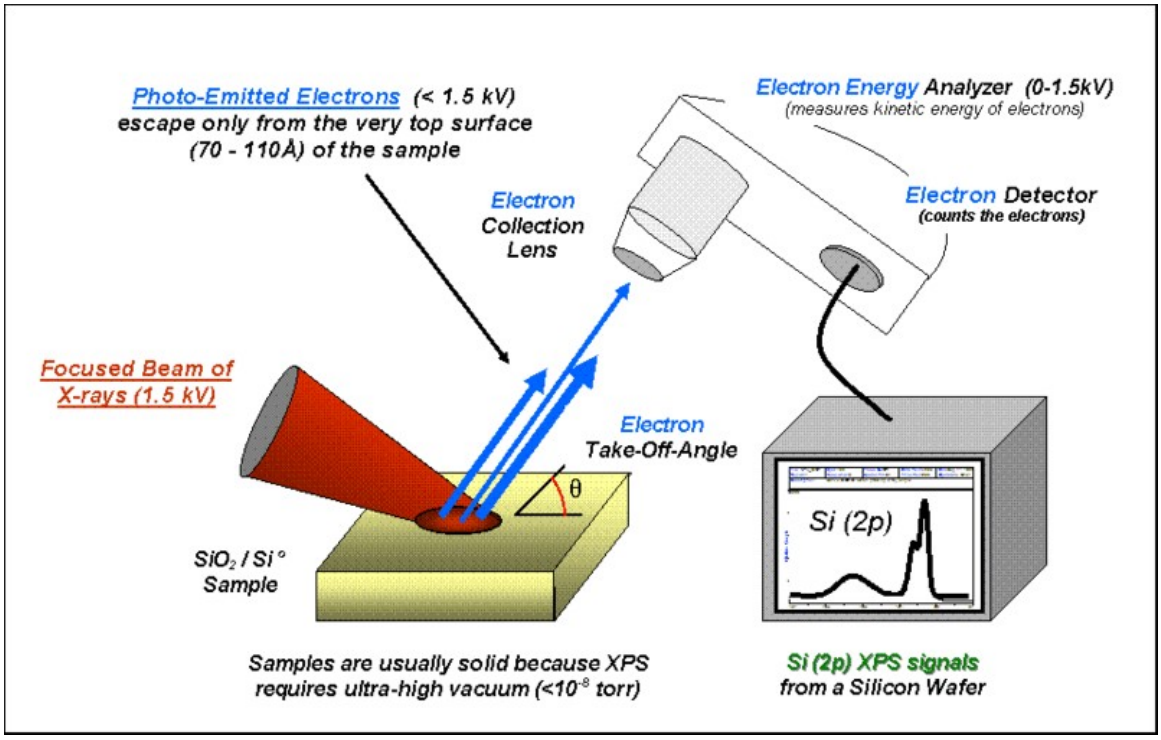

Basic components of a monochromatic XPS system.

X-ray photoelectron spectroscopy (XPS) is a quantitative spectroscopic technique that measures the elemental composition, empirical formula, chemical state and electronic state of the elements that exist within a material. XPS spectra are obtained by irradiating a material with a beam of X-rays while simultaneously measuring the kinetic energy and number of electrons that escape from the top 1 to 10 nm of the material being analyzed. XPS requires ultra high vacuum (UHV) conditions.

XPS is a surface chemical analysis technique that can be used to analyze the surface chemistry of a material in its "as received" state, or after some treatment, for example:

fracturing, cutting or scraping in air or UHV to expose the bulk chemistry, ion beam etching to clean off some of the surface contamination, exposure to heat to study the changes due to heating, exposure to reactive gases or solutions, exposure to ion beam implant, exposure to ultraviolet light.

- XPS is also known as **ESCA**, an abbreviation for **Electron Spectroscopy for Chemical Analysis**.
- XPS detects all elements with an atomic number (Z) of 3 (lithium) and above. It cannot detect hydrogen (Z = 1) or helium (Z = 2) because the diameter of these orbitals is so small, reducing the catch probability to almost zero.
- Detection limits for most of the elements are in the parts per thousand range. Detections limits of parts per million (ppm) are possible, but require special conditions: concentration at top surface or very long collection time (overnight).
- XPS is routinely used to analyze inorganic compounds, metal alloys, semiconductors, polymers, elements, catalysts, glasses, ceramics, paints, papers, inks, woods, plant parts, make-up, teeth, bones, medical implants, bio-materials, viscous oils, glues, ion modified materials and many others.

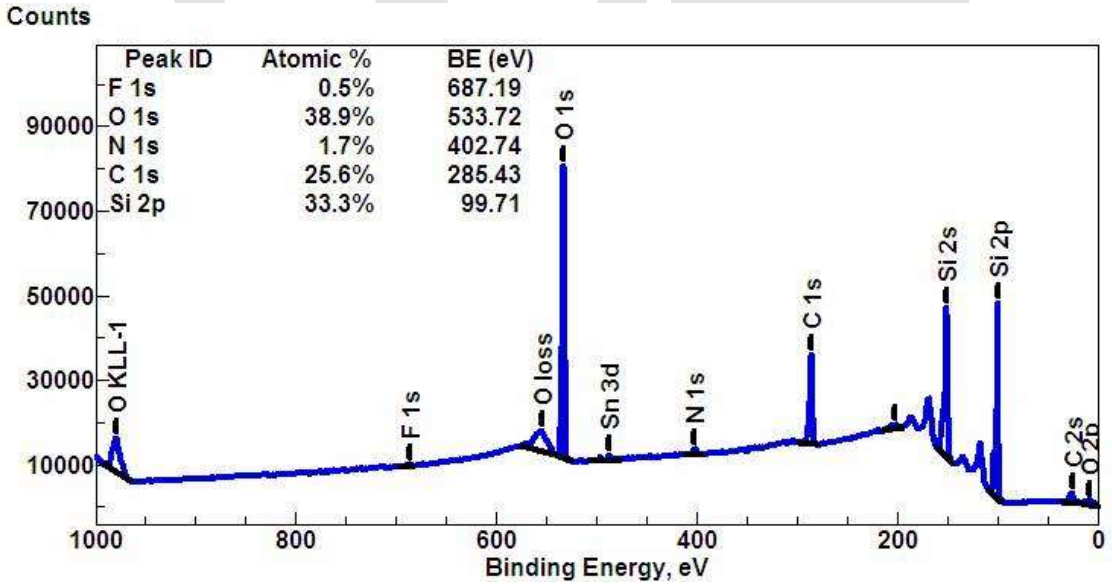

Wide-scan survey spectrum for all elements.

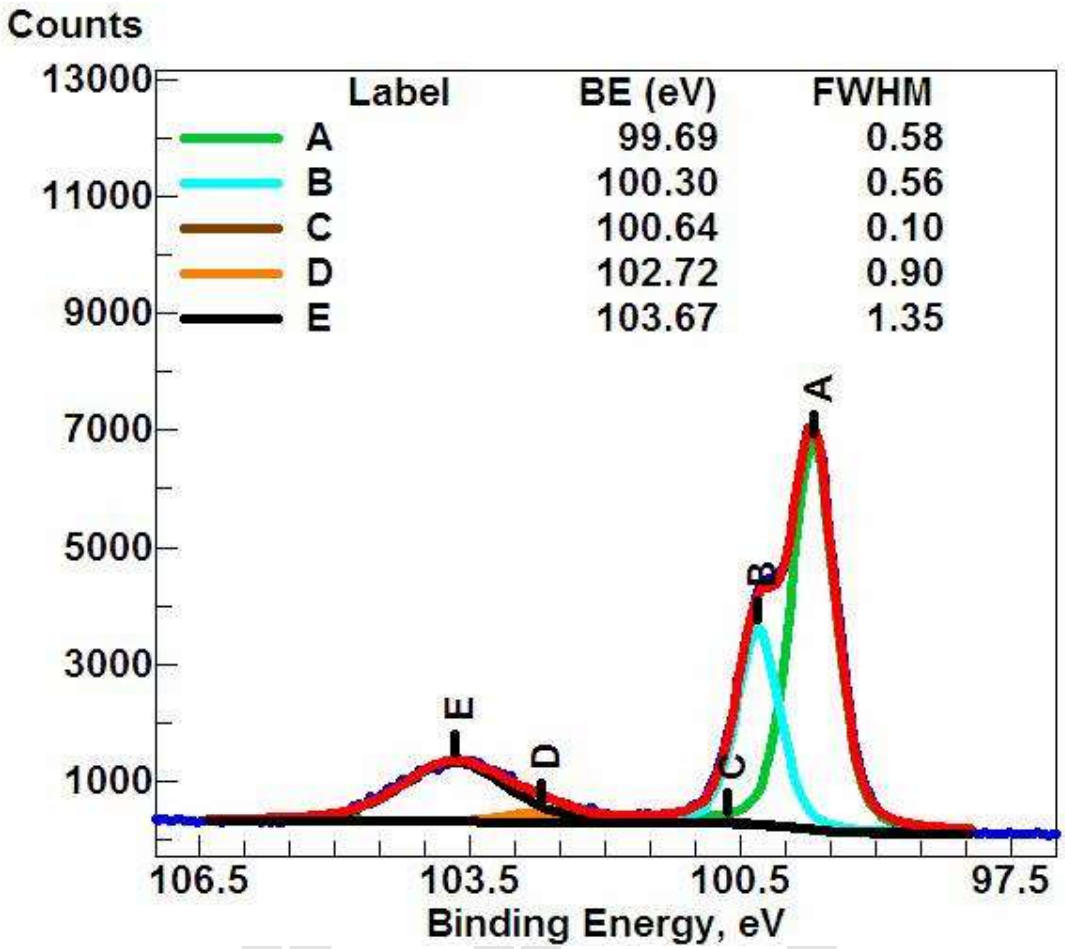

High-resolution spectrum for Si(2p) signal.

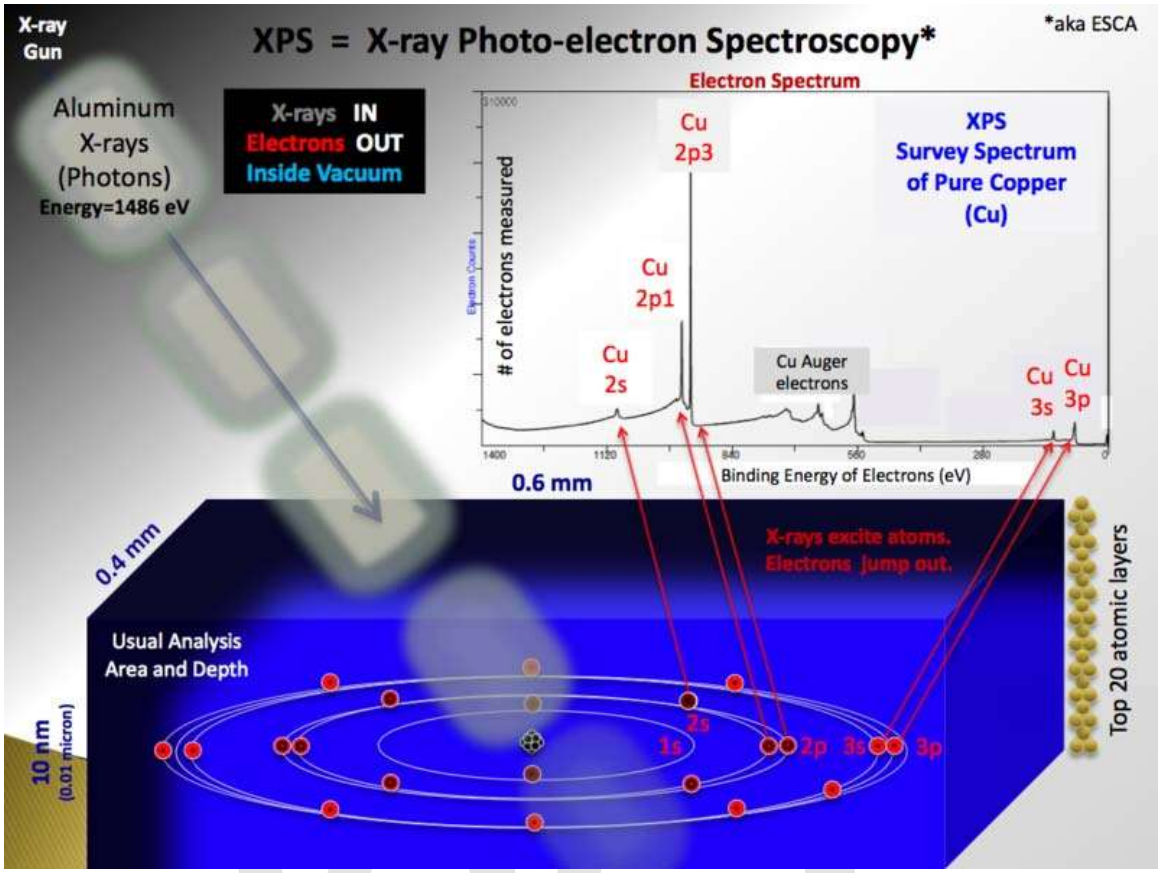

Rough schematic of XPS physics - "Photoelectric Effect.

XPS is used to measure:

- elemental composition of the surface (top 1–10 nm usually)
- empirical formula of pure materials
- elements that contaminate a surface
- chemical or electronic state of each element in the surface
- uniformity of elemental composition across the top surface (or line profiling or mapping)
- uniformity of elemental composition as a function of ion beam etching (or depth profiling)

XPS can be performed using either a commercially built XPS system, a privately built XPS system or a synchrotron-based light source combined with a custom designed electron analyzer. Commercial XPS instruments in the year 2005 used either a highly focused 20 to 200 micrometer beam of monochromatic aluminium Kα X-rays or a broad 10–30 mm beam of non-monochromatic (polychromatic) magnesium X-rays. A few, special design, XPS instruments can analyze volatile liquids or gases, materials at low or high temperatures or materials at roughly 1 torr vacuum, but there are relatively few of these types of XPS systems.

Because the energy of a particular X-ray wavelength is known, the electron binding energy of each of the emitted electrons can be determined by using an equation that is based on the work of Ernest Rutherford (1914):

$$E_{\text{binding}} = E_{\text{photon}} - (E_{\text{kinetic}} + \phi)$$

where E_{binding} is the binding energy (BE) of the electron, E_{photon} is the energy of the X-ray photons being used, E_{kinetic} is the kinetic energy of the electron as measured by the instrument and φ is the work function of the spectrometer (not the material).

History

In 1887, Heinrich Rudolf Hertz discovered the photoelectric effect that was explained in 1905 by Albert Einstein (Nobel Prize in Physics 1921). Two years later, in 1907, P.D. Innes experimented with a Röntgen tube, Helmholtz coils, a magnetic field hemisphere (electron energy analyzer) and photographic plates to record broad bands of emitted electrons as a function of velocity, in effect recording the first XPS spectrum. Other researchers, Henry Moseley, Rawlinson and Robinson, independently performed various experiments trying to sort out the details in the broad bands. Wars halted research on XPS. After WWII, Kai Siegbahn and his group in Uppsala (Sweden) developed several significant improvements in the equipment and in 1954 recorded the first high energy resolution XPS spectrum of cleaved sodium chloride (NaCl) revealing the potential of XPS. A few years later in 1967, Siegbahn published a comprehensive study on XPS bringing instant recognition of the utility of XPS. In cooperation with Siegbahn, Hewlett-Packard in the USA produced the first commercial monochromatic XPS instrument in 1969. Siegbahn received the Nobel Prize in 1981 to acknowledge his extensive efforts to develop XPS into a useful analytical tool.

In parallel with Siegbahn's work, David Turner at Imperial College (and later at Oxford) in the UK developed ultraviolet photoelectron spectroscopy (UPS) on molecular species using helium lamps.

Physics

A typical XPS spectrum is a plot of the number of electrons detected (sometimes per unit time) (Y-axis, ordinate) versus the binding energy of the electrons detected (X-axis, abscissa). Each element produces a characteristic set of XPS peaks at characteristic binding energy values that directly identify each element that exist in or on the surface of the material being analyzed. These characteristic peaks correspond to the electron configuration of the electrons within the atoms, e.g., 1s, 2s, 2p, 3s, etc. The number of detected electrons in each of the characteristic peaks is directly related to the amount of element within the area (volume) irradiated. To generate atomic percentage values, each raw XPS signal must be corrected by dividing its signal intensity (number of electrons detected) by a "relative sensitivity factor" (RSF) and normalized over all of the elements detected.

To count the number of electrons at each kinetic energy value, with the minimum of error, XPS must be performed under ultra-high vacuum (UHV) conditions because electron counting detectors in XPS instruments are typically one meter away from the material irradiated with X-rays.

It is important to note that XPS detects only those electrons that have actually escaped into the vacuum of the instrument. The photo-emitted electrons that have escaped into the vacuum of the instrument are those that originated from within the top 10 to 12 nm of the material. All of the deeper photo-emitted electrons, which were generated as the X-rays penetrated 1– 5 micrometers of the material, are either recaptured or trapped in various excited states within the material. For most applications, it is, in effect, a non-destructive technique that measures the surface chemistry of any material.

Components of an XPS system

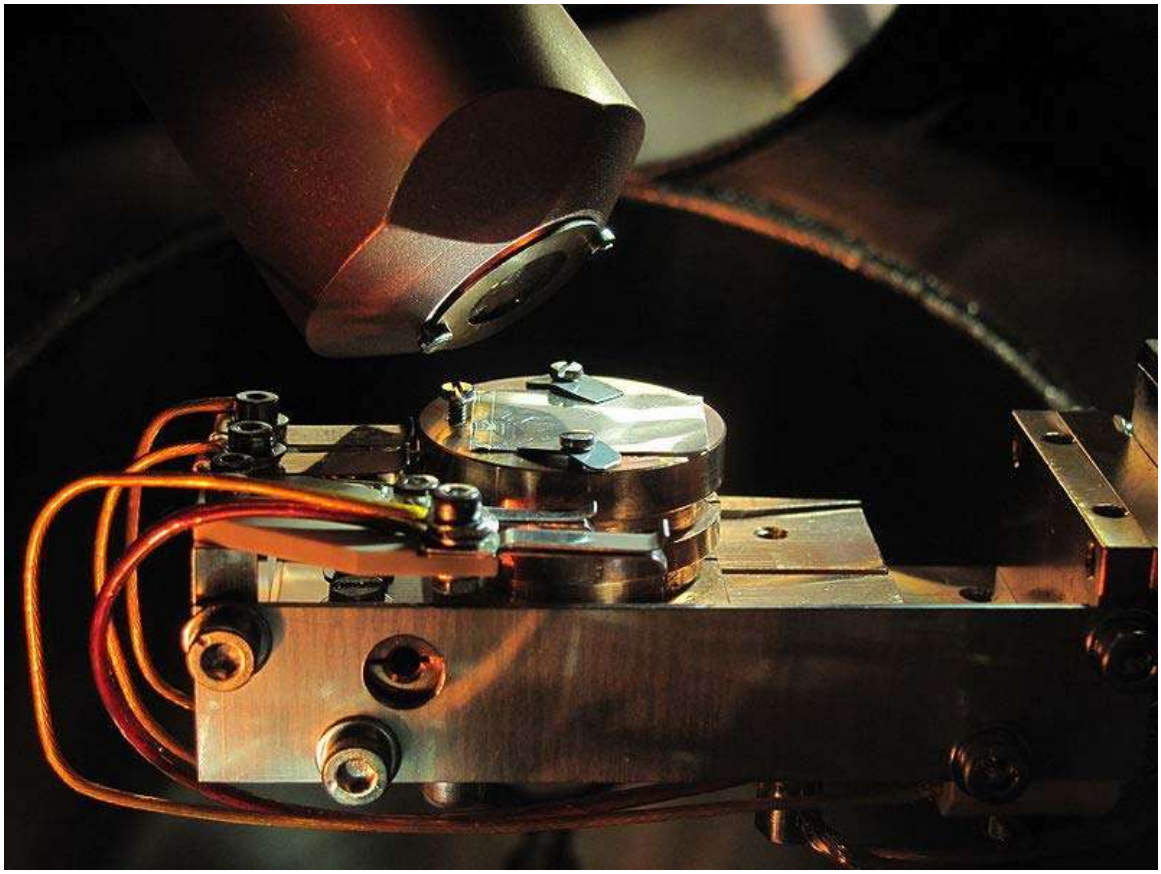

An inside view of an old-type, non-monochromatic XPS system.

The main components of a commercially made XPS system include:

- A source of X-rays
- An ultra-high vacuum (UHV) stainless steel chamber with UHV pumps

- An electron collection lens
- An electron energy analyzer
- Mu-metal magnetic field shielding
- An electron detector system
- A moderate vacuum sample introduction chamber
- Sample mounts
- A sample stage
- A set of stage manipulators

Monochromatic aluminium K-alpha X-rays are normally produced by diffracting and focusing a beam of non-monochromatic X-rays off of a thin disc of natural, crystalline quartz with a <1010> orientation. The resulting wavelength is 8.3386 angstroms (0.83386 nm) which corresponds to a photon energy of 1486.7 eV. The energy width of the monochromated X-rays is 0.16 eV, but the common electron energy analyzer (spectrometer) produces an ultimate energy resolution on the order of 0.25 eV which, in effect, is the ultimate energy resolution of most commercial systems. When working under practical, everyday conditions, high energy resolution settings will produce peak widths (FWHM) between 0.4–0.6 eV for various pure elements and some compounds.

Non-monochromatic magnesium X-rays have a wavelength of 9.89 angstroms (0.989 nm) which corresponds to a photon energy of 1253 eV. The energy width of the non-monochromated X-ray is roughly 0.70 eV, which, in effect is the ultimate energy resolution of a system using non-monochromatic X-rays. Non-monochromatic X-ray sources do not use any crystals to diffract the X-rays which allows all primary X-rays lines and the full range of high energy Bremsstrahlung X-rays (1–12 keV) to reach the surface. The typical ultimate high energy resolution (FWHM) when using this source is 0.9–1.0 eV, which includes with the spectrometer-induced broadening, pass-energy settings and the peak-width of the non-monochromatic magnesium X-ray source.

Uses and capabilities

XPS is routinely used to determine:

- What elements and the quantity of those elements that are present within the top 1-12 nm of the sample surface
- What contamination, if any, exists in the surface or the bulk of the sample
- Empirical formula of a material that is free of excessive surface contamination
- The chemical state identification of one or more of the elements in the sample
- The binding energy of one or more electronic states
- The thickness of one or more thin layers (1–8 nm) of different materials within the top 12 nm of the surface
- The density of electronic states

Capabilities of advanced systems

- Measure uniformity of elemental composition across the top the surface (or *line profiling or mapping*)
- Measure uniformity of elemental composition as a function of depth by ion beam etching (or *depth profiling*)
- Measure uniformity of elemental composition as a function of depth by tilting the sample (or *angle resolved XPS*)

Chemical States from XPS analyses

The ability to produce Chemical State information from the topmost 1-12 nm of any surface makes XPS a unique and invaluable tool for understanding the chemistry of any surface either, as received, or after physical or chemical treatment(s). Because modern systems use monochromatic X-ray sources, XPS measurements leave the surface free of any degradation with few exceptions.

Chemical state analysis of the surface of polymers readily reveals the presence or absence of the chemical states of carbon known as: carbide (C^{2-}), hydrocarbon (C-C), alcohol (C-OH), ketone (C=O), organic ester (COOR), carbonate (CO_3), fluoro-hydrocarbon (CF_2-CH_2), trifluorocarbon (CF_3).

Chemical state analysis of the surface of a silicon wafer readily reveals the presence or absence of the chemical states of silicon known as: n-doped silicon, p-doped silicon, silicon suboxide (Si_2O), silicon monoxide (SiO), Si_2O_3, silicon dioxide (SiO_2).

Industries that use XPS

- Adhesion
- Agriculture
- Automotive
- battery
- Biotechnology
- Canning
- Catalyst
- Ceramic
- Chemical
- Computer
- Cosmetics
- Electronics
- Environmental
- Fabrics
- Food
- Fuel cells
- Geology
- Glass
- Laser

- Lighting
- Lubrication
- Magnetic memory
- Mineralogy
- Mining
- Nanotechnology
- Nuclear
- Packaging
- Paper and wood
- Plating
- Polymer and plastic
- Printing
- Recording
- Semiconductor
- Steel
- Textiles
- Thin-film coating
- Welding

Routine limits of XPS

Quantitative accuracy

- XPS is widely used to generate empirical formula because it readily yields excellent quantitative accuracy from homogeneous solid state materials
- Quantitative accuracy depends on several parameters such as: signal-to-noise ratio, peak intensity, accuracy of relative sensitivity factors, correction for electron transmission function, surface volume homogeneity, correction for energy dependency of electron mean free path, and degree of sample degradation due to analysis.
- Under optimum conditions, the quantitative accuracy of the atomic percent (at%) values calculated from the **Major XPS Peaks** is 90-95% for each major peak. If a high level quality control protocol is used, the accuracy can be further improved.
- Under routine work conditions, where the surface is a mixture of contamination and expected material, the accuracy ranges from 80-90% of the value reported in atomic percent values.
- The quantitative accuracy for the weaker XPS signals, that have peak intensities 10-20% of the strongest signal, are 60-80% of the true value.

Analysis time

- 1–10 minutes for a survey scan that measures the amount of all elements, 1– 10 minutes for high energy resolution scans that reveal chemical state differences, 1–4 hours for a depth profile that measures 4– 5 elements as a function of etched depth (usual final depth is 1,000 nm)

Detection limits

- 0.1–1.0 at% (0.1 at% = 1 part per thousand = 1000 ppm). (Ultimate detection limit for most elements is approximately 100 ppm, which requires 8–16 hours.)

Measured area

- Measured area depends on instrument design. The minimum analysis area ranges from 10 to 200 micrometres. Largest size for a monochromatic beam of X-rays is 1–5 mm. Non-monochromatic beams are 10–50 mm in diameter. Spectroscopic image resolution levels of 200 nm or below has been achieved on latest imaging XPS instruments using synchrotron radiation as X-ray source.

Sample size limits

- Older instruments accept samples: 1×1 to 3×3 cm. Present systems can accept samples up to 30×30 cm.

Degradation during analysis

- Depends on the sensitivity of the material to the wavelength of X-rays used, the total dose of the X-rays, the temperature of the surface and the level of the vacuum. Metals, alloys, ceramics and most glasses are not measurably degraded by either non-monochromatic or monochromatic X-rays. Some, but not all, polymers, catalysts, certain highly oxygenated compounds, various inorganic compounds and fine organics are degraded by either monochromatic or non-monochromatic X-ray sources.
- Non-monochromatic X-ray sources produce a significant amount of high energy Bremsstrahlung X-rays (1– 15 keV of energy) which directly degrade the surface chemistry of various materials. Non-monochromatic X-ray sources also produce a significant amount of heat (100 to 200 °C) on the surface of the sample because the anode that produces the X-rays is typically only 1 to 5 cm (2 in) away from the sample. This level of heat, when combined with the Bremsstrahlung X-rays, acts synergistically to increase the amount and rate of degradation for certain materials. Monochromatic X-ray sources, because they are far away (50– 100 cm) from the sample, do not produce any heat effects. Monochromatic X-ray sources are monochromatic because the quartz monochromator system diffracted the Bremsstrahlung X-rays out of the X-ray beam which means the sample only sees one X-ray energy, for example: 1.486 keV if aluminium K-alpha X-rays are used.
- Because the vacuum removes various gases (e.g. O_2, CO) and liquids (e.g. water, alcohol, solvents) that were initially trapped within or on the surface of the sample, the chemistry and morphology of the surface will continue to change until the surface achieves a steady state. This type of degradation is sometimes difficult to detect.

Materials routinely analyzed by XPS

Inorganic compounds, metal alloys, semiconductors, polymers, pure elements, catalysts, glasses, ceramics, paints, papers, inks, woods, plant parts, make-up, teeth, bones, human implants, biomaterials, viscous oils, glues, ion modified materials

Organic chemicals are not routinely analyzed by XPS because they are readily degraded by either the energy of the X-rays or the heat from non-monochromatic X-ray sources.

Analysis details

Charge compensation techniques

- Low-voltage electron beam (1-20 eV) (or electron flood gun)
- UV light
- Low-voltage argon ion beam with low-voltage electron beam (1-10 eV)
- Aperture mask
- Mesh screen with low-voltage electron beam

Sample preparation

- Sample handling
- Sample cleaning
- Sample mounting

Data processing

Peak identification

The identification of peaks in any survey spectrum is possible because Prof. Kai Siegbahn improved the energy resolution of his XPS instrument to the point that observed signals were both tall and narrow with respect to the energy range measured (0-1400 eV). In the course of improving his XPS instruments, he collected spectra from pure conductive elements. That collection of spectra yielded peaks with energies (reported as BEs) that are characteristic for each specific element. The number of peaks produced by a single element varies from 1 to more than 20. Tables of binding energies (BEs) that identify the shell and spin-orbit of each peak produced by a given element are included with modern XPS instruments, and can be found in various handbooks and websites . Because these experimentally determined BEs are characteristic of specific elements, they can be directly used to identify experimentally measured peaks of a material with unknown elemental composition.

Before beginning the process of peak identification, the analyst must determine if the BEs of the unprocessed survey spectrum (0-1400 eV) have or have not been shifted due to a

positive or negative surface charge. This is most often done by looking for two peaks that due to the presence of carbon and oxygen. {tbc}

Charge referencing insulators

Charge referencing is needed when a sample suffers either a positive (+) or negative (-) charge induced shift of experimental BEs. Charge referencing is needed to obtain meaningful BEs from both wide-scan, high sensitivity (low energy resolution) survey spectra (0-1100 eV), and also narrow-scan, chemical state (high energy resolution) spectra.

Charge induced shifting causes experimentally measured BEs of XPS peaks to appear at BEs that are greater or smaller than true BEs. Charge referencing is performed by adding or subtracting a "Charge Correction Factor" to each of the experimentally measured BEs. In general, the BE of the hydrocarbon peak of the C (1s) XPS signal is used to charge reference (charge correct) all BEs obtained from non-conductive (insulating) samples or conductors that have been deliberately insulated from the sample mount.

Charge induced shifting is normally due to: a modest excess of low voltage (-1 to -20 eV) electrons attached to the surface, or a modest shortage of electrons (+1 to +15 eV) within the top 1-12 nm of the sample caused by the loss of photo-emitted electrons. The degree of charging depends on various factors. If, by chance, the charging of the surface is excessively positive, then the spectrum might appear as a series of rolling hills, not sharp peaks as shown in the example spectrum.

The C (1s) BE of the hydrocarbon species (moieties) of the "Adventitious" carbon that appears on all, air-exposed, conductive and semi-conductive materials is normally found between 284.5 eV and 285.5 eV. For convenience, the C (1s) of hydrocarbon moieties is defined to appear between 284.6 eV and 285.0 eV. A value of 284.8 eV has become popular in recent years. However, some recent reports indicate that 284.9 eV or 285.0 eV represents hydrocarbons attached on metals, not the natural native oxide. The 284.8 eV BE is routinely used as the "Reference BE" for charge referencing insulators. When the C (1s) BE is used for charge referencing, then the charge correction factor is the difference between 284.8 eV and the experimentally measured C (1s) BE of the hydrocarbon moieties.

When using a monochromatic XPS system together with a low voltage electron flood gun for charge compensation the experimental BEs of the C (1s) hydrocarbon peak is often 4-5 eV smaller than the reference BE value (284.8 eV). In this case, all experimental BEs appear at lower BEs than expected and need to be increased by adding a value ranging from 4 to 5 eV. Non-monochromatic XPS systems are not usually equipped with a low voltage electron flood gun so the BEs will normally appear at higher BEs than expected. It is normal to subtract a charge correction factor from all BEs produced by a non-monochromatic XPS system.

Conductive materials and most native oxides of conductors should never need charge referencing. Conductive materials should never be charge referenced unless the topmost layer of the sample has a thick non-conductive film.

Peak-fitting

The process of peak-fitting high energy resolution XPS spectra is still a mixture of art, science, knowledge and experience. The peak-fit process is affected by instrument design, instrument components, experimental settings (aka analysis conditions) and sample variables. Most instrument parameters are constant while others depend on the choice of experimental settings.

Before starting any peak-fit effort, the analyst performing the peak-fit needs to know if the topmost 15 nm of the sample is expected to be a homogeneous material or is expected to be a mixture of materials. If the top 15 nm is a homogeneous material with only very minor amounts of adventitious carbon and adsorbed gases, then the analyst can use theoretical peak area ratios to enhance the peak-fitting process.

Variables that affect or define peak-fit results include:

- FWHMs
- Chemical Shifts
- Peakshapes
- Instrument design factors
- Experimental settings
- Sample factors

FWHMs

When using high energy resolution experiment settings on an XPS equipped with a monochromatic Al K-alpha X-ray source, the FWHM of the major XPS peaks range from 0.3 eV to 1.7 eV. The following is a simple summary of FWHM from major XPS signals:

- Main metal peaks (e.g. 1s, 2p3, 3d5, 4f7) from pure metals have FWHMs that range from 0.30 eV to 1.0 eV
- Main metal peaks (e.g. 1s, 2p3, 3d5, 4f7) from binary metal oxides have FWHMs that range from 0.9 eV to 1.7 eV
- The O (1s) peak from binary metal oxides have FWHMs that, in general, range from 1.0 eV to 1.4 eV
- The C (1s) peak from adventitious hydrocarbons have FWHMs that, in general, range from 1.0 eV to 1.4 eV

Chemical Shifts

Chemical shift values depend on the degree of electron bond polarization between nearest neighbor atoms. A specific chemical shift is the difference in BE values of one specific chemical state versus the BE of the pure element.

Peaks derived from peak-fitting a raw chemical state spectrum are due to the presence of different chemical states.

Peakshapes

Depends on instrument parameters, experimental parameters and sample characteristics

Instrument design factors

FWHM and purity of X-rays used (monochromatic Al, non-monochromatic Mg, Synchrotron, Ag, Zr...)
Design of electron analyzer (CMA, HSA, retarding field...)

Experiment settings

Settings of the electron analyzer (e.g. pass energy, step size)

Sample factors

Physical form of the sample (single crystal, polished, powder, corroded...)
Number of physical defects within the analysis volume (from Argon ion etching, from laser cleaning...)

WT

Chapter- 8

X-ray crystallography (Technique for Nanoparticle Characterization)

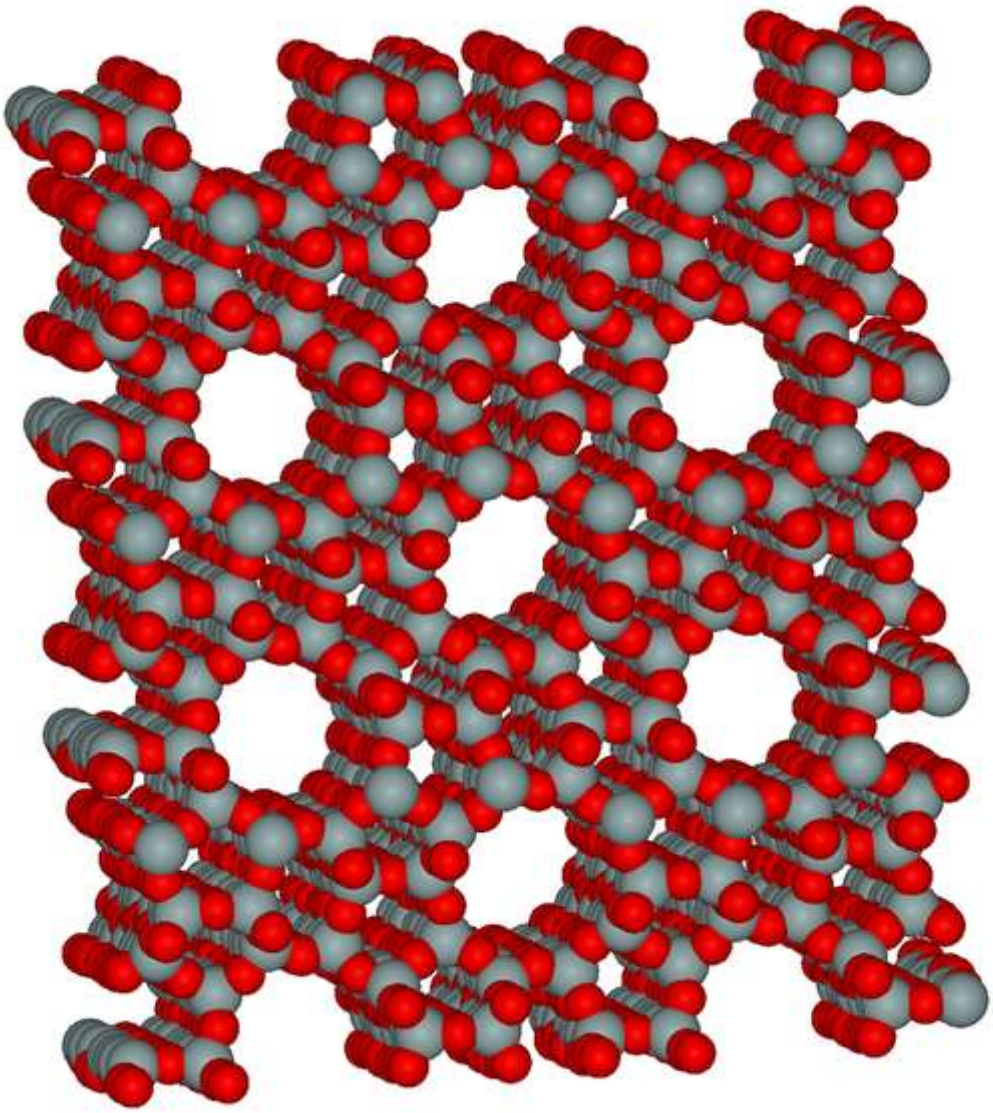

X-ray crystallography can locate every atom in a zeolite, an aluminosilicate with many important applications, such as water purification.

X-ray crystallography is a method of determining the arrangement of atoms within a crystal, in which a beam of X-rays strikes a crystal and diffracts into many specific directions. From the angles and intensities of these diffracted beams, a crystallographer can produce a three-dimensional picture of the density of electrons within the crystal. From this electron density, the mean positions of the atoms in the crystal can be determined, as well as their chemical bonds, their disorder and various other information.

Since many materials can form crystals — such as salts, metals, minerals, semiconductors, as well as various inorganic, organic and biological molecules — X-ray crystallography has been fundamental in the development of many scientific fields. In its first decades of use, this method determined the size of atoms, the lengths and types of chemical bonds, and the atomic-scale differences among various materials, especially minerals and alloys. The method also revealed the structure and functioning of many biological molecules, including vitamins, drugs, proteins and nucleic acids such as DNA. X-ray crystallography is still the chief method for characterizing the atomic structure of new materials and in discerning materials that appear similar by other experiments. X-ray crystal structures can also account for unusual electronic or elastic properties of a material, shed light on chemical interactions and processes, or serve as the basis for designing pharmaceuticals against diseases.

In an X-ray diffraction measurement, a crystal is mounted on a goniometer and gradually rotated while being bombarded with X-rays, producing a diffraction pattern of regularly spaced spots known as *reflections*. The two-dimensional images taken at different rotations are converted into a three-dimensional model of the density of electrons within the crystal using the mathematical method of Fourier transforms, combined with chemical data known for the sample. Poor resolution (fuzziness) or even errors may result if the crystals are too small, or not uniform enough in their internal makeup.

X-ray crystallography is related to several other methods for determining atomic structures. Similar diffraction patterns can be produced by scattering electrons or neutrons, which are likewise interpreted as a Fourier transform. If single crystals of sufficient size cannot be obtained, various other X-ray methods can be applied to obtain less detailed information; such methods include fiber diffraction, powder diffraction and small-angle X-ray scattering (SAXS). If the material under investigation is only available in the form of nanocrystalline powders or suffers from poor crystallinity, the methods of electron crystallography can be applied for determining the atomic structure.

For all above mentioned X-ray diffraction methods, the scattering is elastic; the scattered X-rays have the same wavelength as the incoming X-ray. By contrast, *inelastic* X-ray scattering methods are useful in studying excitations of the sample, rather than the distribution of its atoms.

History

Early scientific history of crystals and X-rays

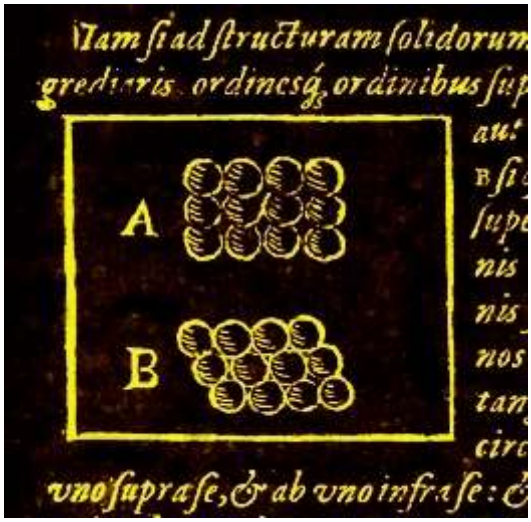

Drawing of square (Figure A, above) and hexagonal (Figure B, below) packing from Kepler's work, *Strena seu de Nive Sexangula*.

Crystals have long been admired for their regularity and symmetry, but they were not investigated scientifically until the 17th century. Johannes Kepler hypothesized in his work *Strena seu de Nive Sexangula* (1611) that the hexagonal symmetry of snowflake crystals was due to a regular packing of spherical water particles.

As shown by X-ray crystallography, the hexagonal symmetry of snowflakes results from the tetrahedral arrangement of hydrogen bonds about each water molecule. The water molecules are arranged similarly to the silicon atoms in the tridymite polymorph of SiO_2.

The resulting crystal structure has hexagonal symmetry when viewed along a principal axis.

Crystal symmetry was first investigated experimentally by Nicolas Steno (1669), who showed that the angles between the faces are the same in every exemplar of a particular type of crystal, and by René Just Haüy (1784), who discovered that every face of a crystal can be described by simple stacking patterns of blocks of the same shape and size. Hence, William Hallowes Miller in 1839 was able to give each face a unique label of three small integers, the Miller indices which are still used today for identifying crystal faces. Haüy's study led to the correct idea that crystals are a regular three-dimensional array (a Bravais lattice) of atoms and molecules; a single unit cell is repeated indefinitely along three principal directions that are not necessarily perpendicular. In the 19th century, a complete catalog of the possible symmetries of a crystal was worked out by Johann Hessel, Auguste Bravais, Yevgraf Fyodorov, Arthur Schönflies and (belatedly) William Barlow. From the available data and physical reasoning, Barlow proposed several crystal structures in the 1880s that were validated later by X-ray crystallography; however, the available data were too scarce in the 1880s to accept his models as conclusive.

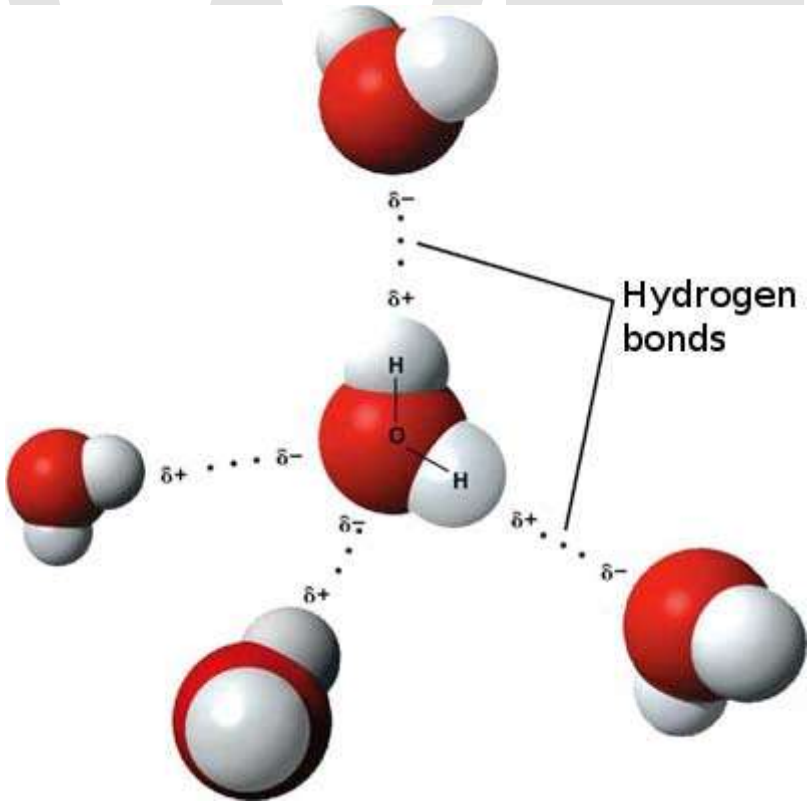

X-ray crystallography shows the arrangement of water molecules in ice, revealing the hydrogen bonds that hold the solid together. Few other methods can determine the structure of matter with such sub-atomic precision (*resolution*).

X-rays were discovered by Wilhelm Conrad Röntgen in 1895, just as the studies of crystal symmetry were being concluded. Physicists were initially uncertain of the nature

of X-rays, although it was soon suspected (correctly) that they were waves of electromagnetic radiation, in other words, another form of light. At that time, the wave model of light — specifically, the Maxwell theory of electromagnetic radiation — was well accepted among scientists, and experiments by Charles Glover Barkla showed that X-rays exhibited phenomena associated with electromagnetic waves, including transverse polarization and spectral lines akin to those observed in the visible wavelengths. Single-slit experiments in the laboratory of Arnold Sommerfeld suggested the wavelength of X-rays was about 1 Angström. However, X-rays are composed of photons, and thus are not only waves of electromagnetic radiation but also exhibit particle-like properties. The photon concept was introduced by Albert Einstein in 1905, but it was not broadly accepted until 1922, when Arthur Compton confirmed it by the scattering of X-rays from electrons. Therefore, these particle-like properties of X-rays, such as their ionization of gases, caused William Henry Bragg to argue in 1907 that X-rays were *not* electromagnetic radiation. Nevertheless, Bragg's view was not broadly accepted and the observation of X-ray diffraction in 1912 confirmed for most scientists that X-rays were a form of electromagnetic radiation.

X-ray analysis of crystals

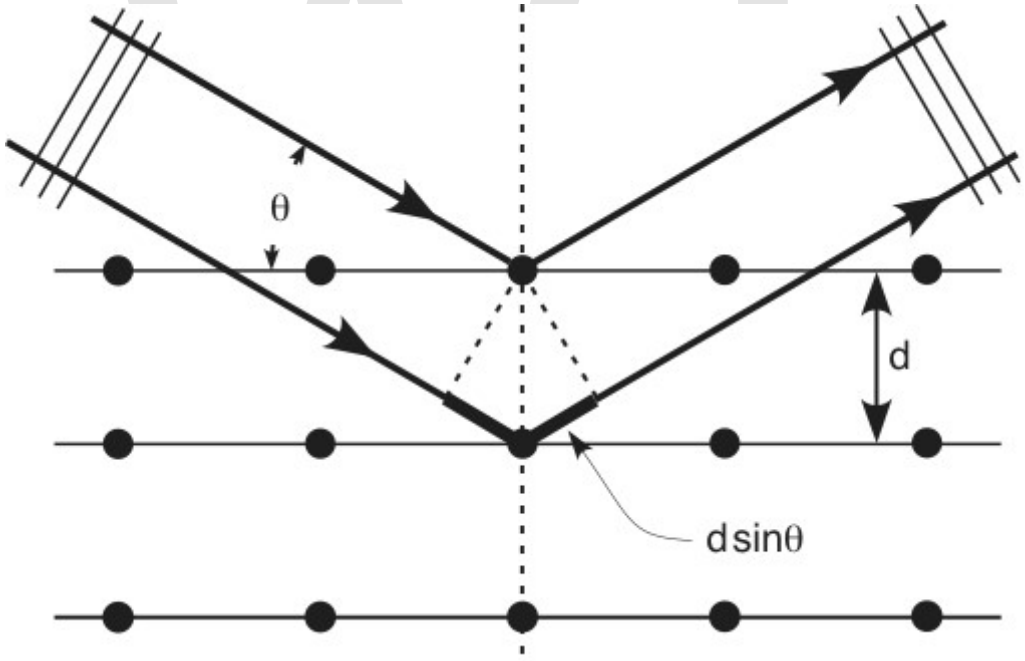

The incoming beam (coming from upper left) causes each scatterer to re-radiate a small portion of its intensity as a spherical wave. If scatterers are arranged symmetrically with a separation *d*, these spherical waves will be in sync (add constructively) only in directions where their path-length difference $2d \sin\theta$ equals an integer multiple of the wavelength λ. In that case, part of the incoming beam is deflected by an angle 2θ, producing a *reflection* spot in the diffraction pattern.

Crystals are regular arrays of atoms, and X-rays can be considered waves of electromagnetic radiation. Atoms scatter X-ray waves, primarily through the atoms' electrons. Just as an ocean wave striking a lighthouse produces secondary circular waves emanating from the lighthouse, so an X-ray striking an electron produces secondary spherical waves emanating from the electron. This phenomenon is known as elastic scattering, and the electron (or lighthouse) is known as the *scatterer*. A regular array of scatterers produces a regular array of spherical waves. Although these waves cancel one another out in most directions through destructive interference, they add constructively in a few specific directions, determined by Bragg's law:

$$2d \sin \theta = n\lambda$$

Here d is the spacing between diffracting planes, θ is the incident angle, n is any integer, and λ is the wavelength of the beam. These specific directions appear as spots on the diffraction pattern called *reflections*. Thus, X-ray diffraction results from an electromagnetic wave (the X-ray) impinging on a regular array of scatterers (the repeating arrangement of atoms within the crystal).

X-rays are used to produce the diffraction pattern because their wavelength λ is typically the same order of magnitude (1-100 Ångströms) as the spacing d between planes in the crystal. In principle, any wave impinging on a regular array of scatterers produces diffraction, as predicted first by Francesco Maria Grimaldi in 1665. To produce significant diffraction, the spacing between the scatterers and the wavelength of the impinging wave should be similar in size. For illustration, the diffraction of sunlight through a bird's feather was first reported by James Gregory in the later 17th century. The first artificial diffraction gratings for visible light were constructed by David Rittenhouse in 1787, and Joseph von Fraunhofer in 1821. However, visible light has too long a wavelength (typically, 5500 Ångströms) to observe diffraction from crystals. Prior to the first X-ray diffraction experiments, the spacings between lattice planes in a crystal were not known with certainty.

The idea that crystals could be used as a diffraction grating for X-rays arose in 1912 in a conversation between Paul Peter Ewald and Max von Laue in the English Garden in Munich. Ewald had proposed a resonator model of crystals for his thesis, but this model could not be validated using visible light, since the wavelength was much larger than the spacing between the resonators. Von Laue realized that electromagnetic radiation of a shorter wavelength was needed to observe such small spacings, and suggested that X-rays might have a wavelength comparable to the unit-cell spacing in crystals. Von Laue worked with two technicians, Walter Friedrich and his assistant Paul Knipping, to shine a beam of X-rays through a copper sulfate crystal and record its diffraction on a photographic plate. After being developed, the plate showed a large number of well-defined spots arranged in a pattern of intersecting circles around the spot produced by the central beam. Von Laue developed a law that connects the scattering angles and the size and orientation of the unit-cell spacings in the crystal, for which he was awarded the Nobel Prize in Physics in 1914.

As described in the mathematical derivation below, the X-ray scattering is determined by the density of electrons within the crystal. Since the energy of an X-ray is much greater than that of a valence electron, the scattering may be modeled as Thomson scattering, the interaction of an electromagnetic ray with a free electron. This model is generally adopted to describe the polarization of the scattered radiation. The intensity of Thomson scattering declines as $1/m^2$ with the mass m of the charged particle that is scattering the radiation; hence, the atomic nuclei, which are thousands of times heavier than an electron, contribute negligibly to the scattered X-rays.

Development from 1912 to 1920

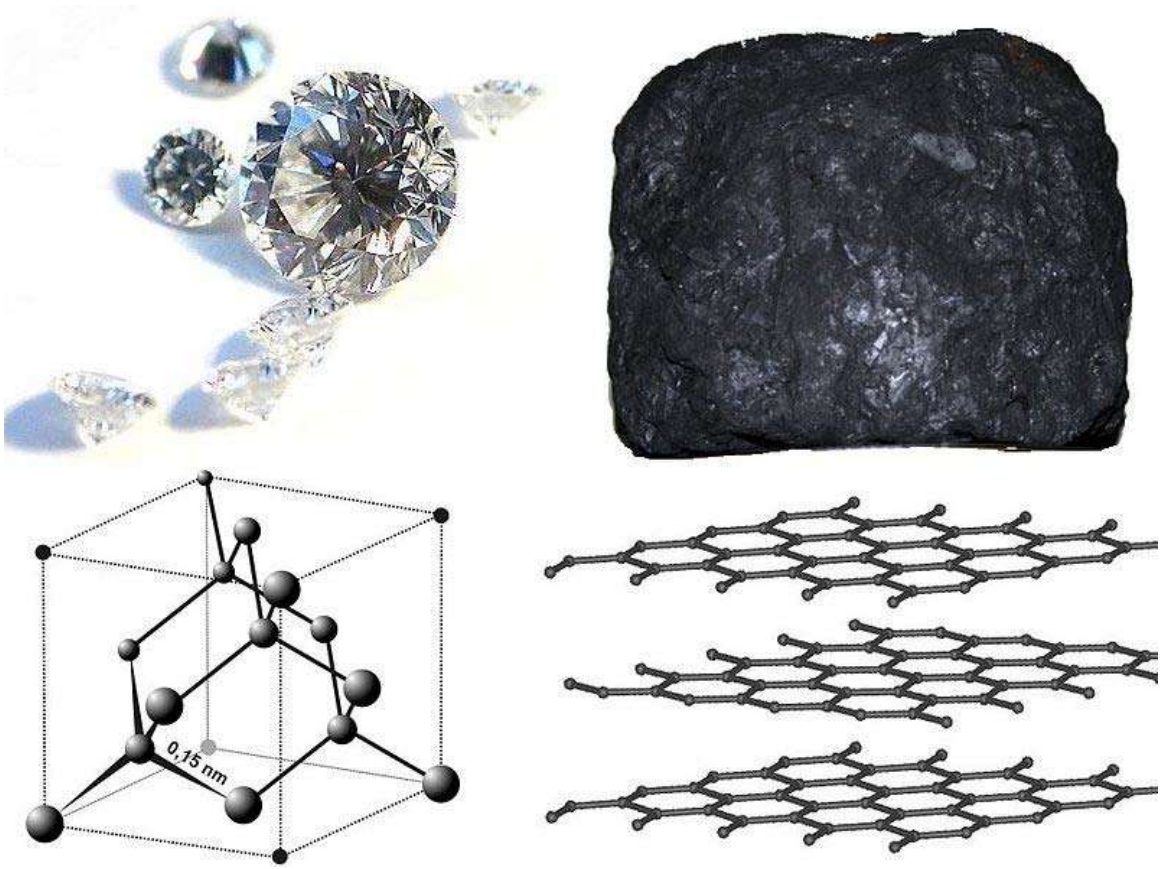

Although diamonds (top left) and graphite (top right) are identical in chemical composition — being both pure carbon — X-ray crystallography revealed the arrangement of their atoms (bottom) accounts for their different properties. In diamond, the carbon atoms are arranged tetrahedrally and held together by single covalent bonds, making it strong in all directions. By contrast, graphite is composed of stacked sheets. Within the sheet, the bonding is covalent and has hexagonal symmetry, but there are no covalent bonds between the sheets, making graphite easy to cleave into flakes.

After Von Laue's pioneering research, the field developed rapidly, most notably by physicists William Lawrence Bragg and his father William Henry Bragg. In 1912-1913, the younger Bragg developed Bragg's law, which connects the observed scattering with

reflections from evenly spaced planes within the crystal. The Braggs, father and son, shared the 1915 Nobel Prize in Physics for their work in crystallography. The earliest structures were generally simple and marked by one-dimensional symmetry. However, as computational and experimental methods improved over the next decades, it became feasible to deduce reliable atomic positions for more complicated two- and three-dimensional arrangements of atoms in the unit-cell.

The potential of X-ray crystallography for determining the structure of molecules and minerals — then only known vaguely from chemical and hydrodynamic experiments — was realized immediately. The earliest structures were simple inorganic crystals and minerals, but even these revealed fundamental laws of physics and chemistry. The first atomic-resolution structure to be "solved" (i.e. determined) in 1914 was that of table salt. The distribution of electrons in the table-salt structure showed that crystals are not necessarily composed of covalently bonded molecules, and proved the existence of ionic compounds. The structure of diamond was solved in the same year, proving the tetrahedral arrangement of its chemical bonds and showing that the length of C–C single bond was 1.52 Ångströms. Other early structures included copper, calcium fluoride (CaF_2, also known as *fluorite*), calcite ($CaCO_3$) and pyrite (FeS_2) in 1914; spinel ($MgAl_2O_4$) in 1915; the rutile and anatase forms of titanium dioxide (TiO_2) in 1916; pyrochroite $Mn(OH)_2$ and, by extension, brucite $Mg(OH)_2$ in 1919;. Also in 1919 sodium nitrate ($NaNO_3$) and cesium dichloroiodide ($CsICl_2$) were determined by Ralph Walter Graystone Wyckoff, and the wurtzite (hexagonal ZnS) structure became known in 1920.

The structure of graphite was solved in 1916 by the related method of powder diffraction, which was developed by Peter Debye and Paul Scherrer and, independently, by Albert Hull in 1917. The structure of graphite was determined from single-crystal diffraction in 1924 by two groups independently. Hull also used the powder method to determine the structures of various metals, such as iron and magnesium.

Contributions to chemistry and material science

X-ray crystallography has led to a better understanding of chemical bonds and non-covalent interactions. The initial studies revealed the typical radii of atoms, and confirmed many theoretical models of chemical bonding, such as the tetrahedral bonding of carbon in the diamond structure, the octahedral bonding of metals observed in ammonium hexachloroplatinate (IV), and the resonance observed in the planar carbonate group and in aromatic molecules. Kathleen Lonsdale's 1928 structure of hexamethylbenzene established the hexagonal symmetry of benzene and showed a clear difference in bond length between the aliphatic C–C bonds and aromatic C–C bonds; this finding led to the idea of resonance between chemical bonds, which had profound consequences for the development of chemistry. Her conclusions were anticipated by William Henry Bragg, who published models of naphthalene and anthracene in 1921 based on other molecules, an early form of molecular replacement.

Also in the 1920s, Victor Moritz Goldschmidt and later Linus Pauling developed rules for eliminating chemically unlikely structures and for determining the relative sizes of atoms. These rules led to the structure of brookite (1928) and an understanding of the relative stability of the rutile, brookite and anatase forms of titanium dioxide.

The distance between two bonded atoms is a sensitive measure of the bond strength and its bond order; thus, X-ray crystallographic studies have led to the discovery of even more exotic types of bonding in inorganic chemistry, such as metal-metal double bonds, metal-metal quadruple bonds, and three-center, two-electron bonds. X-ray crystallography — or, strictly speaking, an inelastic Compton scattering experiment — has also provided evidence for the partly covalent character of hydrogen bonds. In the field of organometallic chemistry, the X-ray structure of ferrocene initiated scientific studies of sandwich compounds, while that of Zeise's salt stimulated research into "back bonding" and metal-pi complexes. Finally, X-ray crystallography had a pioneering role in the development of supramolecular chemistry, particularly in clarifying the structures of the crown ethers and the principles of host-guest chemistry.

In material sciences, many complicated inorganic and organometallic systems have been analyzed using single-crystal methods, such as fullerenes, metalloporphyrins, and other complicated compounds. Single-crystal diffraction is also used in the pharmaceutical industry, due to recent problems with polymorphs. The major factors affecting the quality of single-crystal structures are the crystal's size and regularity; recrystallization is a commonly used technique to improve these factors in small-molecule crystals. The Cambridge Structural Database contains over 500,000 structures; over 99% of these structures were determined by X-ray diffraction.

Mineralogy and metallurgy

Since the 1920s, X-ray diffraction has been the principal method for determining the arrangement of atoms in minerals and metals. The application of X-ray crystallography to mineralogy began with the structure of garnet, which was determined in 1924 by Menzer. A systematic X-ray crystallographic study of the silicates was undertaken in the 1920s. This study showed that, as the Si/O ratio is altered, the silicate crystals exhibit significant changes in their atomic arrangements. Machatschki extended these insights to minerals in which aluminium substitutes for the silicon atoms of the silicates. The first application of X-ray crystallography to metallurgy likewise occurred in the mid-1920s. Most notably, Linus Pauling's structure of the alloy Mg_2Sn led to his theory of the stability and structure of complex ionic crystals.

Early organic and small biological molecules

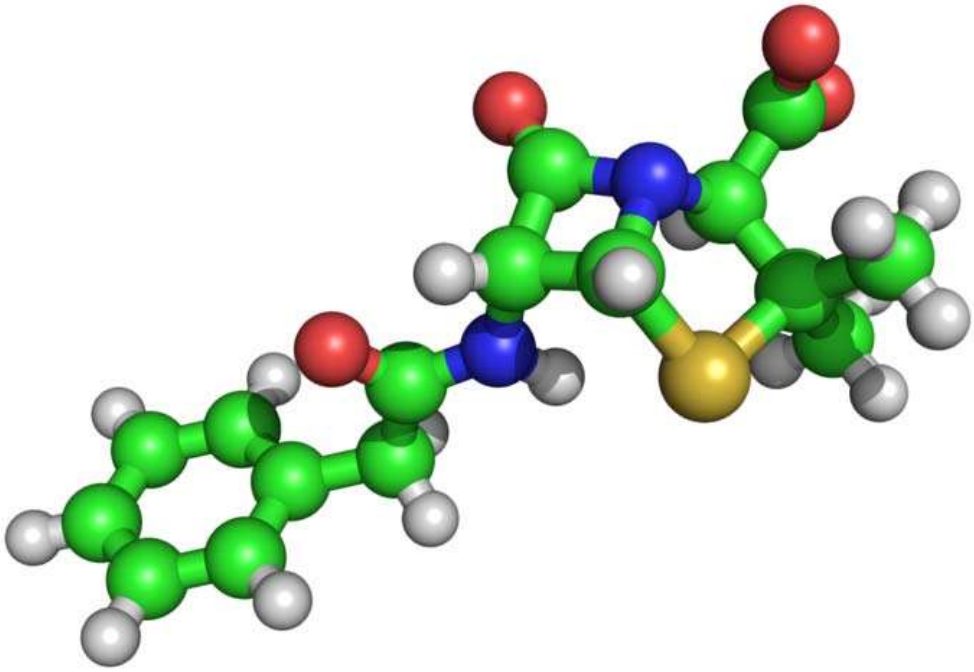

The three-dimensional structure of penicillin, for which Dorothy Crowfoot Hodgkin was awarded the Nobel Prize in Chemistry in 1964. The green, white, red, yellow and blue spheres represent atoms of carbon, hydrogen, oxygen, sulfur and nitrogen, respectively.

The first structure of an organic compound, hexamethylenetetramine, was solved in 1923. This was followed by several studies of long-chain fatty acids, which are an important component of biological membranes. In the 1930s, the structures of much larger molecules with two-dimensional complexity began to be solved. A significant advance was the structure of phthalocyanine, a large planar molecule that is closely related to porphyrin molecules important in biology, such as heme, corrin and chlorophyll.

X-ray crystallography of biological molecules took off with Dorothy Crowfoot Hodgkin, who solved the structures of cholesterol (1937), vitamin B12 (1945) and penicillin (1954), for which she was awarded the Nobel Prize in Chemistry in 1964. In 1969, she succeeded in solving the structure of insulin, on which she worked for over thirty years.

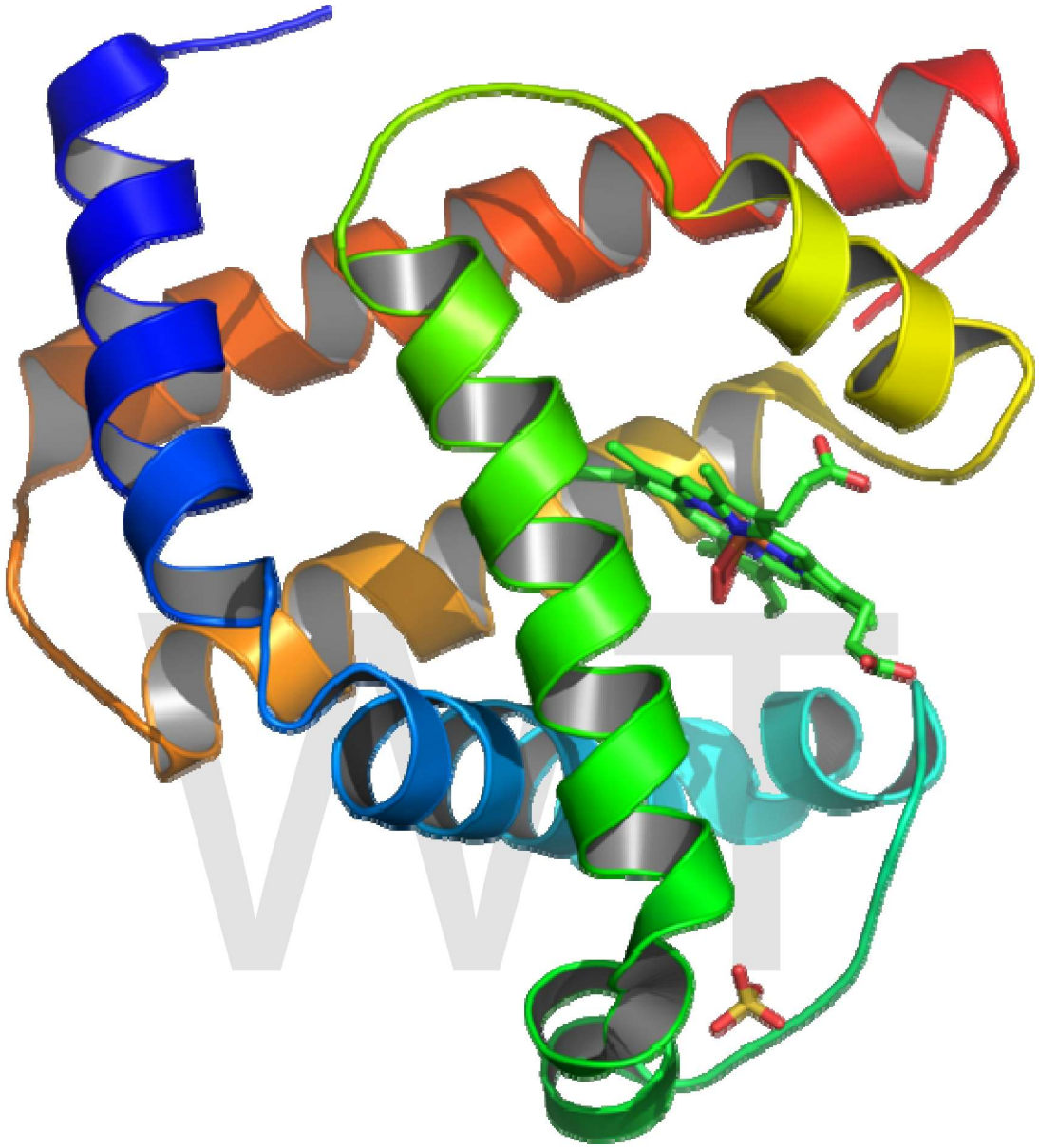

Ribbon diagram of the structure of myoglobin, showing colored alpha helices. Such proteins are long, linear molecules with thousands of atoms; yet the relative position of each atom has been determined with sub-atomic resolution by X-ray crystallography. Since it is difficult to visualize all the atoms at once, the ribbon shows the rough path of the protein polymer from its N-terminus (blue) to its C-terminus (red).

Biological macromolecular crystallography

Crystal structures of proteins (which are irregular and hundreds of times larger than cholesterol) began to be solved in the late 1950s, beginning with the structure of sperm whale myoglobin by Max Perutz and Sir John Cowdery Kendrew, for which they were awarded the Nobel Prize in Chemistry in 1962. Since that success, over 48970 X-ray crystal structures of proteins, nucleic acids and other biological molecules have been

determined. For comparison, the nearest competing method in terms of structures analyzed is nuclear magnetic resonance (NMR) spectroscopy, which has resolved 7806 chemical structures. Moreover, crystallography can solve structures of arbitrarily large molecules, whereas solution-state NMR is restricted to relatively small ones (less than 70 kDa). X-ray crystallography is now used routinely by scientists to determine how a pharmaceutical drug interacts with its protein target and what changes might improve it. However, intrinsic membrane proteins remain challenging to crystallize because they require detergents or other means to solubilize them in isolation, and such detergents often interfere with crystallization. Such membrane proteins are a large component of the genome and include many proteins of great physiological importance, such as ion channels and receptors.

Relationship to other scattering techniques

Elastic vs. inelastic scattering

X-ray crystallography is a form of elastic scattering; the outgoing X-rays have the same energy, and thus same wavelength, as the incoming X-rays, only with altered direction. By contrast, *inelastic scattering* occurs when energy is transferred from the incoming X-ray to the crystal, e.g., by exciting an inner-shell electron to a higher energy level. Such inelastic scattering reduces the energy (or increases the wavelength) of the outgoing beam. Inelastic scattering is useful for probing such excitations of matter, but not in determining the distribution of scatterers within the matter, which is the goal of X-ray crystallography.

X-rays range in wavelength from 10 to 0.01 nanometers; a typical wavelength used for crystallography is 1 Å (0.1 nm), which is on the scale of covalent chemical bonds and the radius of a single atom. Longer-wavelength photons (such as ultraviolet radiation) would not have sufficient resolution to determine the atomic positions. At the other extreme, shorter-wavelength photons such as gamma rays are difficult to produce in large numbers, difficult to focus, and interact too strongly with matter, producing particle-antiparticle pairs. Therefore, X-rays are the "sweetspot" for wavelength when determining atomic-resolution structures from the scattering of electromagnetic radiation.

Other X-ray techniques

Other forms of elastic X-ray scattering include powder diffraction, SAXS and several types of X-ray fiber diffraction, which was used by Rosalind Franklin in determining the double-helix structure of DNA. In general, single-crystal X-ray diffraction offers more structural information than these other techniques; however, it requires a sufficiently large and regular crystal, which is not always available.

These scattering methods generally use *monochromatic* X-rays, which are restricted to a single wavelength with minor deviations. A broad spectrum of X-rays (that is, a blend of X-rays with different wavelengths) can also be used to carry out X-ray diffraction, a technique known as the Laue method. This is the method used in the original discovery of

X-ray diffraction. Laue scattering provides much structural information with only a short exposure to the X-ray beam, and is therefore used in structural studies of very rapid events (Time resolved crystallography). However, it is not as well-suited as monochromatic scattering for determining the full atomic structure of a crystal and therefore works better with crystals with relatively simple atomic arrangements.

The Laue back reflection mode records X-rays scattered backwards from a broad spectrum source. This is useful if the sample is too thick for X-rays to transmit through it. The diffracting planes in the crystal are determined by knowing that the normal to the diffracting plane bisects the angle between the incident beam and the diffracted beam. A Greninger chart can be used to interpret the back reflection Laue photograph.

Electron and neutron diffraction

Other particles, such as electrons and neutrons, may be used to produce a diffraction pattern. Although electron, neutron, and X-ray scattering are based on different physical processes, the resulting diffraction patterns are analyzed using the same coherent diffraction imaging techniques.

As derived below, the electron density within the crystal and the diffraction patterns are related by a simple mathematical method, the Fourier transform, which allows the density to be calculated relatively easily from the patterns. However, this works only if the scattering is *weak*, i.e., if the scattered beams are much less intense than the incoming beam. Weakly scattered beams pass through the remainder of the crystal without undergoing a second scattering event. Such re-scattered waves are called "secondary scattering" and hinder the analysis. Any sufficiently thick crystal will produce secondary scattering, but since X-rays interact relatively weakly with the electrons, this is generally not a significant concern. By contrast, electron beams may produce strong secondary scattering even for relatively thin crystals (>100 nm). Since this thickness corresponds to the diameter of many viruses, a promising direction is the electron diffraction of isolated macromolecular assemblies, such as viral capsids and molecular machines, which may be carried out with a cryo-electron microscope. Moreover the strong interaction of electrons with matter (about 1000 times stronger than for X-rays) allows determination of the atomic structure of extremely small volumes. The field of applications for electron crystallography ranges from bio molecules like membrane proteins over organic thin films to the complex structures of (nanocrystalline) intermetallic compounds and zeolites.

Neutron diffraction is an excellent method for structure determination, although it has been difficult to obtain intense, monochromatic beams of neutrons in sufficient quantities. Traditionally, nuclear reactors have been used, although the new Spallation Neutron Source holds much promise in the near future. Being uncharged, neutrons scatter much more readily from the atomic nuclei rather than from the electrons. Therefore, neutron scattering is very useful for observing the positions of light atoms with few electrons, especially hydrogen, which is essentially invisible in the X-ray diffraction. Neutron scattering also has the remarkable property that the solvent can be made invisible by adjusting the ratio of normal water, H_2O, and heavy water, D_2O.

Methods

Overview of single-crystal X-ray diffraction

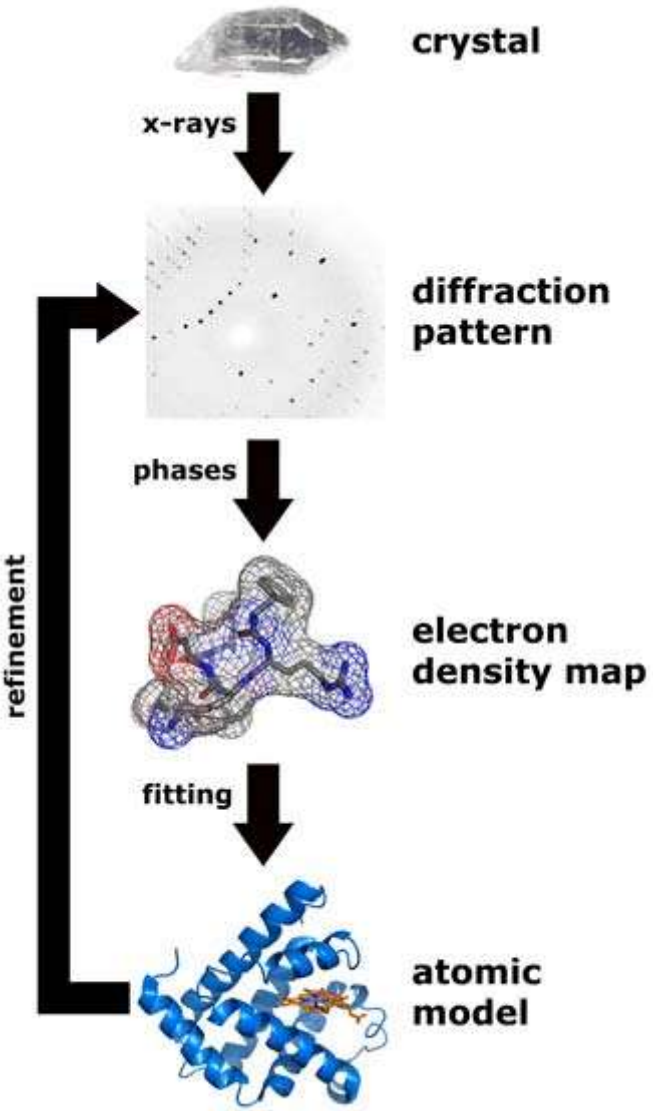

Workflow for solving the structure of a molecule by X-ray crystallography.

The oldest and most precise method of X-ray crystallography is *single-crystal X-ray diffraction*, in which a beam of X-rays strikes a single crystal, producing scattered beams. When they land on a piece of film or other detector, these beams make a *diffraction pattern* of spots; the strengths and angles of these beams are recorded as the crystal is gradually rotated. Each spot is called a *reflection*, since it corresponds to the reflection of the X-rays from one set of evenly spaced planes within the crystal. For single crystals of

sufficient purity and regularity, X-ray diffraction data can determine the mean chemical bond lengths and angles to within a few thousandths of an Ångström and to within a few tenths of a degree, respectively. The atoms in a crystal are not static, but oscillate about their mean positions, usually by less than a few tenths of an Ångström. X-ray crystallography allows measuring the size of these oscillations.

Procedure

The technique of single-crystal X-ray crystallography has three basic steps. The first — and often most difficult — step is to obtain an adequate crystal of the material under study. The crystal should be sufficiently large (typically larger than 0.1 mm in all dimensions), pure in composition and regular in structure, with no significant internal imperfections such as cracks or twinning.

In the second step, the crystal is placed in an intense beam of X-rays, usually of a single wavelength (*monochromatic X-rays*), producing the regular pattern of reflections. As the crystal is gradually rotated, previous reflections disappear and new ones appear; the intensity of every spot is recorded at every orientation of the crystal. Multiple data sets may have to be collected, with each set covering slightly more than half a full rotation of the crystal and typically containing tens of thousands of reflections.

In the third step, these data are combined computationally with complementary chemical information to produce and refine a model of the arrangement of atoms within the crystal. The final, refined model of the atomic arrangement — now called a *crystal structure* — is usually stored in a public database.

Limitations

As the crystal's repeating unit, its unit cell, becomes larger and more complex, the atomic-level picture provided by X-ray crystallography becomes less well-resolved (more "fuzzy") for a given number of observed reflections. Two limiting cases of X-ray crystallography—"small-molecule" and "macromolecular" crystallography—are often discerned. *Small-molecule crystallography* typically involves crystals with fewer than 100 atoms in their asymmetric unit; such crystal structures are usually so well resolved that the atoms can be discerned as isolated "blobs" of electron density. By contrast, *macromolecular crystallography* often involves tens of thousands of atoms in the unit cell. Such crystal structures are generally less well-resolved (more "smeared out"); the atoms and chemical bonds appear as tubes of electron density, rather than as isolated atoms. In general, small molecules are also easier to crystallize than macromolecules; however, X-ray crystallography has proven possible even for viruses with hundreds of thousands of atoms.

Crystallization

Although crystallography can be used to characterize the disorder in an impure or irregular crystal, crystallography generally requires a pure crystal of high regularity to

solve the structure of a complicated arrangement of atoms. Pure, regular crystals can sometimes be obtained from natural or synthetic materials, such as samples of metals, minerals or other macroscopic materials. The regularity of such crystals can sometimes be improved with macromolecular crystal annealing and other methods. However, in many cases, obtaining a diffraction-quality crystal is the chief barrier to solving its atomic-resolution structure.

Small-molecule and macromolecular crystallography differ in the range of possible techniques used to produce diffraction-quality crystals. Small molecules generally have few degrees of conformational freedom, and may be crystallized by a wide range of methods, such as chemical vapor deposition and recrystallization. By contrast, macromolecules generally have many degrees of freedom and their crystallization must be carried out to maintain a stable structure. For example, proteins and larger RNA molecules cannot be crystallized if their tertiary structure has been unfolded; therefore, the range of crystallization conditions is restricted to solution conditions in which such molecules remain folded.

Protein crystals are almost always grown in solution. The most common approach is to lower the solubility of its component molecules very gradually; if this is done too quickly, the molecules will precipitate from solution, forming a useless dust or amorphous gel on the bottom of the container. Crystal growth in solution is characterized by two steps: *nucleation* of a microscopic crystallite (possibly having only 100 molecules), followed by *growth* of that crystallite, ideally to a diffraction-quality crystal. The solution conditions that favor the first step (nucleation) are not always the same conditions that favor the second step (subsequent growth). The crystallographer's goal is to identify solution conditions that favor the development of a single, large crystal, since larger crystals offer improved resolution of the molecule. Consequently, the solution conditions should *disfavor* the first step (nucleation) but *favor* the second (growth), so that only one large crystal forms per droplet. If nucleation is favored too much, a shower of small crystallites will form in the droplet, rather than one large crystal; if favored too little, no crystal will form whatsoever.

It is extremely difficult to predict good conditions for nucleation or growth of well-ordered crystals. In practice, favorable conditions are identified by *screening*; a very large batch of the molecules is prepared, and a wide variety of crystallization solutions are tested. Hundreds, even thousands, of solution conditions are generally tried before finding the successful one. The various conditions can use one or more physical mechanisms to lower the solubility of the molecule; for example, some may change the pH, some contain salts of the Hofmeister series or chemicals that lower the dielectric constant of the solution, and still others contain large polymers such as polyethylene glycol that drive the molecule out of solution by entropic effects. It is also common to try several temperatures for encouraging crystallization, or to gradually lower the temperature so that the solution becomes supersaturated. These methods require large amounts of the target molecule, as they use high concentration of the molecule(s) to be crystallized. Due to the difficulty in obtaining such large quantities (milligrams) of crystallization grade protein, robots have been developed that are capable of accurately

dispensing crystallization trial drops that are in the order of 100 nanoliters in volume. This means that 10-fold less protein is used per-experiment when compared to crystallization trials setup by hand (in the order of 1 microliter).

Several factors are known to inhibit or mar crystallization. The growing crystals are generally held at a constant temperature and protected from shocks or vibrations that might disturb their crystallization. Impurities in the molecules or in the crystallization solutions are often inimical to crystallization. Conformational flexibility in the molecule also tends to make crystallization less likely, due to entropy. Ironically, molecules that tend to self-assemble into regular helices are often unwilling to assemble into crystals. Crystals can be marred by twinning, which can occur when a unit cell can pack equally favorably in multiple orientations; although recent advances in computational methods may allow solving the structure of some twinned crystals. Having failed to crystallize a target molecule, a crystallographer may try again with a slightly modified version of the molecule; even small changes in molecular properties can lead to large differences in crystallization behavior.

Data collection

Mounting the crystal

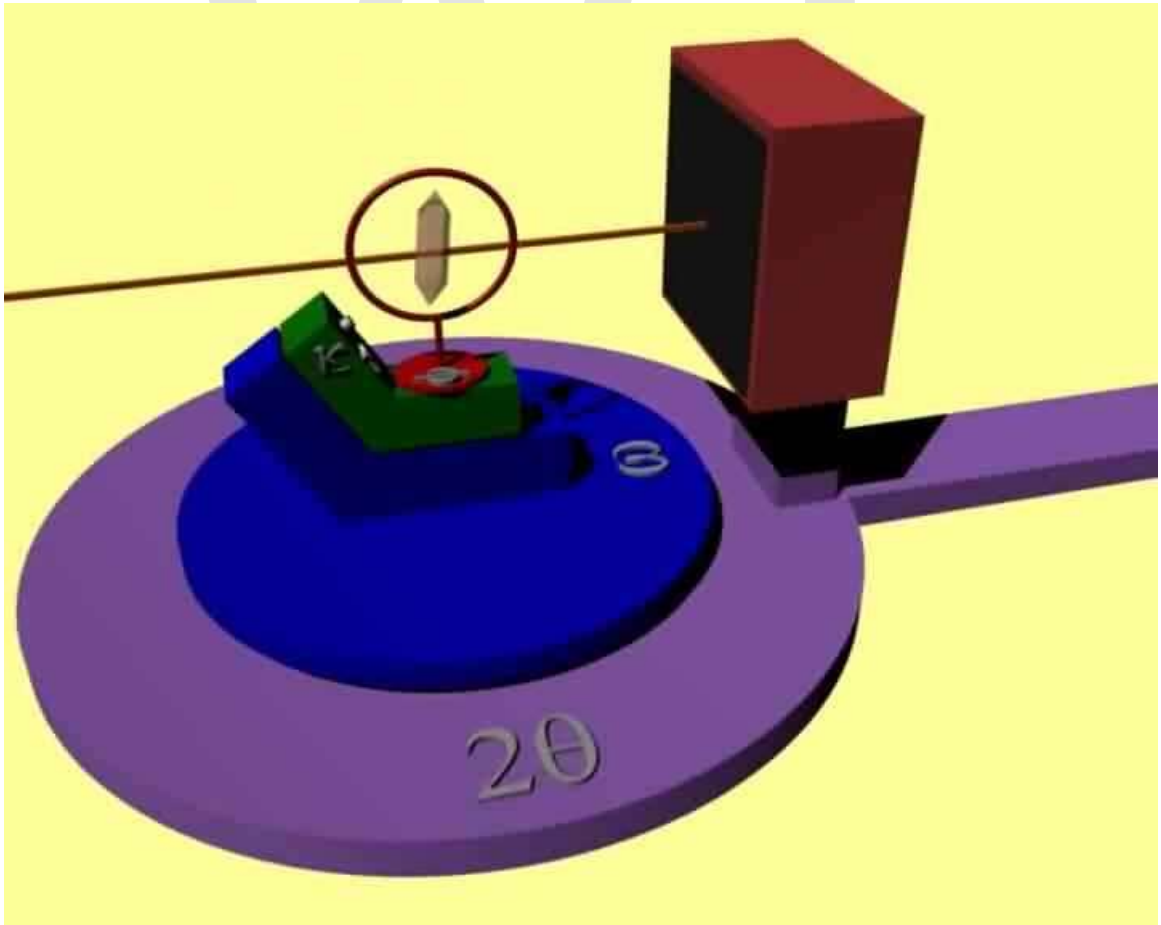

Animation showing the five motions possible with a four-circle kappa goniometer. The rotations about each of the four angles φ, κ, ω and 2θ leave the crystal within the X-ray beam, but change the crystal orientation. The detector (red box) can be slid closer or further away from the crystal, allowing higher resolution data to be taken (if closer) or better discernment of the Bragg peaks.

The crystal is mounted for measurements so that it may be held in the X-ray beam and rotated. There are several methods of mounting. Although crystals were once loaded into glass capillaries with the crystallization solution (the mother liquor), a modern approach is to scoop the crystal up in a tiny loop, made of nylon or plastic and attached to a solid rod, that is then flash-frozen with liquid nitrogen. This freezing reduces the radiation damage of the X-rays, as well as the noise in the Bragg peaks due to thermal motion (the Debye-Waller effect). However, untreated crystals often crack if flash-frozen; therefore, they are generally pre-soaked in a cryoprotectant solution before freezing. Unfortunately, this pre-soak may itself cause the crystal to crack, ruining it for crystallography. Generally, successful cryo-conditions are identified by trial and error.

The capillary or loop is mounted on a goniometer, which allows it to be positioned accurately within the X-ray beam and rotated. Since both the crystal and the beam are often very small, the crystal must be centered within the beam to within ~25 micrometers accuracy, which is aided by a camera focused on the crystal. The most common type of goniometer is the "kappa goniometer", which offers three angles of rotation: the ω angle, which rotates about an axis perpendicular to the beam; the κ angle, about an axis at ~50° to the ω axis; and, finally, the φ angle about the loop/capillary axis. When the κ angle is zero, the ω and φ axes are aligned. The κ rotation allows for convenient mounting of the crystal, since the arm in which the crystal is mounted may be swung out towards the crystallographer. The oscillations carried out during data collection (mentioned below) involve the ω axis only. An older type of goniometer is the four-circle goniometer, and its relatives such as the six-circle goniometer.

X-ray sources

The mounted crystal is then irradiated with a beam of monochromatic X-rays. The brightest and most useful X-ray sources are synchrotrons; their much higher luminosity allows for better resolution. They also make it convenient to tune the wavelength of the radiation, which is useful for multi-wavelength anomalous dispersion (MAD) phasing, described below. Synchrotrons are generally national facilities, each with several dedicated beamlines where data is collected around the clock, seven days a week.

A diffractometer

Smaller, X-ray generators are often used in laboratories to check the quality of crystals before bringing them to a synchrotron and sometimes to solve a crystal structure. In such systems, electrons are boiled off of a cathode and accelerated through a strong electric potential of ~50 kV; having reached a high speed, the electrons collide with a metal plate, emitting *bremsstrahlung* and some strong spectral lines corresponding to the excitation of inner-shell electrons of the metal. The most common metal used is copper, which can be kept cool easily, due to its high thermal conductivity, and which produces strong K_α and K_β lines. The K_β line is sometimes suppressed with a thin (~10 μm) nickel foil. The simplest and cheapest variety of sealed X-ray tube has a stationary anode (the Crookes tube) and produces ~2 kW of X-ray radiation. The more expensive variety has a rotating-anode type source that produces ~14 kW of X-ray radiation.

X-rays are generally filtered (by use of X-Ray Filters) to a single wavelength (made monochromatic) and collimated to a single direction before they are allowed to strike the crystal. The filtering not only simplifies the data analysis, but also removes radiation that degrades the crystal without contributing useful information. Collimation is done either with a collimator (basically, a long tube) or with a clever arrangement of gently curved mirrors. Mirror systems are preferred for small crystals (under 0.3 mm) or with large unit cells (over 150 Å)

Recording the reflections

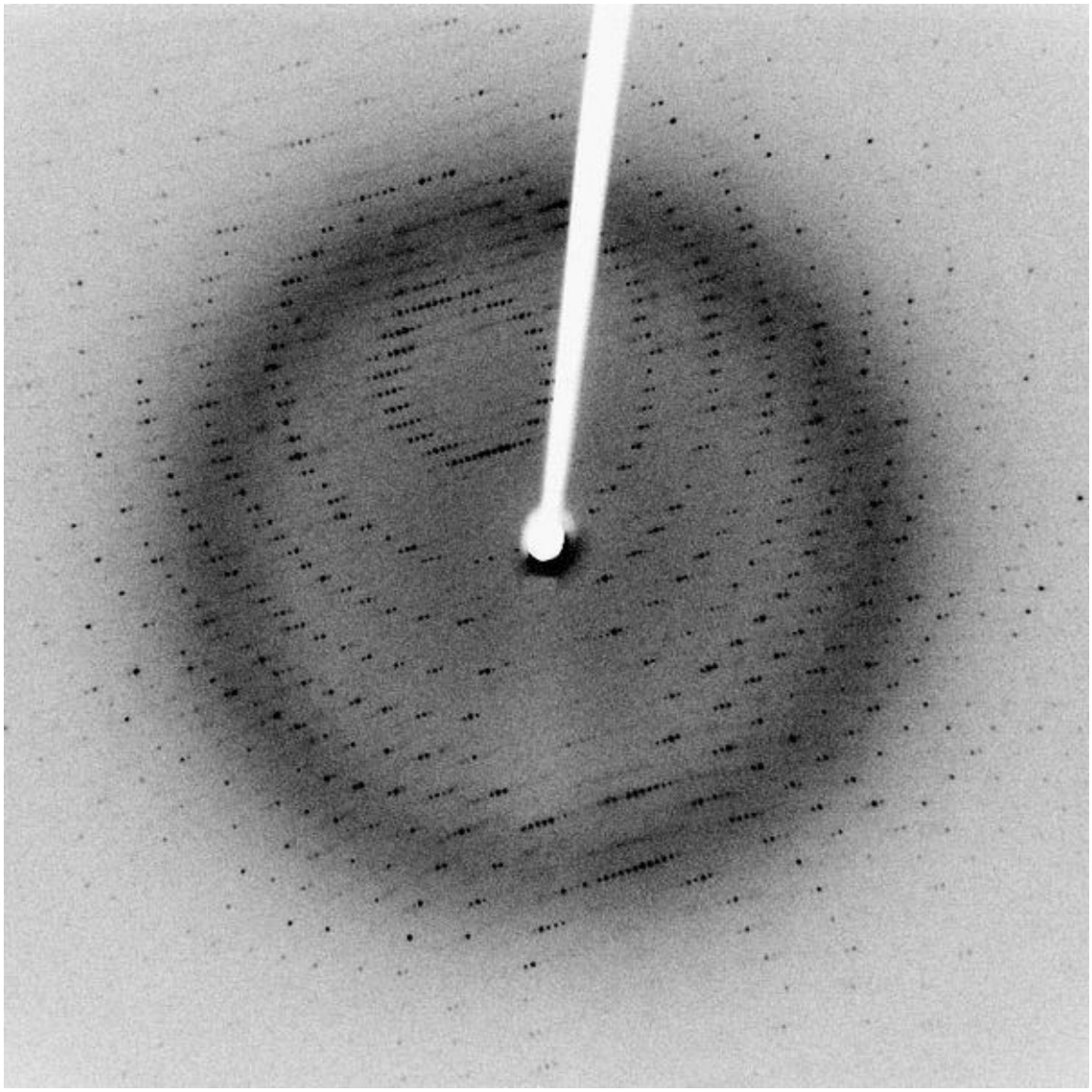

An X-ray diffraction pattern of a crystallized enzyme. The pattern of spots (called *reflections*) can be used to determine the structure of the enzyme.

When a crystal is mounted and exposed to an intense beam of X-rays, it scatters the X-rays into a pattern of spots or *reflections* that can be observed on a screen behind the crystal. A similar pattern may be seen by shining a laser pointer at a compact disc. The relative intensities of these spots provide the information to determine the arrangement of molecules within the crystal in atomic detail. The intensities of these reflections may be recorded with photographic film, an area detector or with a charge-coupled device (CCD) image sensor. The peaks at small angles correspond to low-resolution data, whereas those at high angles represent high-resolution data; thus, an upper limit on the eventual resolution of the structure can be determined from the first few images. Some measures of diffraction quality can be determined at this point, such as the mosaicity of the crystal

and its overall disorder, as observed in the peak widths. Some pathologies of the crystal that would render it unfit for solving the structure can also be diagnosed quickly at this point.

One image of spots is insufficient to reconstruct the whole crystal; it represents only a small slice of the full Fourier transform. To collect all the necessary information, the crystal must be rotated step-by-step through 180°, with an image recorded at every step; actually, slightly more than 180° is required to cover reciprocal space, due to the curvature of the Ewald sphere. However, if the crystal has a higher symmetry, a smaller angular range such as 90° or 45° may be recorded. The rotation axis should be changed at least once, to avoid developing a "blind spot" in reciprocal space close to the rotation axis. It is customary to rock the crystal slightly (by 0.5-2°) to catch a broader region of reciprocal space.

Multiple data sets may be necessary for certain phasing methods. For example, MAD phasing requires that the scattering be recorded at least three (and usually four, for redundancy) wavelengths of the incoming X-ray radiation. A single crystal may degrade too much during the collection of one data set, owing to radiation damage; in such cases, data sets on multiple crystals must be taken.

Data analysis

Crystal symmetry, unit cell, and image scaling

The recorded series of two-dimensional diffraction patterns, each corresponding to a different crystal orientation, is converted into a three-dimensional model of the electron density; the conversion uses the mathematical technique of Fourier transforms, which is explained below. Each spot corresponds to a different type of variation in the electron density; the crystallographer must determine *which* variation corresponds to *which* spot (*indexing*), the relative strengths of the spots in different images (*merging and scaling*) and how the variations should be combined to yield the total electron density (*phasing*).

Data processing begins with *indexing* the reflections. This means identifying the dimensions of the unit cell and which image peak corresponds to which position in reciprocal space. A byproduct of indexing is to determine the symmetry of the crystal, i.e., its *space group*. Some space groups can be eliminated from the beginning. For example, reflection symmetries cannot be observed in chiral molecules; thus, only 65 space groups of 243 possible are allowed for protein molecules which are almost always chiral. Indexing is generally accomplished using an *autoindexing* routine. Having assigned symmetry, the data is then *integrated*. This converts the hundreds of images containing the thousands of reflections into a single file, consisting of (at the very least) records of the Miller index of each reflection, and an intensity for each reflection (at this state the file often also includes error estimates and measures of partiality (what part of a given reflection was recorded on that image)).

A full data set may consist of hundreds of separate images taken at different orientations of the crystal. The first step is to merge and scale these various images, that is, to identify which peaks appear in two or more images (*merging*) and to scale the relative images so that they have a consistent intensity scale. Optimizing the intensity scale is critical because the relative intensity of the peaks is the key information from which the structure is determined. The repetitive technique of crystallographic data collection and the often high symmetry of crystalline materials cause the diffractometer to record many symmetry-equivalent reflections multiple times. This allows calculating the symmetry-related R-factor, a reliability index based upon how similar are the measured intensities of symmetry-equivalent reflections, thus assessing the quality of the data.

Initial phasing

The data collected from a diffraction experiment is a reciprocal space representation of the crystal lattice. The position of each diffraction 'spot' is governed by the size and shape of the unit cell, and the inherent symmetry within the crystal. The intensity of each diffraction 'spot' is recorded, and this intensity is proportional to the square of the *structure factor* amplitude. The structure factor is a complex number containing information relating to both the amplitude and phase of a wave. In order to obtain an interpretable *electron density map*, both amplitude and phase must be known (an electron density map allows a crystallographer to build a starting model of the molecule). The phase cannot be directly recorded during a diffraction experiment: this is known as the phase problem. Initial phase estimates can be obtained in a variety of ways:

- ***Ab initio*** **phasing** or **direct methods -** This is usually the method of choice for small molecules (<1000 non-hydrogen atoms), and has been used successfully to solve the phase problems for small proteins. If the resolution of the data is better than 1.4 Å (140 pm), direct methods can be used to obtain phase information, by exploiting known phase relationships between certain groups of reflections.

- **Molecular replacement -** if a related structure is known, it can be used as a search model in molecular replacement to determine the orientation and position of the molecules within the unit cell. The phases obtained this way can be used to generate *electron density maps*.

- **Anomalous X-ray scattering** (*MAD or SAD phasing*) **-** the X-ray wavelength may be scanned past an absorption edge of an atom, which changes the scattering in a known way. By recording full sets of reflections at three different wavelengths (far below, far above and in the middle of the absorption edge) one can solve for the substructure of the anomalously diffracting atoms and thence the structure of the whole molecule. The most popular method of incorporating anomalous scattering atoms into proteins is to express the protein in a methionine auxotroph (a host incapable of synthesizing methionine) in a media rich in seleno-methionine, which contains selenium atoms. A MAD experiment can then be conducted around the absorption edge, which should then yield the position of any methionine residues within the protein, providing initial phases.

- **Heavy atom methods** (multiple isomorphous replacement) - If electron-dense metal atoms can be introduced into the crystal, direct methods or Patterson-space methods can be used to determine their location and to obtain initial phases. Such heavy atoms can be introduced either by soaking the crystal in a heavy atom-containing solution, or by co-crystallization (growing the crystals in the presence of a heavy atom). As in MAD phasing, the changes in the scattering amplitudes can be interpreted to yield the phases. Although this is the original method by which protein crystal structures were solved, it has largely been superseded by MAD phasing with selenomethionine.

Model building and phase refinement

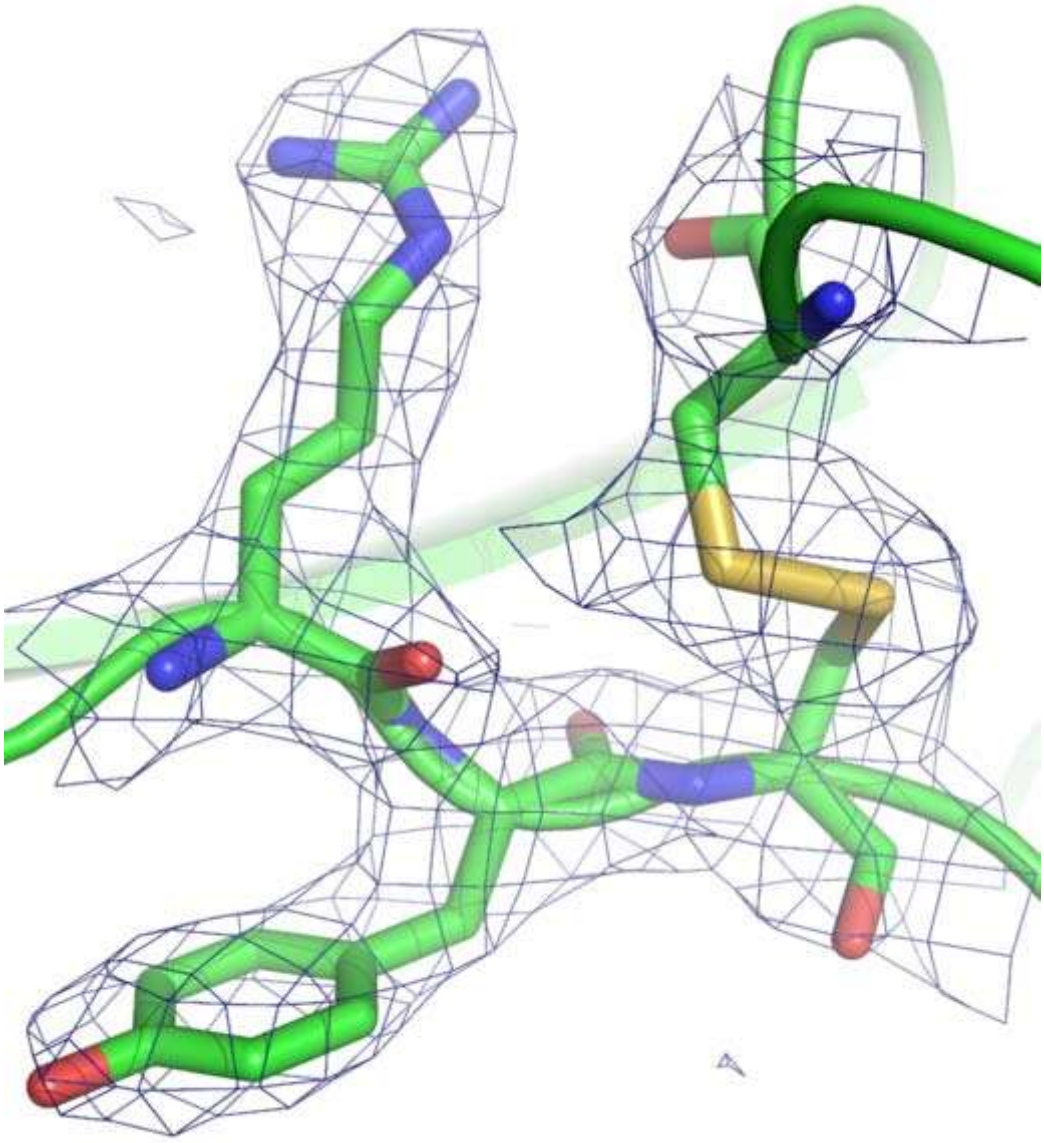

A protein crystal structure at 2.7 Å resolution. The mesh encloses the region in which the electron density exceeds a given threshold. The straight segments represent chemical bonds between the non-hydrogen atoms of an arginine (upper left), a tyrosine (lower left), a disulfide bond (upper right, in yellow), and some peptide groups (running left-right in the middle). The two curved green tubes represent spline fits to the polypeptide backbone.

Having obtained initial phases, an initial model can be built. This model can be used to refine the phases, leading to an improved model, and so on. Given a model of some atomic positions, these positions and their respective Debye-Waller factors (or **B**-factors, accounting for the thermal motion of the atom) can be refined to fit the observed diffraction data, ideally yielding a better set of phases. A new model can then be fit to the new electron density map and a further round of refinement is carried out. This continues until the correlation between the diffraction data and the model is maximized. The agreement is measured by an *R*-factor defined as

$$R = \frac{\sum_{\text{all reflections}} |F_o - F_c|}{\sum_{\text{all reflections}} |F_o|}$$

A similar quality criterion is R_{free}, which is calculated from a subset (~10%) of reflections that were not included in the structure refinement. Both *R* factors depend on the resolution of the data. As a rule of thumb, R_{free} should be approximately the resolution in Ångströms divided by 10; thus, a data-set with 2 Å resolution should yield a final R_{free} ~ 0.2. Chemical bonding features such as stereochemistry, hydrogen bonding and distribution of bond lengths and angles are complementary measures of the model quality. Phase bias is a serious problem in such iterative model building. *Omit maps* are a common technique used to check for this.

It may not be possible to observe every atom of the crystallized molecule - it must be remembered that the resulting electron density is an average of all the molecules within the crystal. In some cases, there is too much residual disorder in those atoms, and the resulting electron density for atoms existing in many conformations is smeared to such an extent that it is no longer detectable in the electron density map. Weakly scattering atoms such as hydrogen are routinely invisible. It is also possible for a single atom to appear multiple times in an electron density map, e.g., if a protein sidechain has multiple (<4) allowed conformations. In still other cases, the crystallographer may detect that the covalent structure deduced for the molecule was incorrect, or changed. For example, proteins may be cleaved or undergo post-translational modifications that were not detected prior to the crystallization.

Deposition of the structure

Once the model of a molecule's structure has been finalized, it is often deposited in a crystallographic database such as the Cambridge Structural Database (for small molecules), the Inorganic Crystal Structure Database (ICSD) (for inorganic compounds) or the Protein Data Bank (for protein structures). Many structures obtained in private

commercial ventures to crystallize medicinally relevant proteins, are not deposited in public crystallographic databases.

Diffraction theory

The main goal of X-ray crystallography is to determine the density of electrons $f(\mathbf{r})$ throughout the crystal, where $\mathbf{r}$ represents the three-dimensional position vector within the crystal. To do this, X-ray scattering is used to collect data about its Fourier transform $F(\mathbf{q})$, which is inverted mathematically to obtain the density defined in real space, using the formula

$$f(\mathbf{r}) = \int \frac{d\mathbf{q}}{(2\pi)^3} F(\mathbf{q}) e^{i\mathbf{q}\cdot\mathbf{r}}$$

where the integral is taken over all values of $\mathbf{q}$. The three-dimensional real vector $\mathbf{q}$ represents a point in reciprocal space, that is, to a particular oscillation in the electron density as one moves in the direction in which $\mathbf{q}$ points. The length of $\mathbf{q}$ corresponds to 2π divided by the wavelength of the oscillation. The corresponding formula for a Fourier transform will be used below

$$F(\mathbf{q}) = \int d\mathbf{r} f(\mathbf{r}) e^{-i\mathbf{q}\cdot\mathbf{r}}$$

where the integral is summed over all possible values of the position vector $\mathbf{r}$ within the crystal.

The Fourier transform $F(\mathbf{q})$ is generally a complex number, and therefore has a magnitude $|F(\mathbf{q})|$ and a phase $\varphi(\mathbf{q})$ related by the equation

$$F(\mathbf{q}) = |F(\mathbf{q})| e^{i\varphi(\mathbf{q})}$$

The intensities of the reflections observed in X-ray diffraction give us the magnitudes $|F(\mathbf{q})|$ but not the phases $\varphi(\mathbf{q})$. To obtain the phases, full sets of reflections are collected with known alterations to the scattering, either by modulating the wavelength past a certain absorption edge or by adding strongly scattering (i.e., electron-dense) metal atoms such as mercury. Combining the magnitudes and phases yields the full Fourier transform $F(\mathbf{q})$, which may be inverted to obtain the electron density $f(\mathbf{r})$.

Crystals are often idealized as being *perfectly* periodic. In that ideal case, the atoms are positioned on a perfect lattice, the electron density is perfectly periodic, and the Fourier transform $F(\mathbf{q})$ is zero except when $\mathbf{q}$ belongs to the reciprocal lattice (the so-called *Bragg peaks*). In reality, however, crystals are not perfectly periodic; atoms vibrate about their mean position, and there may be disorder of various types, such as mosaicity, dislocations, various point defects, and heterogeneity in the conformation of crystallized

molecules. Therefore, the Bragg peaks have a finite width and there may be significant *diffuse scattering*, a continuum of scattered X-rays that fall between the Bragg peaks.

Intuitive understanding by Bragg's law

An intuitive understanding of X-ray diffraction can be obtained from the Bragg model of diffraction. In this model, a given reflection is associated with a set of evenly spaced sheets running through the crystal, usually passing through the centers of the atoms of the crystal lattice. The orientation of a particular set of sheets is identified by its three Miller indices (*h*, *k*, *l*), and let their spacing be noted by *d*. William Lawrence Bragg proposed a model in which the incoming X-rays are scattered specularly (mirror-like) from each plane; from that assumption, X-rays scattered from adjacent planes will combine constructively (constructive interference) when the angle θ between the plane and the X-ray results in a path-length difference that is an integer multiple *n* of the X-ray wavelength λ.

$$2d \sin \theta = n\lambda$$

A reflection is said to be *indexed* when its Miller indices (or, more correctly, its reciprocal lattice vector components) have been identified from the known wavelength and the scattering angle 2θ. Such indexing gives the unit-cell parameters, the lengths and angles of the unit-cell, as well as its space group. Since Bragg's law does not interpret the relative intensities of the reflections, however, it is generally inadequate to solve for the arrangement of atoms within the unit-cell; for that, a Fourier transform method must be carried out.

Scattering as a Fourier transform

The incoming X-ray beam has a polarization and should be represented as a vector wave; however, for simplicity, let it be represented here as a scalar wave. We also ignore the complication of the time dependence of the wave and just focus on the wave's spatial dependence. Plane waves can be represented by a wave vector $\mathbf{k}_{in}$, and so the strength of the incoming wave at time *t=0* is given by

$$Ae^{i\mathbf{k}_{in}\cdot\mathbf{r}}$$

At position **r** within the sample, let there be a density of scatterers $f(\mathbf{r})$; these scatterers should produce a scattered spherical wave of amplitude proportional to the local amplitude of the incoming wave times the number of scatterers in a small volume *dV* about **r**

$$\text{amplitude of scattered wave} = Ae^{i\mathbf{k}\cdot\mathbf{r}}Sf(\mathbf{r})dV$$

where *S* is the proportionality constant.

Let's consider the fraction of scattered waves that leave with an outgoing wave-vector of $\mathbf{k}_{out}$ and strike the screen at $\mathbf{r}_{screen}$. Since no energy is lost (elastic, not inelastic scattering), the wavelengths are the same as are the magnitudes of the wave-vectors $|\mathbf{k}_{in}|=|\mathbf{k}_{out}|$. From the time that the photon is scattered at $\mathbf{r}$ until it is absorbed at $\mathbf{r}_{screen}$, the photon undergoes a change in phase

$$e^{i\mathbf{k}_{out}\cdot(\mathbf{r}_{screen}-\mathbf{r})}$$

The net radiation arriving at $\mathbf{r}_{screen}$ is the sum of all the scattered waves throughout the crystal

$$AS\int d\mathbf{r}\, f(\mathbf{r})e^{i\mathbf{k}_{in}\cdot\mathbf{r}}e^{i\mathbf{k}_{out}\cdot(\mathbf{r}_{screen}-\mathbf{r})} = ASe^{i\mathbf{k}_{out}\cdot\mathbf{r}_{screen}}\int d\mathbf{r}\, f(\mathbf{r})e^{i(\mathbf{k}_{in}-\mathbf{k}_{out})\cdot\mathbf{r}}$$

which may be written as a Fourier transform

$$ASe^{i\mathbf{k}_{out}\cdot\mathbf{r}_{screen}}\int d\mathbf{r}\, f(\mathbf{r})e^{-i\mathbf{q}\cdot\mathbf{r}} = ASe^{i\mathbf{k}_{out}\cdot\mathbf{r}_{screen}}F(\mathbf{q})$$

where $\mathbf{q} = \mathbf{k}_{out} - \mathbf{k}_{in}$. The measured intensity of the reflection will be square of this amplitude

$$A^2S^2|F(\mathbf{q})|^2$$

Friedel and Bijvoet mates

For every reflection corresponding to a point $\mathbf{q}$ in the reciprocal space, there is another reflection of the same intensity at the opposite point $-\mathbf{q}$. This opposite reflection is known as the *Friedel mate* of the original reflection. This symmetry results from the mathematical fact that the density of electrons $f(\mathbf{r})$ at a position $\mathbf{r}$ is always a real number. As noted above, $f(\mathbf{r})$ is the inverse transform of its Fourier transform $F(\mathbf{q})$; however, such an inverse transform is a complex number in general. To ensure that $f(\mathbf{r})$ is real, the Fourier transform $F(\mathbf{q})$ must be such that the Friedel mates $F(-\mathbf{q})$ and $F(\mathbf{q})$ are complex conjugates of one another. Thus, $F(-\mathbf{q})$ has the same magnitude as $F(\mathbf{q})$ but they have the opposite phase, i.e., $\varphi(\mathbf{q}) = -\varphi(\mathbf{q})$

$$F(-\mathbf{q}) = |F(-\mathbf{q})|e^{i\varphi(-\mathbf{q})} = F^*(\mathbf{q}) = |F(\mathbf{q})|e^{-i\varphi(\mathbf{q})}$$

The equality of their magnitudes ensures that the Friedel mates have the same intensity $|F|^2$. This symmetry allows one to measure the full Fourier transform from only half the reciprocal space, e.g., by rotating the crystal slightly more than a 180°, instead of a full turn. In crystals with significant symmetry, even more reflections may have the same intensity (Bijvoet mates); in such cases, even less of the reciprocal space may need to be measured, e.g., slightly more than 90°.

The Friedel-mate constraint can be derived from the definition of the inverse Fourier transform

$$f(\mathbf{r}) = \int \frac{d\mathbf{q}}{(2\pi)^3} F(\mathbf{q}) e^{i\mathbf{q}\cdot\mathbf{r}} = \int \frac{d\mathbf{q}}{(2\pi)^3} |F(\mathbf{q})| e^{i\phi(\mathbf{q})} e^{i\mathbf{q}\cdot\mathbf{r}}$$

Since Euler's formula states that $e^{ix} = \cos(x) + i\sin(x)$, the inverse Fourier transform can be separated into a sum of a purely real part and a purely imaginary part

$$f(\mathbf{r}) = \int \frac{d\mathbf{q}}{(2\pi)^3} |F(\mathbf{q})| e^{i(\phi+\mathbf{q}\cdot\mathbf{r})} = \int \frac{d\mathbf{q}}{(2\pi)^3} |F(\mathbf{q})| \cos(\phi + \mathbf{q}\cdot\mathbf{r}) + i \int \frac{d\mathbf{q}}{(2\pi)^3} |F(\mathbf{q})| \sin(\phi + \mathbf{q}\cdot\mathbf{r}) = I_{cos} + iI_{sin}$$

The function $f(\mathbf{r})$ is real if and only if the second integral $I_{\sin}$ is zero for all values of $\mathbf{r}$. In turn, this is true if and only if the above constraint is satisfied

$$I_{sin} = \int \frac{d\mathbf{q}}{(2\pi)^3} |F(\mathbf{q})| \sin(\phi + \mathbf{q}\cdot\mathbf{r}) = \int \frac{d\mathbf{q}}{(2\pi)^3} |F(-\mathbf{q})| \sin(-\phi - \mathbf{q}\cdot\mathbf{r}) = -I_{sin}$$

since $I_{\sin} = -I_{\sin}$ implies that $I_{\sin}=0$.

Ewald's sphere

Each X-ray diffraction image represents only a slice, a spherical slice of reciprocal space, as may be seen by the Ewald sphere construction. Both $\mathbf{k}_{out}$ and $\mathbf{k}_{in}$ have the same length, due to the elastic scattering, since the wavelength has not changed. Therefore, they may be represented as two radial vectors in a sphere in reciprocal space, which shows the values of $\mathbf{q}$ that are sampled in a given diffraction image. Since there is a slight spread in the incoming wavelengths of the incoming X-ray beam, the values of $|F(\mathbf{q})|$ can be measured only for $\mathbf{q}$ vectors located between the two spheres corresponding to those radii. Therefore, to obtain a full set of Fourier transform data, it is necessary to rotate the crystal through slightly more than 180°, or sometimes less if sufficient symmetry is present. A full 360° rotation is not needed because of a symmetry intrinsic to the Fourier transforms of real functions (such as the electron density), but "slightly more" than 180° is needed to cover all of reciprocal space within a given resolution because of the curvature of the Ewald sphere. In practice, the crystal is rocked by a small amount (0.25-1°) to incorporate reflections near the boundaries of the spherical Ewald shells.

Patterson function

A well-known result of Fourier transforms is the autocorrelation theorem, which states that the autocorrelation $c(\mathbf{r})$ of a function $f(\mathbf{r})$

$$c(\mathbf{r}) = \int d\mathbf{x} f(\mathbf{x}) f(\mathbf{x}+\mathbf{r}) = \int \frac{d\mathbf{q}}{(2\pi)^3} C(\mathbf{q}) e^{i\mathbf{q}\cdot\mathbf{r}}$$

has a Fourier transform $C(\mathbf{q})$ that is the squared magnitude of $F(\mathbf{q})$

$$C(\mathbf{q}) = |F(\mathbf{q})|^2$$

Therefore, the autocorrelation function $c(\mathbf{r})$ of the electron density (also known as the *Patterson function*) can be computed directly from the reflection intensities, without computing the phases. In principle, this could be used to determine the crystal structure directly; however, it is difficult to realize in practice. The autocorrelation function corresponds to the distribution of vectors between atoms in the crystal; thus, a crystal of N atoms in its unit cell may have $N(N-1)$ peaks in its Patterson function. Given the inevitable errors in measuring the intensities, and the mathematical difficulties of reconstructing atomic positions from the interatomic vectors, this technique is rarely used to solve structures, except for the simplest crystals.

Advantages of a crystal

In principle, an atomic structure could be determined from applying X-ray scattering to non-crystalline samples, even to a single molecule. However, crystals offer a much stronger signal due to their periodicity. A crystalline sample is by definition periodic; a crystal is composed of many unit cells repeated indefinitely in three independent directions. Such periodic systems have a Fourier transform that is concentrated at periodically repeating points in reciprocal space known as *Bragg peaks*; the Bragg peaks correspond to the reflection spots observed in the diffraction image. Since the amplitude at these reflections grows linearly with the number N of scatterers, the observed *intensity* of these spots should grow quadratically, like N^2. In other words, using a crystal concentrates the weak scattering of the individual unit cells into a much more powerful, coherent reflection that can be observed above the noise. This is an example of constructive interference.

In a liquid, powder or amorphous sample, molecules within that sample are in random orientations. Such samples have a continuous Fourier spectrum that uniformly spreads its amplitude thereby reducing the measured signal intensity, as is observed in SAXS. More importantly, the orientational information is lost. Although theoretically possible, it is experimentally difficult to obtain atomic-resolution structures of complicated, asymmetric molecules from such rotationally averaged data. An intermediate case is fiber diffraction in which the subunits are arranged periodically in at least one dimension.